THE ROLE OF T CELLS IN THE CHRONIC PHASE AFTER STROKE

Alessio Ricci

Graduate School of Systemic Neurosciences

LMU Munich

Dissertation at the
Graduate School of Systemic Neurosciences
Ludwig-Maximilians-Universität München

January, 2024

Supervisor
Prof. Dr. Arthur Liesz
Institute for Stroke and Dementia Research (ISD)
Klinikum der Universität München

First Reviewer: Prof. Dr. Arthur Liesz
Second Reviewer: Prof. Dr. Thomas Korn
External Reviewer Prof. Dr. Francesca Odoardi

Date of Submission: 19.01.2024
Date of Defense: 11.07.2024

TABLE OF CONTENTS

ABSTRACT

Stroke is a leading cause of mortality and disability worldwide. In recent years, advancements in recanalization therapies have considerably improved acute stroke care, with the main limitation being a restricted time window in which these treatments can be administered. On the other hand, strategies to promote functional recovery in chronic stroke patients are limited to physical rehabilitation, and no pharmacological treatments are available.

Neuroinflammation is a central process that occurs after a stroke and significantly impacts outcomes. In particular, the role of T cells in the acute phase after a stroke has been extensively studied, bringing to light the knowledge that these cells are mostly detrimental. For this reason, the efficacy of leukocyte trafficking blockers, such as Natalizumab, has been tested in stroke patients in two clinical trials. While these strategies were quite effective in preclinical studies, Natalizumab did not show any benefit in stroke patients. A mechanistic understanding of the discrepancy between preclinical and clinical results is currently lacking.

Recent findings suggest that neuroinflammation does not completely resolve in the acute phase after a stroke and instead persists for even months after the ischemic event. In particular, the number of adaptive immune cells tends to increase in the chronic phase. However, what is the phenotype of chronic post-stroke T cells and whether they contribute to functional recovery is unknown.

In our first study, we showed that T cells can proliferate locally in the brain, thus evading the effect of Natalizumab. We took a reverse translational approach and demonstrated that, as in human patients, Natalizumab does not improve functional outcomes in the chronic phase. In fact, while Natalizumab significantly reduces T cell numbers in the acute phase, their number increases in the chronic phase via local expansion within the brain tissue. Importantly, T cells can proliferate in the brain parenchyma both in mice and human patients. Our results stress how a deep mechanistic understanding of pathophysiological processes is of pivotal importance when translating preclinical findings to patients. Furthermore, we described local proliferation as a central mechanism that maintains T cells in the post-stroke brain.

In our second study, we demonstrated that post-stroke T cells acquire a tissue-resident memory (T_{RM}) phenotype. We showed that post-stroke T cells express typical T_{RM} markers, and their maintenance relies on MHC class I and chemokine signaling. Finally, we demonstrated that lymphocytes play a crucial role in restoring functional connectivity after a stroke, likely via microglia-dependent mechanisms. These data offer a comprehensive

description of post-stroke T cell immunophenotype and insights into the mechanisms of tissue residency. Moreover, we showed that lymphocytes have a crucial role in functional recovery also during the chronic phase.

Our studies provide a deeper understanding of T cell biology in the chronic post-stroke brain. Leveraging this knowledge will help overcome the limitations of T cell blockade to treat stroke patients. Furthermore, the molecular mechanisms that we described open up new avenues for immunomodulatory strategies that could provide benefits for stroke recovery.

LIST OF ABBREVIATIONS

AAV	Adeno-Associated Virus
AREG	Amphiregulin
BDNF	Brain-Derived Neurotrophic Factor
Blimp1	B Lymphocyte-Induced Maturation Protein 1
CTLA-4	Cytotoxic T-Lymphocyte Antigen 4
CNS	Central Nervous System
CSF	Cerebrospinal Fluid
DAMP	Damage-Associated Molecular Pattern
DEG	Differentially Expressed Gene
dMCAo	Distal Middle Cerebral Artery Occlusion
EGFR	Epidermal Growth Factor Receptor
EdU	5-Ethynyl-2'-deoxyuridine
FOXP3	Forkhead Box Protein P3
GZMK	Granzyme K
GFAP	Glial Fibrillary Acidic Protein
Hobit	Homolog of Blimp-1 in T cells
Iba1	Ionized Calcium-Binding Adapter Molecule 1
IGF-1	Insulin-Like Growth Factor 1
IFN-γ	Interferon-gamma
IGAL	Integrin Alpha L
IGAM	Integrin Alpha M
ITGA4	Integrin Alpha 4
ITGB1	Integrin Beta 1
ITGAL	Integrin Alpha L
LAG3	Lymphocyte Activation Gene 3
LCMV	Lymphocytic Choriomeningitis Virus
MHC	Major Histocompatibility Complex
MIP-1α	Macrophage Inflammatory Protein 1-alpha
MMP	Matrix Metalloproteinase
moMΦ	Monocyte-Derived Macrophage
NLT	Non-Lymphoid Tissue
NK	Natural Killer

OSM	Oncostatin M
OPN	Osteopontin
OPNR	Osteopontin Receptor
PA-Cre	Photoactivatable Cre
PD-1	Programmed Cell Death Protein 1
PD-L1	Programmed Death-Ligand 1
pMCAo	Proximal Middle Cerebral Artery Occlusion
pRCT	Preclinical Randomized Controlled Multicenter Trial
PT	Photothrombosis
Rag1	Recombination Activating Gene 1
ROS	Reactive Oxygen Species
Runx3	Runt-Related Transcription Factor 3
S1PR1	Sphingosine-1-Phosphate Receptor 1
scSeq	Single-Cell mRNA Sequencing
SLO	Secondary Lymphoid Organ
smFISH	Single-Molecule Fluorescence In Situ Hybridization
STAIR	Stroke Therapy Academic Industry Roundtable
STAT3	Signal Transducer and Activator of Transcription 3
T_{CM}	Central Memory T Cell
TCZ	T Cell Zone
Teff	Effector T Cell
T_{EM}	Effector Memory T Cell
TGF-β	Transforming Growth Factor-beta
TCR	T Cell Receptor
T_{RM}	Tissue-Resident Memory T Cell
Treg	Regulatory T Cell
Tigit	T Cell Immunoreceptor With Ig And ITIM Domains
TNF-α	Tumor Necrosis Factor-alpha
WNV	West Nile Virus

1 INTRODUCTION

1.1 STROKE: EPIDEMIOLOGY AND PATHOMECHANISMS

Stroke is a neurological disorder that manifests as a severe reduction in blood flow to a distinct area of the central nervous system (CNS), resulting in irreversible damage. Two primary classifications of stroke exist: ischemic, characterized by diminished blood flow due to the obstruction of a blood vessel from thrombosis or embolism, and hemorrhagic, in which reduced blood flow results from bleeding in the brain parenchyma or the subarachnoid space (Donkor, 2018). Globally, ischemic and hemorrhagic strokes constitute 62.4% and 37.6% of cases, respectively, with a tendency for a higher prevalence of ischemic strokes in high-income countries (Donkor, 2018; Feigin et al., 2021).

Stroke, ranked as the second leading cause of death worldwide by the World Health Organization, inflicts substantial long-term disability on nearly half of survivors, primarily affecting locomotion, cognition, and speech (Kelly-Hayes et al., 2003). Importantly, the global incidence of stroke is anticipated to rise in the coming years (Pu et al., 2023).

Brain tissue relies on a continuous and abundant supply of oxygen and glucose through blood flow. The abrupt interruption of cerebral blood supply induces rapid brain damage, particularly in the ischemic core, where neurons swiftly succumb to dysfunction due to energy failure, leading to necrosis. At the peripheries of the ischemic territory, referred to as the ischemic penumbra, suboptimal blood perfusion is sustained, enabling neurons to persist for a longer duration. Nonetheless, they remain vulnerable and, without restoration of blood flow, ultimately succumb to excitotoxicity and calcium overload (Iadecola & Anrather, 2011).

The advancement of recanalization approaches such as thrombolysis and thrombectomy has significantly improved acute stroke treatment. However, the critical limitation of these therapies lies in their narrow time window for administration. Furthermore, not all patients qualify for such interventions, and their execution demands highly qualified personnel. Conversely, interventions specifically targeting long-term disability in chronic stroke patients are predominantly confined to rehabilitation. A noteworthy proportion of post-stroke patients spontaneously recover lost functions, emphasizing the imperative to develop strategies that augment this natural recovery process or unlock latent recovery potential in non-responders, thereby alleviating post-stroke long-term disability.

1.2 IMMUNOLOGY OF ISCHEMIC STROKE

1.2.1 Dynamics and Contribution of Immune Cells to Acute Stroke Outcome

Following ischemic brain injury, the initiation of neuroinflammation is triggered by the production of reactive oxygen species (ROS) and the release of damage-associated molecular patterns (DAMPs). Extensive investigation into the dynamics of immune cell activation and infiltration in response to such injuries has been undertaken (Gelderblom et al., 2009). Notably, microglia, the resident macrophage-like cells of the brain, emerge as the first responders to the injury, undergoing proliferation and adopting an activated ameboid-like morphology (Morrison & Filosa, 2013). These activated microglia play a dual role in the inflammatory *milieu*, secreting proinflammatory cytokines while concurrently exhibiting a potential beneficial effect by regulating excitotoxicity (Szalay et al., 2016) and mitigating

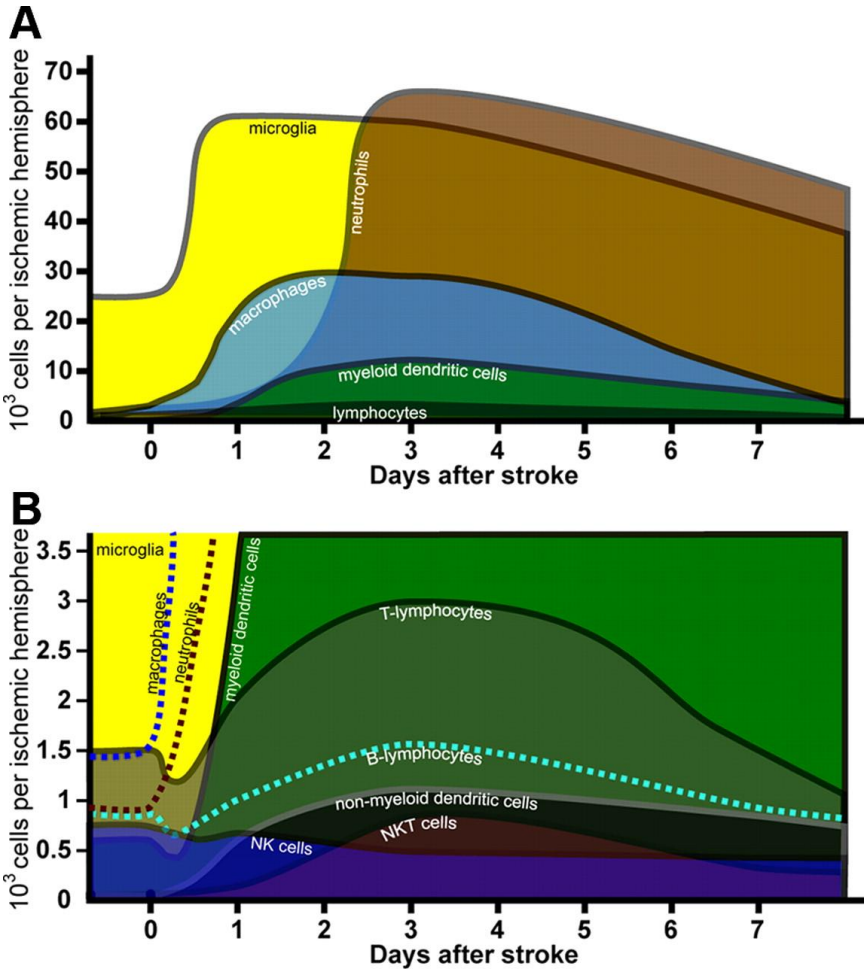

Figure 1. Dynamics of peripheral immune cells during the acute phase after stroke. Cell counts of distinct immune cell populations at different time points after experimental stroke. (A) shows the main myeloid cell populations, while (B) corresponds to a zoom to reveal lymphoid cells. Notably, the quantification reveals a striking distinction, as the number of infiltrating myeloid cells surpasses that of lymphoid cells by more than one order of magnitude. Reproduced with publisher approval from (Gelderblom et al., 2009)

excessive neutrophil infiltration (Otxoa-de-Amezaga et al., 2019).

In response to ischemia, peripheral immune cells infiltrate the brain owing to heightened endothelial activation and the secretion of chemoattractants (Fig. 1). Neutrophils and monocytes are the earliest to migrate into the ischemic brain environment. Neutrophils contribute to an overall detrimental effect by promoting neurotoxicity and tissue damage (Allen et al., 2012; Garcia-Bonilla et al., 2014). Monocytes also migrate into the brain, where they differentiate into macrophages(Garcia-Bonilla et al., 2016). Intriguingly, monocyte-derived macrophages acquire a pro-reparative capacity, and the acute inhibition of monocyte infiltration is associated with a worsened functional outcome (Pedragosa et al., 2020; Wattananit et al., 2016). Subsequently, cells of the adaptive immune system, namely B and T cells, invade the post-stroke brain with a delayed kinetics.

Contrary to earlier perceptions of post-stroke neuroinflammation as a transient phenomenon resolving within weeks (Gelderblom et al., 2009), recent data challenge this assumption. Instead, several indicators of chronic neuroinflammation persist even months after ischemic injury. Although the invasion of peripheral immune cells diminishes in the chronic phase, the numbers of B and T cells steadily increase during this period after stroke (Doyle et al., 2015; Ito et al., 2019). Intriguingly, monocyte-derived macrophages persist in the chronic infarct core, suggesting their long-lived and resident nature in the tissue (Werner et al., 2020). This underscores the importance of reevaluating the temporal dynamics of post-stroke neuroinflammation, acknowledging its prolonged and nuanced trajectory, with implications for potential therapeutic interventions.

1.2.2 The Role of Lymphocytes in the Acute Phase after Stroke

Despite the relatively low numbers of infiltrating T cells following a stroke, these cells play a pivotal role in influencing acute stroke outcomes. Initial investigations demonstrated that lymphocyte-deficient $Rag1^{-/-}$ mice exhibited diminished infarct volumes and improved functional outcomes (Hum et al., 2007). Notably, the protective effect was negated by the adoptive transfer of T cells and not B cells, underscoring the specific contribution of T cells to exacerbating brain damage (Kleinschnitz et al., 2010). Since T cells are characterized by a substantial heterogeneity, it is not surprising that distinct subtypes contribute to stroke outcomes through varied mechanisms. CD8+ cytotoxic T cells employ perforin/granzymes (Mracsko et al., 2014) and FasL (Fan et al., 2020) to exert neurotoxic functions.

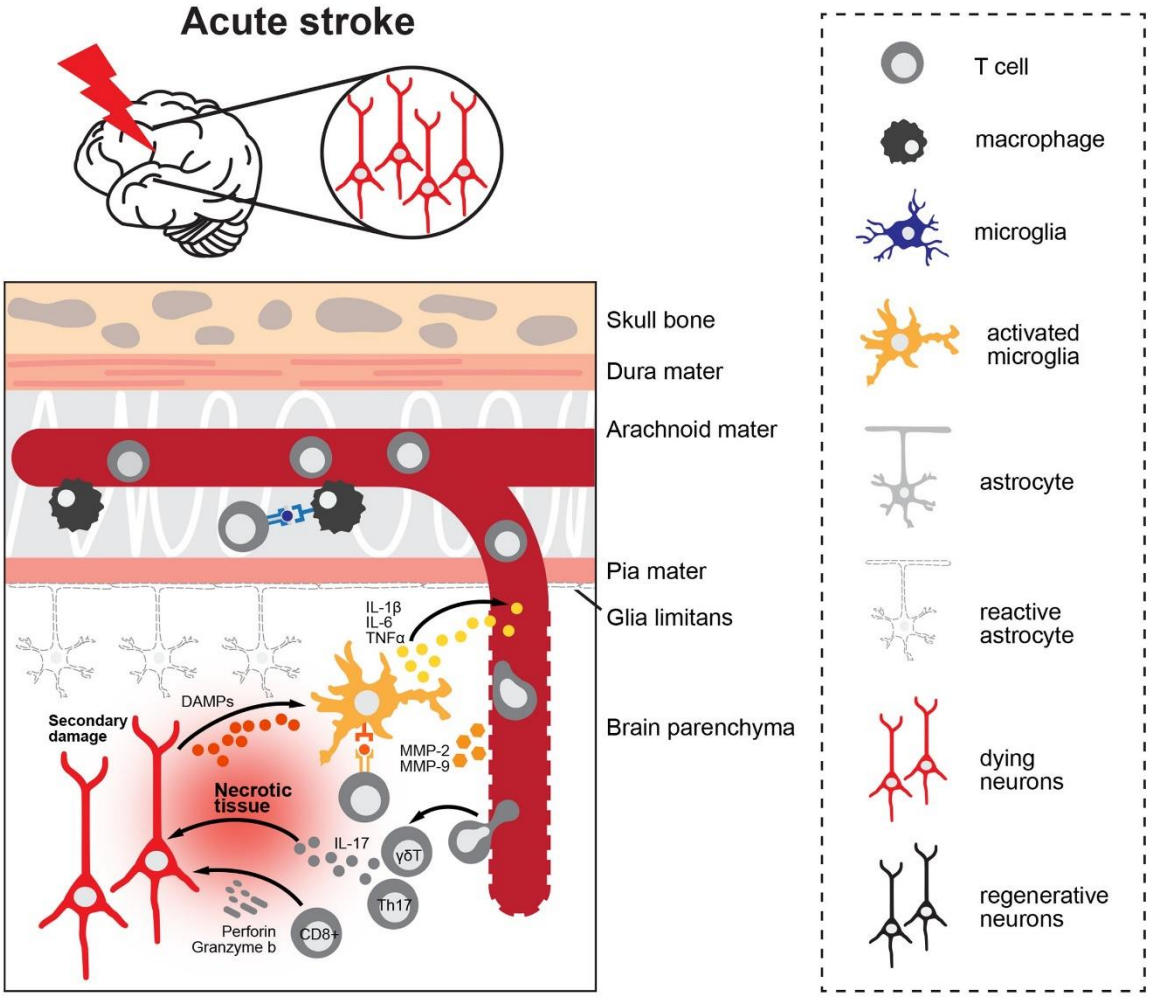

Figure 2. Detrimental effects of T cells in the acute phase after stroke. Ischemic damage initiates the release of Damage-Associated Molecular Patterns (DAMPs) and prompts microglia to release proinflammatory cytokines. In response, T cells infiltrate the brain parenchyma, exacerbating damage through mechanisms such as cytotoxicity induction or the release of cytokines, including IL-17. Reproduced with publisher approval from (Cramer et al., 2019).

In contrast, CD4+ T cells influence stroke outcomes by releasing pro-inflammatory cytokines (Gelderblom et al., 2012) and polarizing microglia toward an activated state (Benakis et al., 2022). Additionally, γδ T cells emerge as the primary source of pro-inflammatory cytokines such as IL-17, contributing to neutrophil recruitment and exacerbation of stroke pathology (Gelderblom et al., 2012; Shichita et al., 2009) (Fig. 2).

In the initial days post-ischemia, brain invasion by T cells occurs in an antigen-independent manner (Kleinschnitz et al., 2010), aligning with the requirement of a 7-10 day timeframe for mounting an adaptive immune response. However, in the early subacute phase, CD8+ T cells rely on antigen recognition for brain accumulation (Mracsko et al., 2014) and exhibit signs of clonal expansion (Liesz et al., 2013). Intriguingly, both CD4+ and CD8+ T cells have demonstrated responsiveness to neural antigens post-stroke (Ortega et al., 2015). Notably, brain antigens have been identified in cervical lymph nodes following ischemic stroke (Planas

et al., 2012). The potential induction of an overt autoimmune response and its precise role in stroke outcomes remain areas for further elucidation.

Despite the overall detrimental role of T cells in the acute phase, therapeutic interventions aiming to block T cell brain invasion have shown promise in preclinical models. Monoclonal antibodies against CD49d, an integrin crucial for leukocyte trafficking in the CNS, successfully inhibited T cell invasion after stroke. This intervention resulted in reduced infarct volumes and improved functional outcomes in numerous studies, including a multicenter randomized preclinical trial (Becker et al., 2001; Langhauser et al., 2014; Liesz et al., 2011; Llovera et al., 2015; Neumann et al., 2015; Relton et al., 2001). Similarly, the immunosuppressive drug Fingolimod, a sphingosine-1-phosphate receptor 1 (S1PR1) modulator that sequesters lymphocytes in lymph nodes, has demonstrated beneficial effects in various preclinical studies (Dang et al., 2021).

While T cells, in general, contribute detrimentally in the acute phase post-ischemia, a specific subpopulation, regulatory T cells (Treg), has shown protective effects. Seminal work by Liesz et al. demonstrated that Treg depletion led to larger infarct volumes and worse outcomes. Treg play a crucial role in dampening inflammation by limiting the production of pro-inflammatory cytokines such as TNF-α, IFN-γ, and IL-1β, and by reducing the infiltration of neutrophils. Mechanistically, Treg secrete the immunomodulatory cytokine IL-10, mediating the observed beneficial effects after stroke (Liesz et al., 2009). Treg are particularly instrumental in restraining microglia activation (Benakis et al., 2022; Xie et al., 2014). Subsequent studies assessing the impact of Treg depletion on stroke outcomes have yielded conflicting results, likely stemming from variations in stroke models and the efficiency of Treg depletion (Liesz & Kleinschnitz, 2016). Nonetheless, therapeutic interventions aimed at enhancing Treg numbers after stroke, including adoptive Treg transfer, CD28 superagonists, and mucosal immunization, have shown a net beneficial effect on stroke outcomes in a recent meta-analysis (Liesz & Kleinschnitz, 2016).

1.2.3 The Role of Lymphocytes in the Chronic Phase after Stroke

A plethora of studies have extensively delved into neuroinflammation during the acute phase post-stroke, however investigations into chronic neuroinflammation remain in their nascent stages.

Numerous reports have demonstrated a significant accumulation of both B and T lymphocytes in the post-stroke brain during the chronic phase (Doyle et al., 2015; Stubbe et al., 2013; Xie et al., 2014). In contrast to their limited role in the acute phase (Kleinschnitz et

al., 2010), B cells have been implicated in delayed cognitive impairment, with genetic or pharmacological ablation of B cells mediating protection (Doyle et al., 2015). Subsequent studies unveiled that brain-infiltrating B cells undergo isotype switching, predominantly producing IgA in a T cell-independent manner (Zbesko et al., 2021). However, the specific contribution of B cells to post-stroke cognitive decline, particularly through antibody secretion, remains to be delineated. Conversely, an alternative study revealed a beneficial role of B cells in post-stroke recovery, as B cell-depleted mice exhibited exacerbated motor deficits, increased anxiety, memory deficits, and reduced neurogenesis (Ortega et al., 2020).

Exploration of the role of T cells in the chronic phase has primarily focused on Treg (Fig. 3). Initial experiments by Stubbe et al. indicated elevated Treg numbers two weeks post-stroke induction, accompanied by heightened proliferation. However, these findings did not establish a clear role for Tregs in long-term outcomes (Stubbe et al., 2013). In contrast, subsequent research demonstrated that delayed blockade or depletion of Treg heightened astrogliosis. Mechanistically, this effect was mediated by Treg-secreted amphiregulin (AREG), which suppressed IL-6-STAT3 signaling in astrocytes and microglia. Notably, post-stroke Treg infiltration was mediated by chemokines CCL1 and CCL20, with their amplification dependent on diverse signaling pathways, including IL-2, IL-33, serotonin, and notably TCR signaling. Additionally, Treg exhibited signs of clonal expansion in the post-ischemic brain (Ito et al., 2019). Another study highlighted the role of Treg in white matter

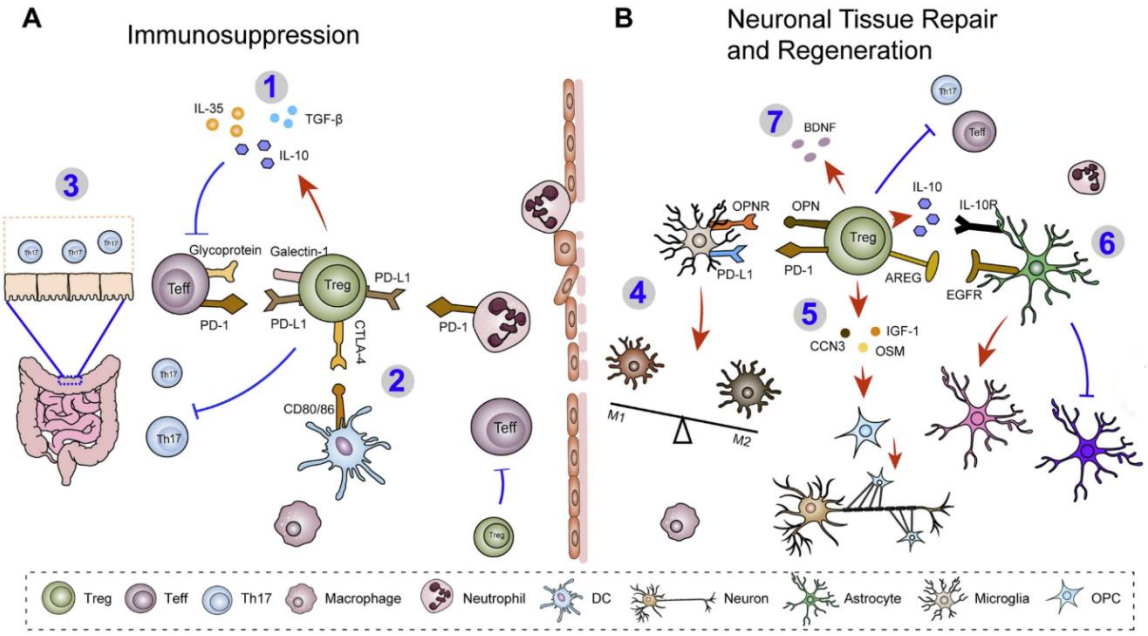

Figure 3. Mechanisms of Treg-mediated protection after ischemic stroke. Treg can mediate immunosuppressive mechanisms by either soluble factors (1), cell-cell contact interactions (2) or by blocking brain invasion of gut-derived γδ T cells. Alternatively, Treg contribute to the tissue repair by shifting microglia phenotype towards a pro-reparative one (4), promoting remyelination (5), suppressing astrogliosis (6) or by secreting neurotrophic factors (7). Reproduced with publisher approval from (Wang et al. 2023)

repair, where Treg-secreted osteopontin (OPN) promoted tissue-reparative microglia and oligodendrogenesis, ultimately enhancing white matter integrity and functional recovery post-stroke. Notably, expanding Treg with IL-2:IL-2-Ab complexes further improved functional outcomes (Shi et al., 2021).

Regarding conventional CD4+ or CD8+ T cells in the chronic phase post-stroke, limited knowledge is available. Delayed depletion of CD8+ T cells resulted in reduced neuroinflammation and modest improvement in functional outcomes, although the underlying molecular mechanisms remain unexplored (Selvaraj et al., 2021). Similarly, delayed depletion of CD4+ T cells decreased chronic B cell accumulation and prevented cognitive decline (Weitbrecht et al., 2021).

It is crucial to note that the majority of lymphocytes in the chronic post-stroke brain reside within the lesion core, segregated from the perilesional parenchyma by the glial scar. Remarkably, the glial scar acts as a permeable barrier to soluble molecules up to 70 kDa, suggesting that mediators secreted by lymphocytes can directly influence nearby neurons, potentially exerting both beneficial and detrimental effects (Zbesko et al., 2018). Moreover, the lesion core is populated by lipid-laden myeloid cells, central in maintaining a heightened inflammatory state. Alleviating their lipid overload with hydroxypropyl-β-cyclodextrin resulted in a significant reduction of both B and T cells (Becktel et al., 2022).

In summary, while preliminary studies indicate that lymphocytes continue to play a role in the recovery process during the chronic phase, further elucidation of the molecular mechanisms governing brain residency and recovery modulation is imperative.

1.2.4 Translation of T Cell-Targeted Therapies to Stroke Patients

Building upon encouraging outcomes in preclinical investigations that targeted T cell invasion post-stroke, several clinical trials have sought to evaluate the efficacy of these agents in human stroke patients. Notably, the anti-CD49d monoclonal antibody Natalizumab, approved for multiple sclerosis and Crohn’s disease, underwent initial scrutiny in the phase 2 clinical trial ACTION. This trial revealed a positive impact on functional independence, assessed through the modified Rankin scale and Barthel index. However, no discernible effects on infarct volume or neurological outcomes at 90 days (National Institute of Health Stroke Scale, NIHSS) were observed (Elkins et al., 2017). A subsequent phase 2b trial, ACTION II, reaffirmed that Natalizumab failed to improve outcomes in ischemic stroke patients (Elkind et al., 2020).

In addition, Fingolimod has been explored in clinical trials involving acute stroke patients. A preliminary study involving 22 participants demonstrated that oral administration of Fingolimod restricted lesion enlargement at 7 days and resulted in improved functional outcomes (Fu et al., 2014). These findings were substantiated by subsequent proof-of-principle studies (Bai et al., 2022). While these pilot studies suggest a potential benefit of Fingolimod administration in stroke patients, conclusive evidence awaits validation through a large-scale clinical trial encompassing diverse ethnic populations beyond the initial Chinese cohorts.

1.3 TISSUE-RESIDENT MEMORY T CELLS

Adaptive immunity is characterized by its specificity and enhanced efficiency in addressing subsequent challenges, a phenomenon termed "immunological memory." This enduring memory is facilitated by the persistence of a subset of cells following the resolution of an initial infection, known as memory cells. Within the T cell subpopulation, two classic subsets of memory cells have been identified based on their recirculation and functional properties: central memory T cells (T_{CM}) and effector memory T cells (T_{EM}). T_{CM} circulate between blood

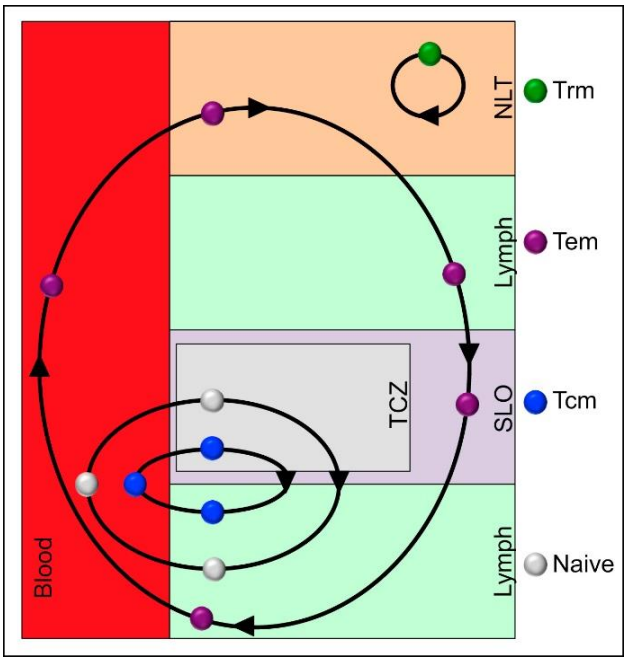

Figure 4. Pattern of recirculation of different memory T cell subtypes. Naïve and T_{CM} recirculate between the blood and the T cell zone (TCZ) of secondary lymphoid organs (SLO). T_{EM} instead can also enter transiently non lymphoid tissues (NLT). T_{RM} permanently reside within NLT. Reproduced with publisher approval from (Schenkel & Masopust, 2014).

and secondary lymphoid organs, displaying high proliferation capacity upon reinfection, while T_{EM} transiently patrol non-lymphoid organs, exhibit potent effector capabilities, and are less proliferative (Mueller et al., 2013).

In recent years, a third subset of memory T cells has emerged, known as tissue-resident memory T cells (T_{RM}). Typically found in border tissues such as skin and mucosae, T_{RM} persist long-term without recirculating, providing a crucial first line of defense against reinfection (Schenkel & Masopust, 2014) (Fig. 4).

T_{RM}, despite some tissue-specific variations, are generally characterized by the expression of the marker CD69. Additionally, they exhibit low levels of tissue egress molecules, including CD62L, S1PR1, and CCR7, while expressing a repertoire of chemokine receptors and integrins that facilitate tissue retention (Schenkel & Masopust, 2014). Recent studies have identified key transcription factors essential for the induction of a T_{RM} program, including *Hobit*, *Blimp1*, *Runx3*, and *Bhlhe40* (Li et al., 2019; Mackay et al., 2016; Milner et al., 2017). The establishment and maintenance of T_{RM} depend on various signaling molecules that induce crucial T_{RM} markers or promote their survival. Among these, TGF-β and IL-15 have been implicated in T_{RM} formation in different organs (K. Yang & Kallies, 2021). Additionally, T_{RM} undergo metabolic changes, prominently relying on fatty acid uptake and degradation for their sustained survival (Pan et al., 2017).

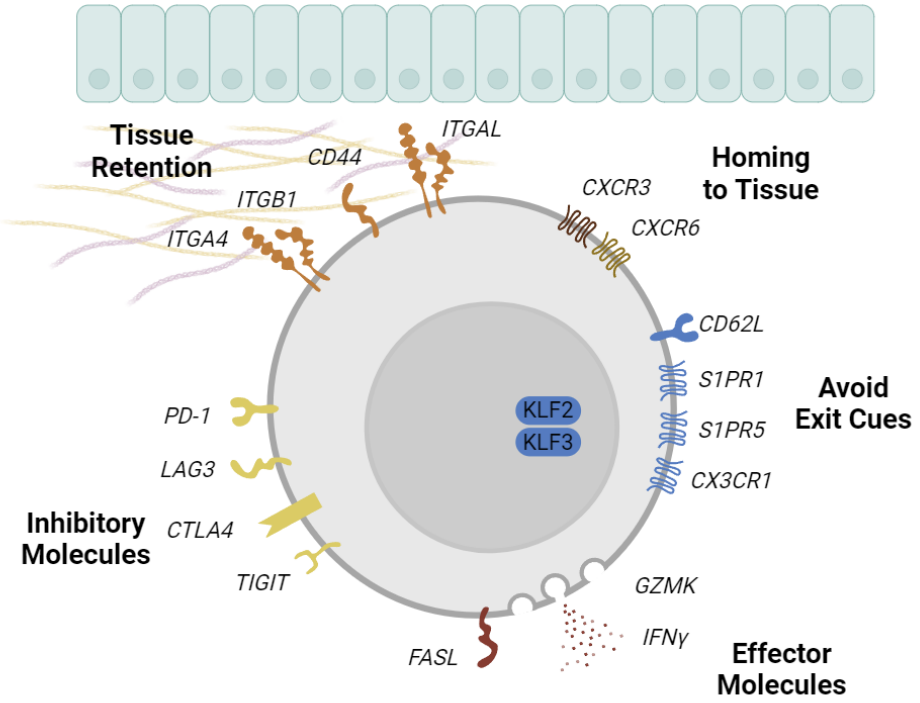

Figure 5. Tissue-resident memory T cell markers. T_{RM} are characterized by upregulation of tissue retention molecules, such as integrins, and tissue homing mediators, such as chemokine receptors. At the same time, they downregulate tissue egress molecules. In addition, they overexpress molecules implicated in both inhibition and effector function. Adapted from (Kumar et al., 2017).

1.3.1 Tissue-Resident Memory T Cells in the Central Nervous System

Pioneering research by Wakim et al. demonstrated the formation of tissue-resident memory T cells in the CNS following viral infection with vesicular stomatitis virus (VSV) (Wakim et al., 2010). This enduring T_{RM} population expressed the integrin CD103 and displayed longevity; however, it did not survive when cultured *in vitro*, emphasizing the critical role of the tissue microenvironment for their persistence (Wakim et al., 2010). Subsequent studies confirmed the emergence of T_{RM} in various viral and bacterial infections of the brain, extending the concept to human subjects in both healthy and diseased conditions (Merkler et al., 2022; Smolders et al., 2018). Interestingly, in the context of acute lymphocytic choriomeningitis virus (LCMV) infections, CD4+ T cells were found to be dispensable for pathogen clearance and CD8+ T_{RM} formation (Steinbach et al., 2016). Conversely, in cases of persistent polyomavirus infection, CD4+ T cell-derived IL-21 played a vital role in the development and functionality of CD8+ T_{RM} (Ren et al., 2020).

Beyond infectious models, T_{RM} populations have been identified in various neurological conditions, including CNS autoimmunity and neurodegeneration. In experimental CNS autoimmunity, CD8+ T_{RM} have been implicated in disease progression, with CD4+ T cells playing a pivotal role in their establishment and function (Frieser et al., 2022; Vincenti et al., 2022). Furthermore, T cells exhibiting a T_{RM} phenotype have been detected in the brain tissue and cerebrospinal fluid of multiple sclerosis patients, highlighting their potential involvement in autoimmune responses (Beltrán et al., 2019; Machado-Santos et al., 2018). In the context of neurodegenerative diseases, particularly Alzheimer's disease (AD), CD8+ T_{RM} presence has been observed in both experimental models and humans (Altendorfer et al., 2022; Chen et al., 2023; Su et al., 2023). Intriguingly, conflicting roles have been proposed, with some studies suggesting a deleterious impact on tau-mediated neurodegeneration, while others propose a protective role through the suppression of proinflammatory microglia. This context- and subtype-dependent functionality underscores the complexity of CD8+ T_{RM} roles in neurodegenerative diseases.

Chemokine receptor signaling plays a central role in T_{RM} formation, with CXCR3 and CXCR6 being typical T_{RM} chemokine receptors (K. Yang & Kallies, 2021). CXCR3 is essential for tissue invasion in various inflammatory contexts, including brain infections (Klein et al., 2005) and autoimmunity (Sporici & Issekutz, 2010). Notably, the CXCR3-CXCL10 axis has been identified as a prominent molecular interaction in a single-cell RNA sequencing database of brain immune cells following ischemic stroke (Garcia-Bonilla et al., 2023). Conversely, CXCR6 regulates long-term maintenance in tissues such as the lung and liver (Tse et al., 2014; Wein et al., 2019). In brain infections with West Nile virus (WNV), CXCR6 and its

ligand CXCL16 are crucial for T_{RM} maintenance and the acquisition of typical T_{RM} markers (Rosen et al., 2022). Similarly, CXCR6 signaling is fundamental for tissue maintenance, T_{RM} program establishment, and clonal expansion in a mouse model of AD (Su et al., 2023).

2 AIM OF THE STUDY

Natalizumab is an efficient drug that blocks leukocyte infiltration in the context of neuroinflammation. This approach has shown a robust benefit in a number of preclinical studies, but it failed to show efficacy when evaluated in clinical trials. Importantly, preclinical work has focused on the acute phase after a stroke, while the primary endpoints of the clinical trials were in the subacute/chronic phase (90 days post-stroke). First, we set out to address whether Natalizumab also shows a lack of efficacy during the chronic phase in a murine model of experimental stroke, using a combination of behavioral tests and wide-field calcium imaging. Furthermore, we evaluated whether the lack of Natalizumab efficacy in the chronic phase could be linked to "evasion mechanisms" that allow T cells to accumulate in the brain despite the treatment.

The presence of T cells in the chronic post-stroke brain has been previously recognized, but a detailed immunophenotyping of this cell population is currently lacking. Given the vast heterogeneity of T cells, we performed an in-depth characterization utilizing high-parametric flow cytometry and single-cell mRNA sequencing. T cells rely on antigen presentation to recognize a specific target. Therefore, we employed inducible knock-out mouse models to assess whether this mechanism is involved in long-term brain residency after a stroke. In parallel, we also investigated the role of chemokine signaling and employed adoptive transfer of T cells in lymphocyte-deficient mice to determine which pathways are necessary for tissue residency. Finally, we evaluated the role of lymphocytes in the recovery process by assessing functional connectivity in lymphocyte-deficient mice.

3 RESEARCH ARTICLES

3.1 CHRONIC T CELL PROLIFERATION IN BRAINS AFTER STROKE COULD INTERFERE WITH THE EFFICACY OF IMMUNOTHERAPIES

3.1.1 Summary

Neuroinflammation has emerged as a focal point in translational stroke research, with preclinical investigations highlighting the pivotal role played by brain-invading lymphocytes in post-stroke pathophysiology. The application of anti-CD49d antibodies has consistently demonstrated efficacy in mitigating cerebral lymphocyte invasion, thereby improving outcomes during the acute phase in experimental stroke models. Despite promising results in preclinical studies, clinical trials employing this approach failed to exhibit efficacy in stroke patients when assessing chronic outcomes three months post-stroke.

In this context, we pinpoint the persistence of T cell accumulation in the brain beyond the acute phase—despite the application of anti-CD49d antibodies—as a potential mechanistic explanation for the observed disparity between preclinical and clinical studies. This phenomenon manifested in both murine models and human autopsy samples, spanning a period of over one month post-stroke. Notably, anti-CD49d treatment failed to yield functional benefits in the chronic phase following stroke, as assessed through calcium imaging-inferred functional connectivity. Upon deeper investigation, we revealed that the sustained accumulation of T cells in the post-ischemic brain primarily resulted from heightened local T cell proliferation rather than continual invasion.

This pivotal observation prompts a re-evaluation of existing immunotherapeutic strategies that target circulating lymphocytes with the objective of fostering recovery after stroke. The focus should shift towards understanding and addressing the intricate dynamics of local T cell proliferation in the post-ischemic brain, providing valuable insights for the development of more effective therapeutic interventions.

3.1.2 Reference

The paper was published in the “Journal of Experimental Medicine” under the following reference:

Heindl, S., **A. Ricci**, O. Carofiglio, Q. Zhou, T. Arzberger, N. Lenart, N. Franzmeier, T. Hortobagyi, P.T. Nelson, A.M. Stowe, A. Denes, D. Edbauer, and A. Liesz. 2021. Chronic T cell proliferation in brains after stroke could interfere with the efficacy of immunotherapies. J Exp Med. 218. doi:10.1084/jem.20202411

JEM Journal of Experimental Medicine

BRIEF DEFINITIVE REPORT

Chronic T cell proliferation in brains after stroke could interfere with the efficacy of immunotherapies

Steffanie Heindl[1], Alessio Ricci[1], Olga Carofiglio[1], Qihui Zhou[2], Thomas Arzberger[3,4], Nikolett Lenart[5], Nicolai Franzmeier[1], Tibor Hortobagyi[6], Peter T. Nelson[7], Ann M. Stowe[7], Adam Denes[5], Dieter Edbauer[2,8], and Arthur Liesz[1,8]

Neuroinflammation is an emerging focus of translational stroke research. Preclinical studies have demonstrated a critical role for brain-invading lymphocytes in post-stroke pathophysiology. Reducing cerebral lymphocyte invasion by anti-CD49d antibodies consistently improves outcome in the acute phase after experimental stroke models. However, clinical trials testing this approach failed to show efficacy in stroke patients for the chronic outcome 3 mo after stroke. Here, we identify a potential mechanistic reason for this phenomenon by detecting chronic T cell accumulation—evading the systemic therapy—in the post-ischemic brain. We observed a persistent accumulation of T cells in mice and human autopsy samples for more than 1 mo after stroke. Cerebral T cell accumulation in the post-ischemic brain was driven by increased local T cell proliferation rather than by T cell invasion. This observation urges re-evaluation of current immunotherapeutic approaches, which target circulating lymphocytes for promoting recovery after stroke.

Introduction

Stroke is one of the leading causes of death and permanent disability worldwide (World Health Organization, 2017). Despite the enormous medical need, specific therapies for stroke patients are still limited to vascular recanalization approaches within the acute phase after stroke (Emberson et al., 2014; Fiehler and Gerloff, 2015; Hacke et al., 2008). In the search for alternative therapeutic strategies, post-stroke neuroinflammation has come into focus in current translational stroke research (Iadecola and Anrather, 2011). Neuroinflammation after stroke is a crucial pathomechanism contributing to secondary brain injury, neurodegeneration, and recovery (Iadecola and Anrather, 2011; Moskowitz et al., 2010). While different leukocyte cell populations have been implicated in the neuroinflammatory response to stroke, T cells have been consistently shown to be a key cell population driving secondary brain injury (Chamorro et al., 2012; Macrez et al., 2011). Consequently, several therapeutic strategies targeting the brain invasion of lymphocytes have been tested using antibodies against key adhesion molecules or by reducing the number of circulating lymphocytes (Chamorro et al., 2012; Cramer et al., 2019a).

A prominent and controversial example of this translational approach is the use of anti-CD49d antibodies (Natalizumab), which reduces the invasion of circulating lymphocytes to the brain by blocking a key adhesion molecule. The repurposing of this drug used for patients with multiple sclerosis improved outcome in the acute phase after experimental stroke in the majority of preclinical studies (Becker et al., 2001; Langhauser et al., 2014; Liesz et al., 2011; Neumann et al., 2015; Relton et al., 2001), which was validated in a first-ever multicenter, randomized preclinical trial (Llovera et al., 2015). In a first phase 2 clinical trial (ACTION), Natalizumab treatment significantly improved functional outcome (modified Rankin scale) in the subacute phase (30 d), but this effect was not evident anymore in the chronic phase (90 d; Elkins et al., 2017). Correspondingly, a follow-up phase 2b trial (ACTION-II) also did not report any improvement with Natalizumab treatment in the stroke outcome at 90 d (Elkind et al., 2020).

Failed translations from promising experimental studies to clinical trials are commonly attributed to differences in study design, target engagement, or lack of statistical robustness of the preclinical findings (Endres et al., 2008; Howells et al., 2014; Macleod et al., 2014). However, the efficacy of Natalizumab in preclinical models has been extraordinarily well characterized, and clinical trials have closely mimicked the efficient

[1]Institute for Stroke and Dementia Research, University Hospital, Ludwig Maximilians University Munich, Munich, Germany; [2]German Center for Neurodegenerative Diseases, Munich, Germany; [3]Department of Psychiatry and Psychotherapy, University Hospital, Ludwig Maximilians University Munich, Munich, Germany; [4]Center for Neuropathology and Prion Research, Ludwig Maximilians University Munich, Munich, Germany; [5]Momentum Laboratory of Neuroimmunology, Institute of Experimental Medicine, Budapest, Hungary; [6]ELKH-DE Cerebrovascular and Neurodegenerative Research Group, Department of Neurology, University of Debrecen, Debrecen, Hungary; [7]University of Kentucky, Lexington, KY; [8]Munich Cluster for Systems Neurology (SyNergy), Munich, Germany.

Correspondence to Arthur Liesz: arthur.liesz@med.uni-muenchen.de.

therapeutic approaches in animal models in the design of the treatment regimen and investigated outcome parameters, with the exception of analyzing different time points after stroke: Clinical trials analyzed the chronic phase after stroke as the primary endpoint in contrast to preclinical studies, where only the acute phase was studied. Therefore, we took a reverse translational approach and tested whether the design of the clinical trials—analyzing chronic stroke outcome between patient groups with similar baseline characteristics after stroke—would have been efficacious in the murine experimental stroke model. Confirming a lack of efficacy on chronic post-stroke recovery also in animal models further prompted us to study the potentially underlying mechanisms of the diverging effects in acute versus chronic phases after stroke.

Results and discussion

Natalizumab treatment does not improve post-stroke recovery and neuronal plasticity

To model the clinical study design of Natalizumab treatment for stroke from the two clinical trials in an animal model, we used a photothrombotic stroke (PT) model resulting in equal lesion volumes and behavioral deficits in both treatment groups at the acute phase, corresponding to the equal characteristics of the study populations with Natalizumab or control treatment in the clinical trials. Mice of mixed sex then received anti-CD49d or an isotype control antibody i.p. 2 h after stroke, followed by injections every second week over a period of 3 mo, based on previous reports and the pharmacokinetic analyses of cellular anti-CD49d saturation (Fig. S1, A–D). We used a panel of in vivo imaging techniques for cortical plasticity, behavior tests, the assessment of lesion size and synaptic plasticity, which were proven to sensitively detect therapeutic effects on chronic post-stroke recovery (Cramer et al., 2019b; Cserép et al., 2020; Sadler et al., 2020). Anti-CD49d treatment did not improve long-term lesion involution based on in vivo widefield imaging (Fig. 1, A and B; and Fig. S1 D) and also had no effect on histologically quantified lesion volumes after PT as well as in an independent stroke model of distal middle cerebral artery occlusion (dMCAo) used in the majority of previous reports on the effects in the acute post-stroke phase (Fig. 1 C and Fig. S1 E). Moreover, recovery of behavior deficits using a well-established multiparameter neuroscore (Llovera et al., 2015) and cylinder test (Llovera et al., 2014) also did not differ between treatment groups throughout the observation period of 3 mo after stroke (Fig. 1 D). Additionally, we examined functional neuronal connectivity using in vivo widefield calcium imaging. We observed equal network disturbances in pairwise comparisons of functional cortical areas in both treatment groups after stroke (Fig. 1 E). Moreover, we did not detect anti-CD49d-associated improvement in neuronal network connectivity after stroke neither within the ischemic hemisphere nor across homotopic areas of both brain hemispheres (Fig. 1 F). Correspondingly, quantification of synaptic spine density as a marker of synaptic plasticity at 3 mo after stroke did not reveal a difference between treatment groups, which were both returned to baseline levels (naive). These results clearly indicate a lack of efficacy for anti-CD49d to improve functional recovery in the chronic post-stroke phase in two preclinical stroke models, which is comparable to the outcome of the clinical trials testing the efficacy of Natalizumab in stroke patients (Elkind et al., 2020; Elkins et al., 2017; Liesz et al., 2011; Llovera et al., 2015).

Anti-CD49d only transiently reduces cerebral lymphocyte counts after stroke

Therefore, we next aimed to analyze the biological efficacy of anti-CD49d treatment in reducing long-term lymphocyte invasion to the injured brain, which could not be studied in the clinical trials. To this end, we performed quantitative flow cytometric analyses at acute and chronic time points after stroke. Corresponding to previous studies by us and others, anti-CD49d significantly decreased cerebral lymphocyte invasion at the acute phase in male and female animals (Fig. 2 A and Fig. S3 A). In contrast, no difference in cerebral leukocyte count was detectable between treatment groups at 1 mo after stroke for any of the T cell subtypes, which we quantified in a multidimensional flow cytometric analysis (Fig. 2, B and C). Interestingly, we found T cells among leukocyte populations to specifically accumulate in the chronic phase after stroke (Fig. S2). Next, we performed immunofluorescence labeling of $CD3^+$ T cells to analyze the spatial distribution of T cells after stroke. Consistent with our flow cytometric results and a previous report (Doyle et al., 2015), we found dense T cell accumulation within the chronic lesion but did not detect a difference in intralesional T cell density between control or anti-CD49d–treated groups at 28 d after stroke (Fig. 2 D). We analyzed the spatial clustering of T cells by calculating the Clark–Evans agglomeration index (R index), which indicates cell clustering for an $R < 1$ (Fig. 2 E). Interestingly, the R index ranged between 0.3 and 0.7 for both acute (day 7) as well as for chronic (day 28) time points, regardless of treatment groups. Additionally, chronic T cell accumulation and their local clustering was confirmed in the dMCAo stroke model for both treatment groups (Fig. S3 B). Thus, the chronic accumulation of T cells in the post-ischemic brain associates with local clustering of T cells likely due to local, intracerebral proliferation. This finding could potentially explain the difference in treatment efficacy of anti-CD49d between the acute stroke outcome (with transiently reduced cerebral T cell invasion) and long-term recovery. Taken together, our approach to monitor the treatment efficacy of anti-CD49d for chronic recovery in two independent stroke models could have predicted the inefficacy of Natalizumab in clinical stroke trials. Moreover, this first-ever analysis of long-term effects of anti-CD49d treatment on the cerebral lymphocyte pool provides a mechanistic rationale for the futile treatment effects in the chronic post-stroke phase.

T cells proliferate intracerebrally after stroke

We next aimed to distinguish chronic recruitment versus local proliferation as the potential cause of the chronic lymphocyte accumulation in the post-stroke brain. Therefore, we administered 5-ethynyl-2′-deoxyuridine (EdU), a thymidine analogue labeling proliferating cells, in the drinking water over a 7-d time period, starting either the day of surgery (days 0–7) or 3 wk later

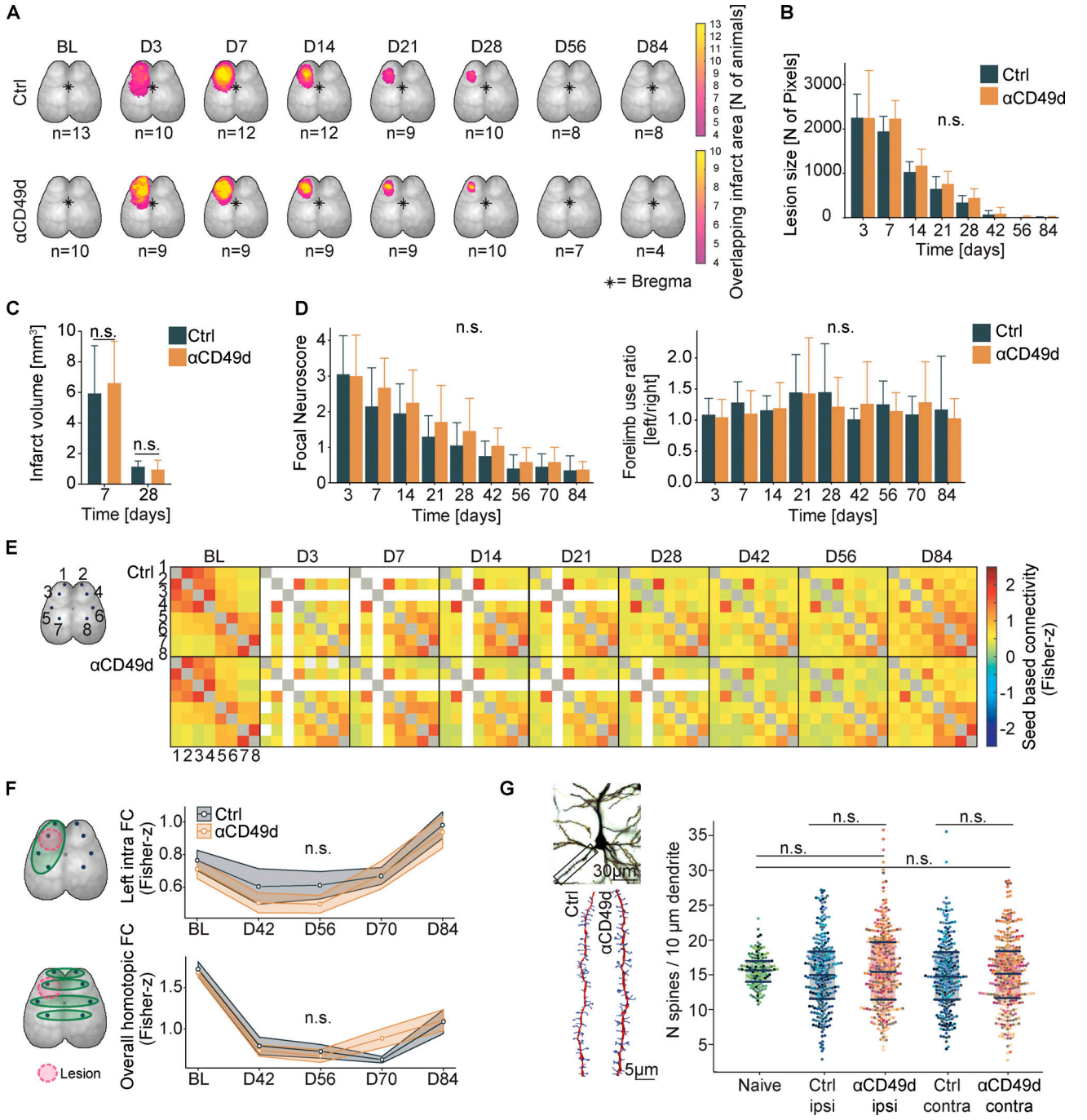

Figure 1. **Longitudinal evaluation of post-stroke recovery in mice receiving anti-CD49d treatment. (A)** The lesion area based on autofluorescence after stroke of individual animals was superimposed to depict the lesion throughout the observation period of 84 d in Thy1-GCaMP6s animals. The color code indicates the sum of overlapping lesion pixels of individual mice per acquisition time point. Data were generated in two independent experiments. BL, baseline; D, day. **(B)** Quantification of the number of autofluorescent pixels seen in calcium imaging of Thy1-GCaMP6s animals. Control (Ctrl): n = 10, anti-CD49d: n = 13, P = 0.716. Data are shown as mean ± SD, linear-mixed-models, group-by-time interaction. Data were generated in two independent experiments. **(C)** The lesion volume was quantified at 7 and 28 d after stroke and shows no difference between treatment groups. Control 7 d: n = 6, control 28 d: n = 11, anti-CD49d 7 d: n = 5, anti-CD49d 28 d: n = 8, all WT animals. Data are shown as mean ± SD. Ordinary one-way ANOVA + Tukey's post-hoc test. Data were generated in at least three independent experiments per time point. **(D)** Evaluation of the multi-parameter neuroscore and cylinder test shows no difference between treatment groups. Control: n = 10, anti-CD49d: n = 13, P (neuroscore) = 0.560, P (cylinder) = 0.691. Data are shown as median ± SE, linear-mixed models, group-by-time interaction. Data were generated in two independent experiments in Thy1-GCaMP6s animals. **(E)** Illustrative pixelmaps show the group-wise averaged seed-based FC between eight seeds representing functional cortical areas over an observation period of 84 d after stroke by longitudinal in vivo calcium imaging: 1, left rostral forelimb; 2, right rostral forelimb; 3, left caudal forelimb; 4, right caudal forelimb; 5, left forelimb sensory area; 6, right forelimb sensory area; 7, left hindlimb sensory area; 8, right hindlimb sensory area.. Gray squares indicate excluded seed autocorrelation, and white squares indicate excluded seeds due to the stroke lesion, when excluded in more than three animals. Data are shown as Fisher z-transformed connectivity scores and were generated in two independent experiments in Thy1-GCaMP6s animals. **(F)** Schematic illustration for longitudinal in vivo widefield calcium imaging acquisition; left intrahemispheric and whole cortex homotopic FC

of the eight previously defined functional areas. Time course of left intrahemispheric FC (intra FC; P = 0.127) and overall homotopic FC (P = 0.295). Data are shown as median ± SE, linear-mixed models, group-by-time interaction. Data were generated in two independent experiments in Thy1-GCaMP6s animals. **(G)** Representative images of a Golgi-Cox–stained pyramidal neuron layer II/III in a naive animal (scale bar = 30 µm) and 3D reconstruction of pyramidal neuron dendrites (red) with dendritic spines (blue, scale bar = 5 µm). Dendritic spines were quantified in layer II/III in naive (untreated) animals and 84 d after stroke in stroke ipsi- and contralateral hemispheres. Naive: *n* = 5, control: *n* = 10, anti-CD49d: *n* = 13. Data are shown as median ± interquartile range. Wilcoxon rank-sum test with continuity correction and Bonferroni correction for multiple comparisons were used. Data were generated in at least two independent experiments. All data in this figure were obtained in a mixed-sex cohort (anti-CD49d: four male, nine female; control: three male, seven female), except for C (only male mice).

(days 21–28). Then, the rate of proliferating T cells was determined in blood, spleen, and the ischemic brain hemisphere after acute (day 7) or chronic (day 28) EdU labeling in untreated mice (Fig. 3 A). As expected for the acute inflammatory response, we observed an increase in the proliferation rate (percentage of EdU^+ cells) for cerebral T cells in comparison to splenic and blood T cells at 7 d after stroke. Surprisingly, the proliferation rate in the chronic phase was still significantly (more than twofold) increased for the cerebral T cell population compared with peripheral organs. In contrast, using systemic antibody labeling of circulating T cells over 3 d (days 25–28), we detected only a small number of T cells still de novo–invading the brain in the chronic phase after stroke (Fig. S3 C). To additionally confirm the local proliferation of cerebral T cells, we analyzed histologically the expression of the direct proliferation marker Ki67 to quantify the percentage of proliferating T cells within the chronic stroke lesion (Fig. 3 B). We found independent of the treatment group a substantial number of >5% $Ki67^+$ T cells, confirming the local intralesional proliferation of T cells 28 d after PT (Fig. 3 C), which was also confirmed in the dMCAo stroke model with comparable findings (Fig. S3 D). These results suggest that—regardless of anti-CD49d treatment—sustained and local proliferation of T cells in the post-stroke brain drives chronic cerebral T cell accumulation after stroke.

Evidence for chronic T cell accumulation in human brain autopsy samples

To verify chronic T cell accumulation after stroke in brains of human stroke patients, we obtained 10 individual samples from two brain banks (Lexington and Debrecen) of six individual stroke patients dying during the acute and chronic phase after confirmed cerebral ischemia and excluding other brain disorders or immunological or inflammatory diseases (Table S1). The area covering the ischemic lesion within the samples was identified based on H&E staining for quantitative analyses. Using immunohistochemical staining, we detected $CD3^+$ T cells in all 10 human brain samples (Fig. 3 D). The number of detected T cells ranged from ∼300 to >9,000 cells/cm^2 of tissue section, with an average of 80% located within the lesion area. Additionally, the spatial distribution of T cells within the stroke lesions was determined and showed strong local clustering, with an R index ranging from 0.28 to 0.55 (Fig. 3 E). A Spearman correlation analysis for T cell density and time since stroke revealed a highly significant positive association. These results clearly demonstrate that T cells accumulate chronically and cluster locally in the ischemic lesion of human stroke patients. We additionally performed immunofluorescence staining for $CD3^+$ T cells and Ki67 in the most chronically collected patient sample (124 d after stroke) and detected double-positive cells (Fig. 3 F), confirming that the phenomenon of local, intracerebral proliferation of T cells in the chronic phase after stroke also applies to human stroke patients.

Taken together, we describe here chronic T cell accumulation most likely due to local proliferation after ischemic stroke in mice and human brains, constituting a previously unrecognized potential confounder for immunotherapeutic studies after ischemic stroke. None of the current pharmacological approaches block completely the cerebral invasion of T cells after stroke (in contrast to experimental T cell–depletion approaches; Liesz et al., 2009; Liesz et al., 2011) but rather reduce numbers of invading T cells by various degrees (Liesz et al., 2011; Llovera et al., 2015). Therefore, despite the therapeutic intervention, some T cells invade the ischemic brain. Once in the cerebral microenvironment, T cells might become autonomous from the peripheral immune system and establish a tissue-resident population by local proliferation. Here, we confirm chronic T cell accumulation and local proliferation in two independent experimental stroke models (PT and dMCAo). However, further mechanistic studies will be required to explore the biological function and therapeutic implications of this unexpected phenomenon.

For this study, we mainly used the PT model, which induces a pronounced cellular neuroinflammatory response and allows for sensitive analysis of neuromodulatory effects in the chronic recovery phase after stroke (Cotrina et al., 2017; Sadler et al., 2020). Key findings on lesion volume, T cell accumulation, and proliferation have additionally been confirmed in a widely used dMCAo model with similar findings in male and female animals. However, considering previous reports on model differences concerning the extent and dynamics of the neuroinflammatory response to stroke, future clinical trials need to consider not only potentially unexpected long-term effects, as reported in this study, but also potentially drastic differences in the role of neuroinflammation between stroke subtypes regarding lesion location, size, and etiology (Cotrina et al., 2017; Cramer et al., 2019a; Zhou et al., 2013).

As such, our findings have high clinical relevance for many ongoing or planned immunotherapeutic trials in stroke that target circulating lymphocytes, their endothelial adhesion, or cerebral invasion. According to the ClinicalTrials.gov registry of clinical intervention trials, more than 40 trials are exploring such strategies with pending outcome as of March 2021. The therapeutic approaches in these studies cover a broad range of potential therapies, including (autologous) cell therapies, polarization of T cell responses, or modulating lymphocyte migration. Several of these studies use repurposing of drugs that

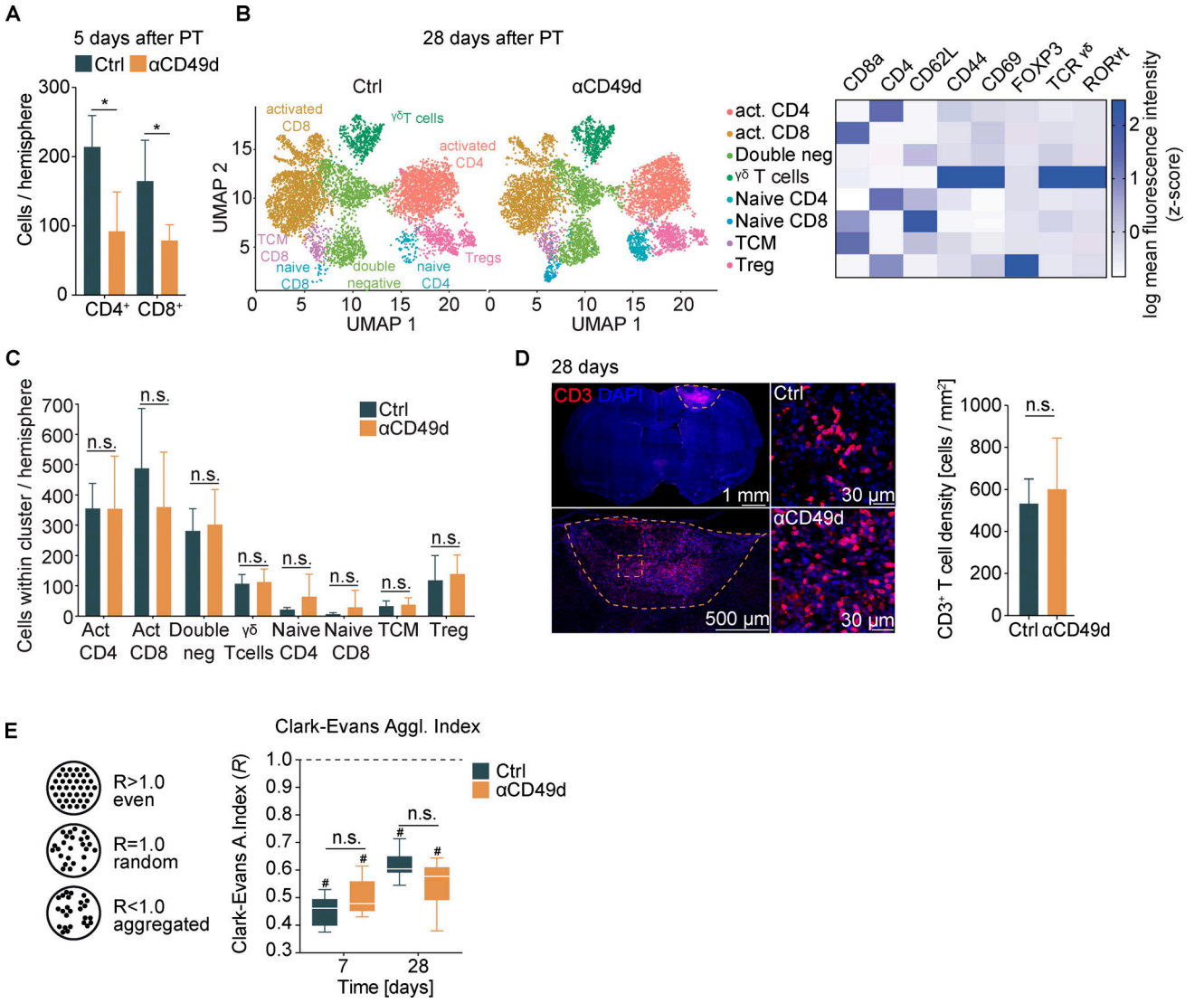

Figure 2. **T cells chronically accumulate in the post-ischemic brain independent of anti-CD49d treatment. (A)** Flow cytometric quantification of CD4⁺ T helper cells and CD8⁺ cytotoxic T cells per ipsilateral stroke hemisphere at 5 d after stroke. *n* = 5 per group. Data are shown as mean ± SD, unpaired *t* test with Holm–Sidak's post-hoc test. Data were generated in two independent experiments in WT animals. **(B)** Quantification of T cell subtypes by multidimensional flow cytometry 28 d after stroke from the ipsilateral stroke hemisphere was achieved by dimensionality reduction using UMAP (Uniform Manifold Approximation and Projection). The individual clusters were identified as CD3⁺ T cell subtypes by the MFI of CD8a, CD4, CD62L, CD44, CD69, Foxp3, γδ TCR, and RORγt, as shown in the heatmap on the right, including activated (act.) CD4⁺ T helper cells (CD4⁺CD69⁺CD62L⁻), activated CD8⁺ cytotoxic T cells (CD8⁺CD69⁺CD62L⁻ RORγt⁺), double-negative T cells (CD4⁻CD8⁻), γδ T cells (TCRγδ⁺CD44⁺CD69⁺), naive CD4⁺ T helper cells (CD4⁺CD69⁻CD62L⁺), naive CD8⁺ cytotoxic T cells (CD8⁺CD69⁻CD62L⁺), central memory T cells (TCM; CD8⁺CD69⁻CD62L⁺CD44⁺), and regulatory T cells (Treg; CD4⁺FOXP3⁺). **(C)** Quantification of numbers of T cell subtypes per cluster in the ipsilateral stroke hemisphere shown in B. Control: *n* = 5, anti-CD49d: *n* = 7. Data are shown as mean ± SD; unpaired *t* test and Holm–Sidak post-hoc test. The data were generated in three independent experiments in WT animals. **(D)** Representative immunofluorescence images of CD3⁺ T cells in the brain 28 d after stroke of the whole section with demarcation of the lesion (upper left, scale bar = 1 mm), the lesion area (lower left, scale bar = 500 µm), and an area within the lesion from control and anti-CD49d animals (right, scale bars = 30 µm). The T cell density within the lesion (cells per square millimeter) showed no difference between groups. Control: *n* = 11, anti-CD49d: *n* = 8. Data are shown as mean ± SD; unpaired *t* test. The data were generated in at least three independent experiments in WT animals. **(E)** Schematic representation of the R index for describing cell clustering (left) and the R index for CD3⁺ T cells within the lesion at 7 and 28 d after stroke for both treatment groups (right). Control 7 d: *n* = 6, control 28 d: *n* = 11, anti-CD49d 7 d: *n* = 5, anti-CD49d 28 d: *n* = 8. Data are shown as median ± interquartile range. *, P < 0.05; #, P (clustered [R < 1]) <0.0001; ordinary one-way ANOVA + Tukey's post-hoc test. Data were generated in at least three independent experiments per time point in WT animals.

have been established and approved for multiple sclerosis, a disease that not only differs drastically in its pathogenesis but also has distinct neuroimmunological features. However, the differences between acute ischemic lesions and chronic autoimmune brain disorders have not yet been fully characterized and may pose a threat to the success of immunotherapeutic stroke trials.

In light of these findings, current clinical trials targeting lymphocyte migration or brain recruitment (lymphocyte-depleting antibodies, fingolimod, and cell therapy approaches)

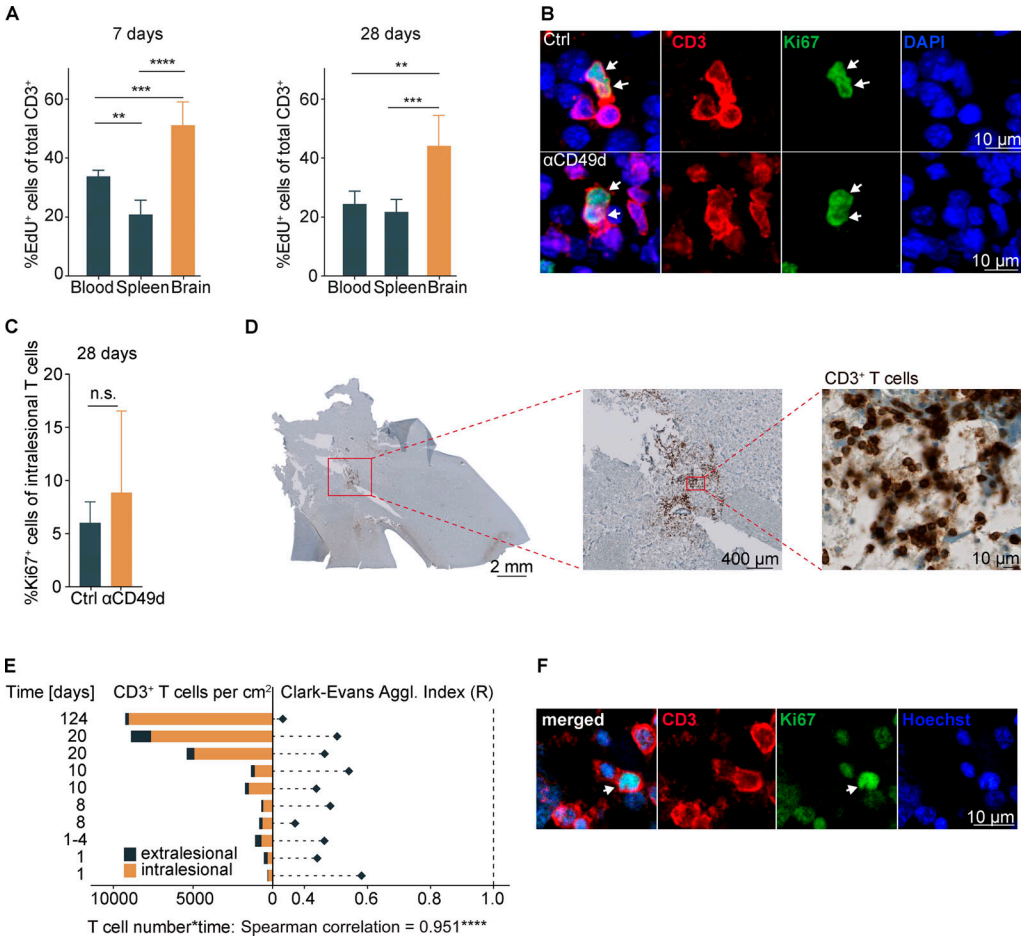

Figure 3. **T cells chronically proliferate in the postischemic brain in mice and stroke patients. (A)** The percentage of EdU+ T cells was quantified by flow cytometry in the spleen, blood, and ipsilateral stroke hemisphere at day 7 and day 28 after stroke (n = 5 per group). Data are shown as mean ± SD; ordinary one-way ANOVA and Tukey's post-hoc test. Two independent experiments per time point were performed in WT animals. **(B)** Representative images show immunofluorescence staining for CD3 and Ki67 within the lesion area for the detection of intracerebral T cell proliferation 28 d after stroke in both treatment groups (upper row, control; lower row, anti-CD49d). Arrows point to CD3 and Ki67 double-positive T cells. Scale bars = 10 µm. **(C)** Quantification of the percentage of Ki67+ T cells from (B) within the lesion 28 d after stroke showed no difference between the treatment groups. control: n = 11, anti-CD49d: n = 8. Data are shown as mean ± SD. Unpaired t test. The data were generated in at least three independent experiments in WT animals. **(D)** Representative images are shown for CD3+ DAB staining on consecutive brain sections from a human sample (124 d since stroke onset). Higher magnification images are shown from respective indicated areas. Scale bars: left, 1 mm; middle, 400 µm; right, 10 µm. **(E)** Cell density (cells/square centimeter) of intra- and extralesional CD3 T cells and cell clustering by R index were quantified. P (clustered [R < 1] <0.0001) for all analyzed samples. Correlation analysis (Spearman) between T cell density and time since stroke onset per sample. **(F)** Representative images of immunofluorescence staining for CD3 and Ki67 within the previously histopathologically identified lesion area are shown for the patient samples with the highest detected T cell count (124 d since stroke onset). Arrows point to CD3 and Ki67 double-positive T cells. Scale bar = 10 µm. **, P < 0.01; ***, P < 0.001; ****, P < 0.0001.

need to be fundamentally reconsidered. Mechanisms of chronic neuroinflammation after stroke and the consequences for post-stroke recovery need to be better understood for the rationale design of efficient immunotherapies in stroke.

Materials and methods

Animals

All experiments in this study were conducted in accordance with the national guidelines for animal experiments and approved by the German governmental committees (Regierungpraesidium Oberbayern, Munich, Germany). For flow cytometric and immunohistochemical analyses, the animals were 8–12-wk-old male or female C57BL/6J mice (Charles River Laboratories). For in vivo widefield calcium imaging and dendritic Golgi spine analysis, the animals were 12–15-wk-old male and female C57BL/6J-Tg(Thy1-GCaMP6s)GP4.12Dkim/J (here termed Thy1-GCaMP6s; Dana et al., 2014) heterozygous mice bred at the Institute for Stroke and Dementia Research, Munich (>12 generations back-crossed on C57Bl6/J WT mice). The animals were housed under controlled temperature (22 ± 2°C) with a 12-h light/dark cycle and access to food and water ad libitum. All animal experiments were performed and reported in accordance with the ARRIVE guidelines (Kilkenny et al., 2010).

Stroke surgery

For PT induction, mice were anaesthetized with isoflurane, delivered in a mixture of 30% O_2 and 70% N_2O. Mice were placed

into a stereotactic frame, and body temperature was maintained at 37°C with a mouse warming pad. Dexpanthenol eye ointment was applied to both eyes. Animals received 10 µl/g body weight of 1% Rose Bengal (198250-5g; Sigma-Aldrich) in saline i.p. 5 min before the induction of anesthesia (5% isoflurane). A skin incision was used to expose the skull. Bregma was located, and the lesion location was marked in the left hemisphere (1.5 mm lateral and 1.0 mm rostral to bregma). For in vivo widefield calcium imaging experiments, PT was induced as previously described (Cramer et al., 2019b). In brief, an independent vector analysis was performed based on baseline resting-state imaging, which allowed us to define cortical functional regions as independent components. The independent component in the primary motor cortex was then used to individually define the lesion location for every mouse. Shielding was placed on the skull, allowing a 2.0-mm-diameter circular light exposure over the lesion area. 10 min after Rose Bengal injection, the laser (25 mV output) was applied to the lesion area for 17 min (Cobolt Jive 50, 561 nm power at 25 mV; Fiber Collimation Package: 543 nm, f = 7.66 mm, beam diameter [d] ≈ (4)(0.000561 mm)[7.86 mm/(pi × 0.004 mm)] = 1.4 mm). The sham procedure was performed as described previously but without laser illumination.

dMCAo was performed as previously described (Llovera et al., 2014). Briefly, the mouse was positioned on its side and skin was incised between the ear and the eye. After, the temporal muscle was detached from the bone and a craniotomy was performed on top of the middle cerebral artery. The vessel was permanently coagulated, proximal and distal to the MCA bifurcation, with electrocoagulation forceps. Finally, the muscle was placed back and the wound sutured.

Anti-CD49d antibody treatment

Animals were treated with 300 µg anti-CD49d (clone PS/2, catalog no. BE0071; Bio X Cell) or isotype control (LTF-2, catalog no. BE0090; Bio X Cell) in 0.01 M PBS 2 h after PT induction, followed by injection every second week until termination of the experiment. The treatment groups were assigned after randomization, and experimenters were blinded to group assignment.

Neuroscore

The multiparametric neuroscore was assessed as previously described (Orsini et al., 2012). Briefly, the score is composed of the assessment of several subtests of both global and focal deficits. Assessment of global deficits included grooming, status of ears and eyes, posture, spontaneous activity, and epileptic behavior. Focal deficits were evaluated by gait, grip, forelimb asymmetry during tail suspension, circling behavior of the entire body or only a forelimb, body symmetry, and whisker response. Total score ranges from 0 to 54 points (26 points for general and 28 for focal deficits), with a higher score indicating worse deficits. Data were acquired once before stroke and on days 3, 7, 14, 21, 28, 42, 56, 70, and 84 after stroke.

Cylinder test

The cylinder test was assessed as previously described (Llovera et al., 2014). Briefly, the animals were placed in a transparent acrylic glass cylinder (diameter, 8 cm; height, 25 cm) in front of two mirrors, and video was recorded for 10 min. The frequency of forelimb use during a full rear and landing with only one forelimb was counted. At least 20 contacts for one forelimb were counted using slow-motion or frame-by-frame function. The ratio was calculated as the total number of left forelimb contacts divided by the total number of right forelimb contacts with the cylinder wall.

Flow cytometry

Mice were deeply anesthetized and perfused with 20 ml saline. Both brain and spleen were dissected, and blood was collected in EDTA tubes after cardiac puncture. For brain, both hemispheres were carefully removed, and cells were isolated by mechanical dissociation. Cell preparation and staining were performed as previously described (Llovera et al., 2017). Mononuclear cells were enriched using discontinuous Percoll gradients. Cell stainings were performed using the following antibodies: CD45-eF450 (1:250, 48–0451-82, clone: 30-F11; Invitrogen), CD3-FITC (1:250, 11–0032-82, clone: 17A2; Invitrogen), CD8-PE (1:250, 12–0081-82, clone: 53–6.7; Invitrogen), CD4-PerCP-Cy5 (1:250, 45–0042-82, clone: RM4-5; Invitrogen), TCRyd-APC (1:250, 118116, clone: GL3; BioLegend), NK1.1-PE-Cy7 (1:250, 25–5941-82, clone: PK136; Invitrogen), CD19-APC-Cy7 (1:250, 47–0193-82, clone: eBio1D3; Invitrogen), CD11b-PerCP-Cy5 (1:250, 45–0112-82, clone: M1/70; Invitrogen), MHCII-PE (1:250, 12–5322-81, clone: NIMR-4; eBioscience), Ly6C-APC (1:500, 17–5932-82, clone: HK1.4; eBioscience), Ly6G-PE-Cy7 (1:333, 25–5931-82, clone: RB6-8C5; eBioscience), and CD11c-APC-Cy7 (1:250, 117324, clone: N418; BioLegend). Stained cells were analyzed on a BD FACSVerse flow cytometer (BD Biosciences), and analysis was performed using FlowJo software (version 10.0).

For high-dimensional flow cytometry (Fig. 2, B and C), mice were injected i.v. with 3 µg CD45-APC-Cy7 (103116, clone: 30-F11; BioLegend), 3 min before transcardiac perfusion, to exclude blood contamination. Mononuclear cells were then isolated as described above. The samples were stained first with Zombie NIR Fixable Viability Kit (1:200; BioLegend) and surface markers, diluted in Brilliant Stain Buffer (BD Biosciences). The following antibodies were used: CXCR3-BV421 (1:100, 126522, clone: CXCR3-127; BioLegend), CD27-SB436 (1:100, 62–0271-82, clone: LG.7F9; eBioscience), CD69-BV480 (1:50, 746813, clone: H1.2F3; BD Biosciences), CD19-BV570 (1:200, 115535, clone: 6D5; BioLegend), CD11b-BV570 (1:200, 101233, clone: M1/70; BioLegend), PD-1-BV605 (1:100, 563059, clone: J43; BD Biosciences), CD62L-BV650 (1:100, 564108, clone MEL-14; BD Biosciences), TCR-γδ-BV750 (1:100, 746962, clone: GL3; BD Biosciences), CCR7-BV785 (1:100, 120127, clone: 4B12; BioLegend), CD44-AF532 (1:200, 58–0441-82, clone: IM7; eBioscience), CD127-PE-CF594 (1:100, 562419, clone: SB/199; BD Biosciences), NK1.1-AF700 (1:100, 56–5941-82, clone: PK136; eBioscience), CD8a-BV510 (1:200, 563068, clone: 53-6.7; BD Biosciences), CD3-FITC (1:200, 11–0032-82, clone: 17A2; eBioscience), KLRG1-PE (1:200, 138408, clone: 2F1/KLRG1; BioLegend), CD103-PE-Cy7 (1:200, 121426, clone: 2E7; BioLegend), CD4-PerCP-Cy5.5 (1:200, 45–0042-82, clone: RM4-5; eBioscience). For intracellular staining, Foxp3 / Transcription Factor Staining Buffer Set was used following the provider guidelines. The following antibodies

for intracellular staining were used: FoxP3-AF647 (1:100, 126408, clone: MF-14; BioLegend), T-bet-BV711 (1:100, 644820, clone: 4B10; BioLegend), ROR-γt-APC (1:100, 17–6981-82, clone B2D; eBioscience). Stained cells were analyzed on a Norther Light spectral flow cytometer (Cytek) and analysis performed by FlowJo software (version 10.0).

In vivo proliferation analysis

For analysis of in vivo cell proliferation, mice were treated with EdU (0.5 mg/ml; Invitrogen) in sucrose-enriched drinking water (5 g sucrose in 100 ml) for 7 d before saline perfusion. EdU was detected using a Click-iT EdU Alexa Fluor 647 Flow Cytometry Assay Kit (C10419; Invitrogen) following the manufacturer's instructions. Subsequently, FACS antibody staining was performed as described above using the following cell surface antibodies: CD11b-PE-Cy7 (1:250, 25–0112-82, clone: M1/70; Invitrogen), CD45-BV510 (1:250, 563891, clone: 30-F11; BD Biosciences), CD3-FITC (1:250, 11–0032-82, clone: 17A2; Invitrogen), CD19-eF450 (1:250, 48–0193-82, clone: eBio1D3; eBioscience), CD4-PerCP-Cy5.5 (1:250, 45–0042-82, clone: RM4-5; Invitrogen), and CD8-PE (1:250, Invitrogen, 12–0081-82, clone: 53–6.7). Stained cells were then analyzed on a BD FACSVerse flow cytometer (BD Biosciences), and analysis was performed using FlowJo software (version 10.0).

Pharmacokinetic analysis

To determine cellular anti-CD49d saturation levels, venous blood was collected in EDTA tubes after cardiac puncture, and mononuclear cells were enriched using a Histopaque-1077 gradient (Sigma-Aldrich). Cells were diluted to a concentration of 10^6 cells/ml and stained with a mouse anti-Rat IgG2b PE-conjugated secondary antibody (1:20, clone R2B-7C3; eBioscience) to detect cell-bound anti-CD49d for 30 min at 4°C. For determination of anti-CD49d saturation, cells were incubated with a saturating amount of anti-CD49d (10 µg/ml) for 30 min at room temperature and subsequently stained with the antibody as described above. Stained cells were then analyzed on a BD FACSVerse flow cytometer (BD Biosciences), and analysis was performed using FlowJo software (version 10.0). The anti-CD49d saturation level was then calculated as percentage of the mean fluorescence intensity (MFI) from in vivo bound anti-CD49d from the MFI of in vitro saturated cells by the following equation:

$$\text{anti} - \text{CD49d saturation} = \frac{\text{MFI in vivo } \textit{bound anti} - \textit{CD49d}}{\text{MFI in vitro saturated anti} - \text{CD49d}} \times 100.$$

The number of anti-CD49d molecules per cell was determined using a PE fluorescence quantitation kit (BD Quantibrite PE, #340495; BD Biosciences) following the manufacturer's instructions.

Mouse anti-rat IgG ELISA

To analyze neutralizing mouse anti-rat IgG antibodies in mice, we used a customized modification of a commercial ELISA (#88-50400; Thermo Fisher Scientific). Flat-bottom 96-well ELISA plates were coated overnight with the same rat anti-CD49d antibody (100 ng/ml) at 4°C as used for the in vivo treatment (clone PS/2, Cat. BE0071; Bio X Cell). After washing, the antibody-coated plates were incubated for 1 h at room temperature with mouse plasma obtained 28 d after stroke (i.e., two doses of anti-CD49d at 2 h and 14 d) or control plasma from a naive mouse that had been spiked at ∼10 ng/ml with the capture antibody of the ELISA kit. Subsequent detection and biochemiluminescent analysis using a microplate reader (Bio-Rad) was performed following the manufacturer's instructions.

Dendritic spine analysis

Following saline perfusion, mice were perfused 84 d after PT with aldehyde fixative solution (003780; Bioenno). Brains were then carefully removed and placed in fixative solution at 4°C overnight. Brains were then sliced at 100 µm using a vibratome and collected in 0.1 M PBS. Slices were placed in impregnation slice Golgi Kit (003760; Bioenno) solution for 5 d in the dark. Staining and post-staining was performed as described by the manufacturer (Bioenno). Images of dendrites were obtained within 500 µm around the lesion area in cortical layer 2/3. In total, 25 dendrites per animal (5 dendrites from 5 neurons) in both hemispheres were recorded using an Axio Imager.M2 and a 100× objective (EC Plan-Neofluar, numerical aperture [NA] = 1.3, oil immersion, acquisition at 18–20°C) using the AxioCam MRc and AxioVision 4.8.2 software. Dendrites from the images were then 3D reconstructed and the spine density evaluated on the reconstructed 3D surface using Imaris x64 (8.4.0; Bitplane).

In vivo widefield neuronal calcium imaging

In vivo widefield calcium imaging was performed as previously published (Cramer et al., 2019b). Briefly, Thy1-GCaMP6s heterozygous mice were scalped and transparent dental cement was placed upon the intact skull at least 3 d before start of the experiment. Resting-state in vivo imaging was performed in mild anesthesia (0.5 mg/kg body weight of medetomidine with 0.75% isoflurane inhalation). Mice were placed in a stereotactic frame below a customized macroscopic imaging setup, and mouse cortex was illuminated with 450-nm blue LED light. Resting-state calcium activity was recorded for 4 min (6 × 1,000 frames) with a high-precision 2/3" Interline charge-coupled device camera (Adimec-1000m/D, pixel size 7.4 × 7.4 µm, acquisition at 20–22°C; Adimec) at a 25-Hz frame rate using longDaq software (Optical Imaging).

In vivo calcium imaging analysis

Functional imaging data were preprocessed as previously described (Cramer et al., 2019b). In particular, the seed-to-seed FCs between eight previously defined seeds were calculated as Pearson's correlation between the time course of each of these seeds and Fisher's z transformation. For left intrahemispheric connectivity, the mean of the Fisher's z-transformed Pearson's correlation coefficient of each connection between the seeds located in the left hemisphere was calculated. The overall homotopic connectivity was calculated as the mean of all Fisher's z-transformed Pearson's correlation coefficients of each homotopic connection between the seeds in both hemispheres. The time course of left intrahemispheric and overall homotopic

connectivity was displayed from baseline and days 42 to 84 after stroke, ensuring the visibility of all seeds after disappearance of the autofluorescent lesion. Fisher's z-transformed Pearson's correlation was calculated using MATLAB (MathWorks R2016b with Optimization Toolbox, Statistics and Machine Learning Toolbox, Signal Processing Toolbox and Image Processing Toolbox; MathWorks).

Lesion involution quantification

The lesion size was determined by autofluorescence of the ischemic tissue in Thy1-GCaMP6s animals used for in vivo widefield calcium imaging for every time point of imaging acquisition. The area of autofluorescent pixels was previously defined by thresholding and converted into a mask to exclude autofluorescent tissue from the connectivity analysis. The lesion was determined as the size of the exclusion mask by quantification of all pixels within the mask.

Lesion volumetry

Mice were transcardially perfused 28 d after PT or dMCAo stroke induction with saline and 4% paraformaldehyde solution. To protect the cortical lesion from damage, the whole skull was isolated and stored in 4% paraformaldehyde overnight at 4°C and then placed in 0.3 M EDTA for 7 d for decalcification. Subsequently, the brains were dehydrated for 2 d in 30% sucrose in 0.01 M PBS and then snap-frozen in isopentane. Cresyl Violet staining for infarct volumetry was performed as previously described (Llovera et al., 2014), and the lesion size was quantified using FIJI ImageJ.

Immunohistochemical staining of mouse coronal brain sections

Fluorescent immunohistochemical staining for $CD3^+$ and $Ki67^+$ to determine the number of proliferating T cells in control versus anti-CD49d treated animals was performed on 20-µm-thick paraformaldehyde-fixed coronal sections from mice at 7 and/or 28 d after PT or dMCAo. Sections were fixed with cold acetone for 10 min at room temperature and washed with 0.01 M PBS before blocking with goat serum blocking buffer for 1 h at room temperature. Subsequently, sections were stained overnight at 4°C with primary antibody (1:200, CD3e, hamster anti-mouse, clone 500A2; BD PharMingen; and 1:200, Ki-67, rabbit mAb, clone D3B5; Cell Signaling Technology). After washing with 0.1% Triton X-100 in 0.01 M PBS, secondary antibody staining was applied for 2 h at room temperature (1:200, goat anti-hamster, Alexa Fluor 594; Thermo Fisher Scientific; and 1:200, goat anti-rabbit, Alexa Fluor 647; Life Technologies). Nuclei were stained with DAPI (1:5,000; Invitrogen) for 5 min at room temperature.

Per animal, three images for cell quantification were recorded as 6-µm-high tile-scan Z-stacks (slice thickness, 0.4 µm) on a Zeiss confocal microscope (LSM880) with 25× objective (LCI Plan-Neofluar 25×, NA = 0.8, ImmKorr differential interference contrast, water immersion, acquisition at 18°C). The lesion was marked and measured in the tile-scan image and cells were quantified using the Cell Counter Plugin in FIJI. Cell density was calculated as number of cells per square millimeter. The R index for quantification of clustering of cells per area was calculated using the clarkevans.test R function (R package spatstat; Baddeley et al., 2005). For evaluation of clustering, the ratio of the observed average nearest-neighbor distance r (rA) to the expected pattern for a Poisson point process of the same intensity (rE): $R=\frac{rA}{rE}$. An R index of >1.0 indicates ordered spatial distribution, R = 0 indicates even distribution, and R < 1.0 indicates aggregation. Hypothesis testing was performed against the null hypothesis, which is complete spatial randomness/a uniform Poisson process. For every animal, the cell density and R index were calculated and averaged among the three acquired images. Whole-slice images were acquired using a 10× objective (EC Plan-Neofluar 10×, NA = 0.3, air immersion, acquisition at 18°C) and high-resolution images were acquired using a 40× objective (EC Plan-Neofluar 40×, NA = 1.3 oil differential interference contrast, oil immersion, acquisition at 18–20°C).

Patient characteristics for postmortem histological analyses

Ethical approval for the use of human postmortem material was granted according to institutional ethics board protocol and national regulations by the Hungarian Medical Research Council Scientific and Research Ethics Board (19312/2016/EKU) and the University of Kentucky Medical Institutional Review Board (UK IRB #44009), respectively. Clinical information was provided by the respective brain bank (Table S1).

Histological and immunohistochemical staining of human brain tissue samples

Histochemical and immunohistochemical staining was performed on sections cut to 6 µm from paraffin-embedded tissue blocks. Randomly chosen sections of every patient were deparaffinated and rehydrated and subsequently stained with H&E. Immunohistochemistry for CD3 (polyclonal rabbit anti-human CD3, diluted 1:50, A0452; Dako) was performed on sections adjacent to H&E-stained sections with the Ventana Benchmark GX automated staining system using a CC1 (Roche) pretreatment and the iView DAB Detection Kit (Roche). Sections were counterstained with hematoxylin and coverslipped with Entellan (Merck) as mounting medium. Age of infarcts was estimated by two experienced and independent neuropathologists (T. Arzberger and P.T. Nelson) on H&E sections according to published criteria (Mena et al., 2004). CD3 stains were scanned with Zeiss Axio Scan Z1 using a 20× objective. The infarct area was demarcated, and the absolute numbers and coordinates of intra- and extralesional $CD3^+$ T cells were assessed manually using Qupath (version 0.2.2). Cell density was calculated as number of cells per cm^2 of defined lesion area. The R index for quantification of cell clustering per area was calculated as described above in R (version 3.6.0). Intralesional cell density was correlated with time after stroke onset for each sample.

Immunofluorescence staining of human brain tissue samples

Immunofluorescence staining was performed on sections cut to 6 µm from paraffin-embedded tissue blocks. Randomly selected sections were deparaffinated and blocked in 3% H_2O_2. After heat-induced antigen retrieval in Tris-buffered EDTA (pH 9.0) for 30 min at 95°C, sections were blocked with 5% donkey serum for 4 h at room temperature. Then, sections were incubated in

antibody staining solution (0.3% Triton X-100 and 20 mM sodium azide containing 0.05 M Tris-buffered saline [TBS], pH 7.4) overnight at 4°C (1:50, CD3, polyclonal rabbit anti-human, reference A0452; and 1:100, Ki67, monoclonal mouse anti-human, clone MIB-1, reference M7240; Dako). After washing with 0.05 M TBS, secondary antibody staining was performed with antibody staining solution (0.3% Triton X-100 and 20 mM sodium azide containing 0.05 M TBS, pH 7.4) for 2.5 h at room temperature in the dark (1:500, donkey anti-rabbit, Alexa Fluor 594, reference 711–586-152; and 1:500, donkey anti-mouse, Alexa Fluor 488, reference 715–546-151; Jackson ImmunoResearch). For nuclear staining, Hoechst 33334 (0.02 mg/ml diluted in 0.05 M TBS, pH 7.4, reference 62249; Thermo Fisher Scientific) was applied for 30 min at room temperature. After staining, an autofluorescence eliminator reagent (reference 2160; EMD Millipore) was applied for 5 min before mounting the slides with Fluoromount-G (reference 0100–01; Southern Biotech). The images were acquired at 20× magnification (objective: Plan Apo VC 20×, NA = 0.75, working distance = 1 mm, field of view = 645.12 µm, calibration: 0.62 µm/pixel or with 5× optical zoom, calibration: 0.12 µm/pixel, acquisition at 21°C) using a Nikon Ni C2 confocal microscope.

Statistics

To assess whether the lesion involution (number of autofluorescent pixels), behavioral recovery (neuroscore and cylinder test) or FC (left intra-FC and overall homotopic FC) between anti-CD49d–treated and control-treated animals were significantly different, we performed linear-mixed models for calculating group-by-time interaction in R (version 3.6.0). To test for statistical difference in infarct volume between treatment groups, we used one-way ANOVA and Tukey's post-hoc test. Next, we assessed the difference in dendritic spine numbers between anti-CD49d–treated and control-treated animals using the Wilcoxon rank-sum test with continuity correction and Bonferroni post-hoc correction for multiple testing in R (Version 3.6.0). To test for significantly different numbers of infiltrating T cells between anti-CD49d– and control-treated animals, we used unpaired *t* tests and Holm–Sidak's correction for multiple testing. For determining significant differences in histologically quantified T cells, we used an unpaired *t* test. To assess significant differences in the R index between treatment groups at different time points, we used one-way ANOVA and Tukey's test for correction of multiple comparisons. We next quantified significant differences between the number of EdU^+ T cells in different organs using one-way ANOVA and Tukey's test for correction of multiple comparisons. To test for significant differences in the percentage of $Ki67^+$ T cells between treatment groups, we used an unpaired *t* test. We used linear regression analysis to test for a correlation between the intralesional T cell density in stroke patients and time after stroke onset. Unless otherwise mentioned all analyses were performed in GraphPad Prism (version 7.0a). For all analyses, an α level of adjusted $P < 0.05$ was considered statistically significant.

Online supplemental material

Fig. S1 provides pharmacokinetic analysis data for the rationale of the treatment regimen with anti-CD49d and additional results on infarct volumetry supporting the findings in the Fig. 1 in the PT and dMCAo stroke model. Fig. S2 provides information on the temporal dynamics of cerebral invasion on innate and adaptive immune subpopulations over 1 mo after experimental stroke. Fig. S3 shows comparable findings for chronic T cell accumulation in female mice as shown in the main figures for male mice. Additionally, this figure confirms chronic T cell accumulation and proliferation in the dMCAo stroke model. Table S1 lists patient data.

Acknowledgments

We would like to thank Kerstin Thuβ-Silczak and Christina Fürle for technical support as well as Juliet Stowe for the selection and preparation of human tissue samples from the Sanders Brown Center on Aging (supported by National Institutes of Health grant P30 AG028383).

This work was funded by the European Research Council (grant ERC-StGs 802305 to A. Liesz and grant ERC-PoC 875677 to D. Edbauer), the American Heart Association (grant 19EIA34760279 to A.M. Stowe), the Hungarian Brain Research Program (grant 2017-1.2.1-NKP-2017-00002), and the German Research Foundation under Germany's Excellence Strategy (EXC 2145 SyNergy, ID 390857198) through the collaborative research center TRR274 (project ID 408885537) and under grants LI-2534/6-1 and LI-2534/7-1. D. Edbauer received funding from the NOMIS Foundation.

Author contributions: S. Heindl conceptualized experiments, performed most of the experiments, analyzed the data, and wrote the manuscript. A. Ricci performed and analyzed experiments. O. Carofiglio, Q. Zhou, T. Arzberger, and N. Lenart performed experiments. N. Franzmeier analyzed FC data. T. Hortobagyi, P.T. Nelson, A.M. Stowe, and A. Denes selected and provided the human tissue samples. D. Edbauer provided experimental resources. A. Liesz initiated the study, conceptualized and supervised the research, and wrote the manuscript. All authors reviewed the manuscript.

Disclosures: The authors declare no competing interests exist.

Submitted: 11 November 2020
Revised: 31 March 2021
Accepted: 28 April 2021

References

Baddeley, A., E. Rubak, and R. Turner. 2005. Spatial Point Patterns: Methodology and Applications with R. Chapman and Hall/CRC Press, London.

Becker, K., D. Kindrick, J. Relton, J. Harlan, and R. Winn. 2001. Antibody to the alpha4 integrin decreases infarct size in transient focal cerebral ischemia in rats. *Stroke.* 32:206–211. https://doi.org/10.1161/01.STR.32.1.206

Chamorro, Á., A. Meisel, A.M. Planas, X. Urra, D. van de Beek, and R. Veltkamp. 2012. The immunology of acute stroke. *Nat. Rev. Neurol.* 8:401–410. https://doi.org/10.1038/nrneurol.2012.98

Cotrina, M.L., N. Lou, J. Tome-Garcia, J. Goldman, and M. Nedergaard. 2017. Direct comparison of microglial dynamics and inflammatory profile in photothrombotic and arterial occlusion evoked stroke. *Neuroscience.* 343:483–494. https://doi.org/10.1016/j.neuroscience.2016.12.012

Cramer, J.V., C. Benakis, and A. Liesz. 2019a. T cells in the post-ischemic brain: Troopers or paramedics? *J. Neuroimmunol.* 326:33–37. https://doi.org/10.1016/j.jneuroim.2018.11.006

Cramer, J.V., B. Gesierich, S. Roth, M. Dichgans, M. Düring, and A. Liesz. 2019b. In vivo widefield calcium imaging of the mouse cortex for analysis of network connectivity in health and brain disease. *Neuroimage.* 199:570–584. https://doi.org/10.1016/j.neuroimage.2019.06.014

Cserép, C., B. Pósfai, N. Lénárt, R. Fekete, Z.I. László, Z. Lele, B. Orsolits, G. Molnár, S. Heindl, A.D. Schwarcz, et al. 2020. Microglia monitor and protect neuronal function through specialized somatic purinergic junctions. *Science.* 367:528–537. https://doi.org/10.1126/science.aax6752

Dana, H., T.W. Chen, A. Hu, B.C. Shields, C. Guo, L.L. Looger, D.S. Kim, and K. Svoboda. 2014. Thy1-GCaMP6 transgenic mice for neuronal population imaging in vivo. *PLoS One.* 9:e108697. https://doi.org/10.1371/journal.pone.0108697

Doyle, K.P., L.N. Quach, M. Solé, R.C. Axtell, T.-V.V. Nguyen, G.J. Soler-Llavina, S. Jurado, J. Han, L. Steinman, F.M. Longo, et al. 2015. B-lymphocyte-mediated delayed cognitive impairment following stroke. *J. Neurosci.* 35:2133–2145. https://doi.org/10.1523/JNEUROSCI.4098-14.2015

Elkind, M.S.V., R. Veltkamp, J. Montaner, S.C. Johnston, A.B. Singhal, K. Becker, M.G. Lansberg, W. Tang, R. Kasliwal, and J. Elkins. 2020. Natalizumab in acute ischemic stroke (ACTION II): A randomized, placebo-controlled trial. *Neurology.* 95:e1091–e1104. https://doi.org/10.1212/WNL.0000000000010038

Elkins, J., R. Veltkamp, J. Montaner, S.C. Johnston, A.B. Singhal, K. Becker, M.G. Lansberg, W. Tang, I. Chang, K. Muralidharan, et al. 2017. Safety and efficacy of natalizumab in patients with acute ischaemic stroke (ACTION): a randomised, placebo-controlled, double-blind phase 2 trial. *Lancet Neurol.* 16:217–226. https://doi.org/10.1016/S1474-4422(16)30357-X

Emberson, J., K.R. Lees, P. Lyden, L. Blackwell, G. Albers, E. Bluhmki, T. Brott, G. Cohen, S. Davis, G. Donnan, et al. Stroke Thrombolysis Trialists' Collaborative Group. 2014. Effect of treatment delay, age, and stroke severity on the effects of intravenous thrombolysis with alteplase for acute ischaemic stroke: a meta-analysis of individual patient data from randomised trials. *Lancet.* 384:1929–1935. https://doi.org/10.1016/S0140-6736(14)60584-5

Endres, M., B. Engelhardt, J. Koistinaho, O. Lindvall, S. Meairs, J.P. Mohr, A. Planas, N. Rothwell, M. Schwaninger, M.E. Schwab, et al. 2008. Improving outcome after stroke: overcoming the translational roadblock. *Cerebrovasc. Dis.* 25:268–278. https://doi.org/10.1159/000118039

Fiehler, J., and C. Gerloff. 2015. Mechanical Thrombectomy in Stroke. *Dtsch. Arztebl. Int.* 112:830–836.

Hacke, W., M. Kaste, E. Bluhmki, M. Brozman, A. Dávalos, D. Guidetti, V. Larrue, K.R. Lees, Z. Medeghri, T. Machnig, et al. ECASS Investigators. 2008. Thrombolysis with alteplase 3 to 4.5 hours after acute ischemic stroke. *N. Engl. J. Med.* 359:1317–1329. https://doi.org/10.1056/NEJMoa0804656

Howells, D.W., E.S. Sena, and M.R. Macleod. 2014. Bringing rigour to translational medicine. *Nat. Rev. Neurol.* 10:37–43. https://doi.org/10.1038/nrneurol.2013.232

Iadecola, C., and J. Anrather. 2011. The immunology of stroke: from mechanisms to translation. *Nat. Med.* 17:796–808. https://doi.org/10.1038/nm.2399

Kilkenny, C., W.J. Browne, I.C. Cuthill, M. Emerson, and D.G. Altman. 2010. Improving bioscience research reporting: the ARRIVE guidelines for reporting animal research. *PLoS Biol.* 8:e1000412. https://doi.org/10.1371/journal.pbio.1000412

Langhauser, F., P. Kraft, E. Göb, J. Leinweber, M.K. Schuhmann, K. Lorenz, M. Gelderblom, S. Bittner, S.G. Meuth, H. Wiendl, et al. 2014. Blocking of α4 integrin does not protect from acute ischemic stroke in mice. *Stroke.* 45:1799–1806. https://doi.org/10.1161/STROKEAHA.114.005000

Liesz, A., E. Suri-Payer, C. Veltkamp, H. Doerr, C. Sommer, S. Rivest, T. Giese, and R. Veltkamp. 2009. Regulatory T cells are key cerebroprotective immunomodulators in acute experimental stroke. *Nat. Med.* 15:192–199. https://doi.org/10.1038/nm.1927

Liesz, A., W. Zhou, É. Mracskó, S. Karcher, H. Bauer, S. Schwarting, L. Sun, D. Bruder, S. Stegemann, A. Cerwenka, et al. 2011. Inhibition of lymphocyte trafficking shields the brain against deleterious neuroinflammation after stroke. *Brain.* 134:704–720. https://doi.org/10.1093/brain/awr008

Llovera, G., S. Roth, N. Plesnila, R. Veltkamp, and A. Liesz. 2014. Modeling stroke in mice: permanent coagulation of the distal middle cerebral artery. *J. Vis. Exp.* (89):e51729. https://doi.org/10.3791/51729

Llovera, G., K. Hofmann, S. Roth, A. Salas-Pérdomo, M. Ferrer-Ferrer, C. Perego, E.R. Zanier, U. Mamrak, A. Rex, H. Party, et al. 2015. Results of a preclinical randomized controlled multicenter trial (pRCT): Anti-CD49d treatment for acute brain ischemia. *Sci. Transl. Med.* 7:299ra121. https://doi.org/10.1126/scitranslmed.aaa9853

Llovera, G., C. Benakis, G. Enzmann, R. Cai, T. Arzberger, A. Ghasemigharagoz, X. Mao, R. Malik, I. Lazarevic, S. Liebscher, et al. 2017. The choroid plexus is a key cerebral invasion route for T cells after stroke. *Acta Neuropathol.* 134:851–868. https://doi.org/10.1007/s00401-017-1758-y

Macleod, M.R., S. Michie, I. Roberts, U. Dirnagl, I. Chalmers, J.P. Ioannidis, R. Al-Shahi Salman, A.W. Chan, and P. Glasziou. 2014. Biomedical research: increasing value, reducing waste. *Lancet.* 383:101–104. https://doi.org/10.1016/S0140-6736(13)62329-6

Macrez, R., C. Ali, O. Toutirais, B. Le Mauff, G. Defer, U. Dirnagl, and D. Vivien. 2011. Stroke and the immune system: from pathophysiology to new therapeutic strategies. *Lancet Neurol.* 10:471–480. https://doi.org/10.1016/S1474-4422(11)70066-7

Mena, H., D. Cadavid, and E.J. Rushing. 2004. Human cerebral infarct: a proposed histopathologic classification based on 137 cases. *Acta Neuropathol.* 108:524–530. https://doi.org/10.1007/s00401-004-0918-z

Moskowitz, M.A., E.H. Lo, and C. Iadecola. 2010. The science of stroke: mechanisms in search of treatments. *Neuron.* 67:181–198. https://doi.org/10.1016/j.neuron.2010.07.002

Neumann, J., M. Riek-Burchardt, J. Herz, T.R. Doeppner, R. König, H. Hütten, E. Etemire, L. Männ, A. Klingberg, T. Fischer, et al. 2015. Very-late-antigen-4 (VLA-4)-mediated brain invasion by neutrophils leads to interactions with microglia, increased ischemic injury and impaired behavior in experimental stroke. *Acta Neuropathol.* 129:259–277. https://doi.org/10.1007/s00401-014-1355-2

Orsini, F., P. Villa, S. Parrella, R. Zangari, E.R. Zanier, R. Gesuete, M. Stravalaci, S. Fumagalli, R. Ottria, J.J. Reina, et al. 2012. Targeting mannose-binding lectin confers long-lasting protection with a surprisingly wide therapeutic window in cerebral ischemia. *Circulation.* 126:1484–1494. https://doi.org/10.1161/CIRCULATIONAHA.112.103051

Relton, J.K., K.E. Sloan, E.M. Frew, E.T. Whalley, S.P. Adams, and R.R. Lobb. 2001. Inhibition of alpha4 integrin protects against transient focal cerebral ischemia in normotensive and hypertensive rats. *Stroke.* 32:199–205. https://doi.org/10.1161/01.STR.32.1.199

Sadler, R., J.V. Cramer, S. Heindl, S. Kostidis, D. Betz, K.R. Zuurbier, B.H. Northoff, M. Heijink, M.P. Goldberg, E.J. Plautz, et al. 2020. Short-Chain Fatty Acids Improve Poststroke Recovery via Immunological Mechanisms. *J. Neurosci.* 40:1162–1173. https://doi.org/10.1523/JNEUROSCI.1359-19.2019

World Health Organization. 2017. Top 10 Causes of Death. In World Health Organization. World Health Organization, Geneva.

Zhou, W., A. Liesz, H. Bauer, C. Sommer, B. Lahrmann, N. Valous, N. Grabe, and R. Veltkamp. 2013. Postischemic brain infiltration of leukocyte subpopulations differs among murine permanent and transient focal cerebral ischemia models. *Brain Pathol.* 23:34–44. https://doi.org/10.1111/j.1750-3639.2012.00614.x

Supplemental material

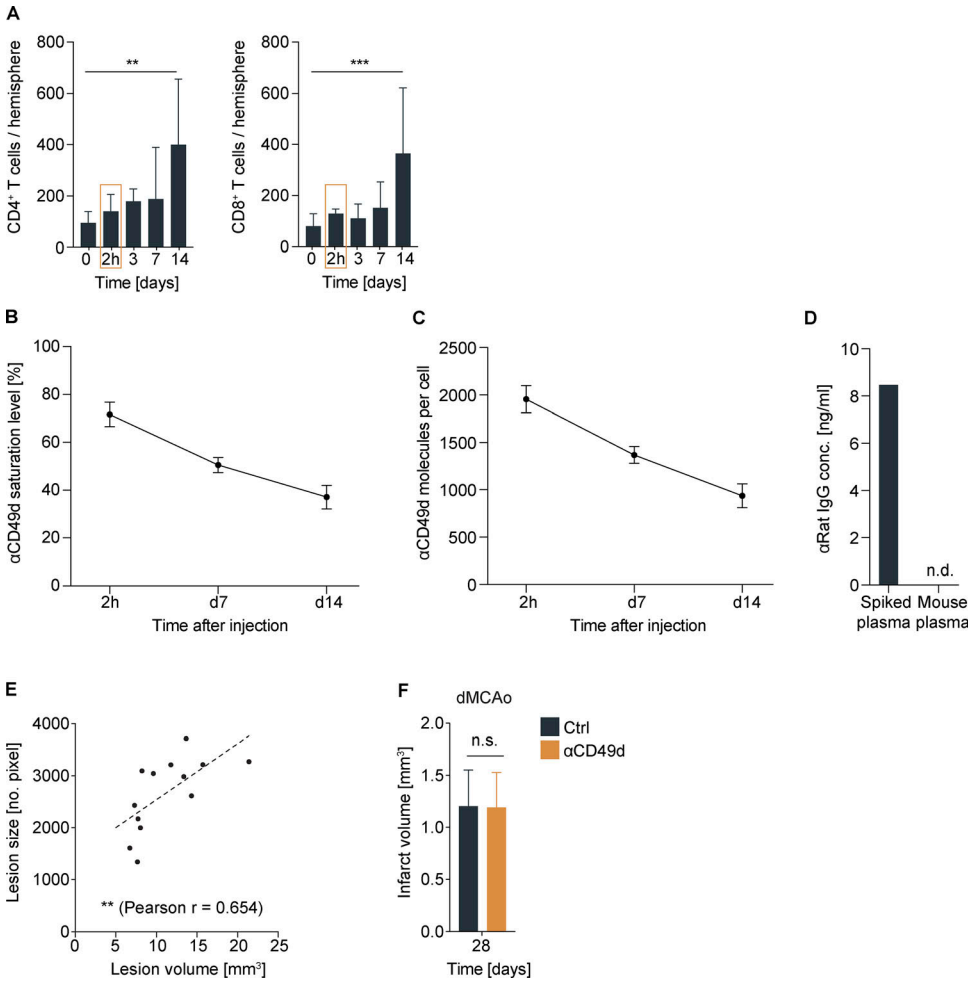

Figure S1. **Rationale for anti-CD49d treatment regimen and infarct volumetric assessment. (A)** Flow cytometric analysis of acute CD4⁺ and CD8⁺ T cell infiltration into the ipsilateral hemisphere after photothrombosis; *n* (0 = sham) = 10, *n* (2 h) = 3, n (3 d) = 6, *n* (7 d) = 6, *n* (14 d) = 5. Data are shown as mean + SD; ordinary one-way ANOVA + Dunnett's post-hoc test. At least two independent experiments were performed per time point in WT animals. **(B)** Saturation levels of anti-CD49d measured at 2 h and 7 and 14 d after i.p. injection of 300 µg anti-CD49d per animal; *n* = 3–4 per time point. Data are shown as mean + SD. Data were acquired in at least two independent experiments in WT animals. **(C)** Quantification of anti-CD49d molecules bound per cell at 2 h and 7 and 14 d after anti-CD49d treatment; *n* = 3–4 per time point. Data were acquired in at least two independent experiments in WT animals. **(D)** Mouse plasma concentration of anti-rat IgG is shown at day 28 from mice receiving two injections of 300 µg anti-CD49d at 2 h and 14 d after stroke. Naive mouse plasma was spiked with monoclonal anti-rat IgG as a positive control (spiked plasma); *n* = 3. **(E)** Correlation of lesion volume (histological analysis) and lesion size (autofluorescent pixels). Pearson correlation *n* = 13. Data were acquired in two independent experiments in Thy1GCaMP6s animals. **(F)** Infarct volume 28 d after distal middle cerebral occlusion; *n* (control) = 6, *n* (αCD49d) = 5. Data are shown as mean + SD. Unpaired *t* test. Data were acquired in three independent experiments in WT animals. **, P < 0.01; ***, P < 0.001.

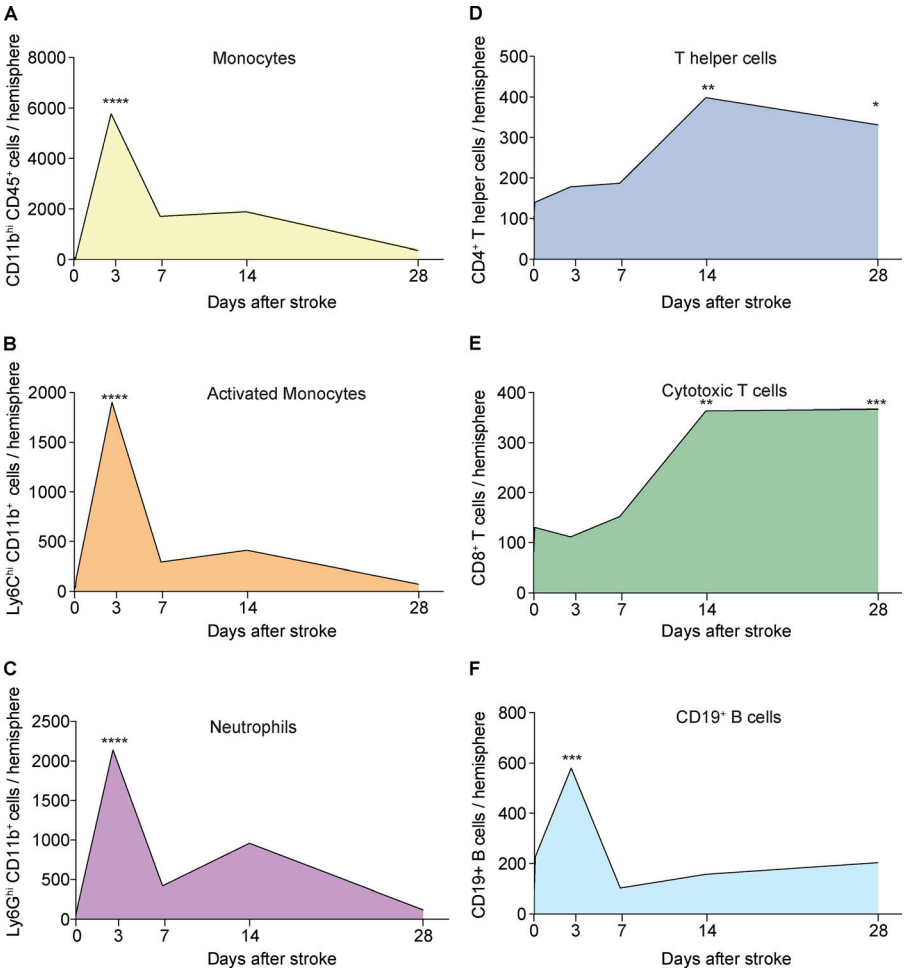

Figure S2. **Temporal dynamics of myeloid and lymphoid immune cell infiltration after stroke. (A–F)** Absolute counts of monocytes (A), activated monocytes (B), neutrophils (C), CD4$^+$ T helper cells (D), CD8$^+$ cytotoxic T cells (E), and CD19$^+$ B cells (F) were assessed using flow cytometry at 2 h and 3–28 d after stroke, as well as after sham surgery (day 0) in the ipsilateral hemisphere; *n* (sham) = 10, *n* (2 h) = 3, *n* (3 d) = 5–6, *n* (7 d) = 5–6, *n* (14 d) = 5, *n* (28 d) = 5. Mean values are shown per time point. Ordinary one-way ANOVA + Dunnett's post-hoc test. At least two independent experiments were performed per time point in WT animals. *, P < 0.05; **, P < 0.01; ***, P < 0.001; ****, P < 0.0001.

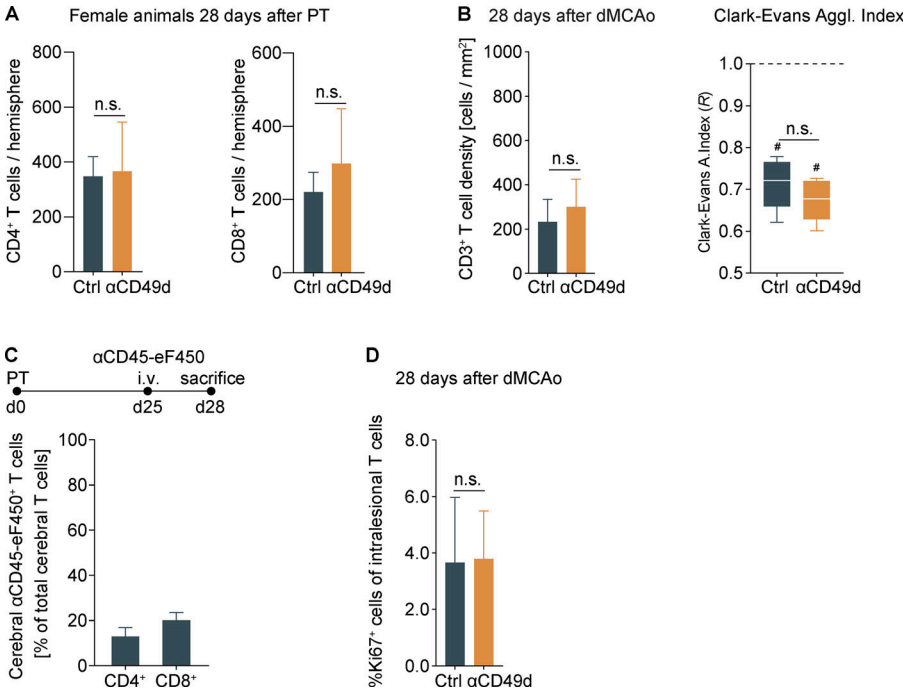

Figure S3. **Chronic T cell accumulation in female mice and after dMCAo. (A)** Flow cytometric analysis of CD4⁺ and CD8⁺ T cells 28 d after stroke in female mice; *n* = 7–8 per group, unpaired *t* test. Data are shown as mean + SD. **(B)** Evaluation of cell density and cell agglomeration of CD3⁺ intralesional T cells 28 d after dMCAo; *n* = 5 per group, unpaired *t* test. Data are shown as mean + SD/median and interquartile range. **(C)** i.v. labeling of circulating CD45⁺ leukocytes over 3 d before flow cytometric brain analysis 28 d after stroke reveals only a small fraction of brain-invading CD4⁺ and CD8⁺ T cells out of total cerebral T cells in the ischemic hemisphere; *n* = 4. Data are shown as mean + SD. **(D)** Percentage of Ki67⁺ T cells 28 d after dMCAo; *n* = 5 per group, unpaired *t* test. Data are shown as mean + SD. All data were generated in three independent experiments in WT animals. #, P < 0.05 for R < 1.0.

Table S1 is provided online as a Word document and lists patient data.

3.2 STROKE INDUCES DEVELOPMENT OF A BRAIN-RESIDENT T CELL POPULATION WHICH PROMOTES FUNCTIONAL RECOVERY

3.2.1 Summary

Acute brain injuries trigger an immediate inflammatory response that does not completely resolve and instead gives rise to chronic, long-lasting neuroinflammation. T cells contribute substantially to acute stroke outcomes. Recent studies have shown that T cells exhibit chronic accumulation in the brain following ischemic stroke, yet their specific identity and mechanisms of tissue residency remain elusive. Furthermore, whether chronically resident T cells contribute to functional recovery is largely unexplored.

In this study, we elucidate the development of a self-sustaining brain tissue-resident memory T cell (T_{RM}) population after a stroke and delineate their pivotal contribution in reinstating cortical connectivity. Combining high-dimensional flow cytometry and single-cell mRNA sequencing, we confirmed that post-stroke T cells express typical T_{RM} markers. Our observations reveal that the accumulation of post-stroke T_{RM} is contingent upon both major histocompatibility complex class I (MHC-I) and chemokine signaling mediated through CXCR3 and CXCR6 receptors. Intriguingly, local depletion of the brain T_{RM} population prompts rapid repopulation through local proliferation, crucial for maintaining homeostatic population levels. Furthermore, in lymphocyte-deficient mice, we observe impaired recovery of the neuronal networks after stroke, suggesting a plausible mediation by microglia-dependent synaptic pruning.

These findings offer novel insights into the molecular mechanisms underpinning T cell brain residency subsequent to brain ischemia. In addition, our data challenge the common conception of a mostly harmful contribution of T cells to stroke outcomes and reveal an intrinsic pro-regenerative role of post-stroke brain T_{RM}. Harnessing and enhancing such potential emerges as a promising avenue for novel cell-based therapeutic approaches aimed at facilitating functional recovery.

3.2.2 Reference

The paper is not yet accepted for publication

Ricci A., S. Heindl, O. Carofiglio, A. Simats, S. Bittner, E. Beltran, R. Fekete, A. Denes, and A. Liesz. 2024

BRIEF REPORT

Stroke Induces Development of a Brain-Resident T cell Population which Promotes Functional Recovery

Alessio Ricci[1], Steffanie Heindl[1], Olga Carofiglio[1], Alba Simats[1], Stefan Bittner[2], Eduardo Beltran[3], Rebeka Fekete[4], Adam Denes[4], Arthur Liesz[1,5]*

1 Institute for Stroke and Dementia Research, University Hospital, Ludwig Maximilians University Munich, Munich, Germany

2 Department of Neurology, Focus Program Translational Neuroscience (FTN) and Immunotherapy (FZI), RhineMain Neuroscience Network (rmn(2)), University Medical Center of the Johannes Gutenberg University Mainz, Mainz, Germany.

3 Institute of Clinical Neuroimmunology, University Hospital, LMU Munich, Munich, Germany

4 Momentum Laboratory of Neuroimmunology, Institute of Experimental Medicine, Budapest, Hungary

5 Munich Cluster for Systems Neurology (SyNergy), Munich, Germany

* correspondence to: Arthur.Liesz@med.uni-muenchen.de

Keywords: ischemic stroke; tissue residency; T cell; neuroinflammation; antigen presentation; chemokines.

Abstract

Acute brain injuries induce not only an immediate inflammatory response but result in chronic neuroinflammation. T cells accumulate in the brain chronically after ischemic stroke, however their identity, mechanisms of tissue residency and contribution to post-stroke recovery are unknown. Here, we describe the development of a self-maintained brain tissue-resident memory T cell (T_{RM}) population after stroke and demonstrated their role in restoring cortical connectivity. We observed that post-stroke T_{RM} accumulation relied both on MHC-I and chemokine signaling via CXCR3 and CXCR6. Local depletion of the brain T_{RM} population led to rapid repopulation by local proliferation for homeostatic population maintenance. Furthermore, lymphocyte-deficient mice show an impaired recovery of neuronal network after stroke, likely mediated by microglia-dependent synaptic pruning. These data provide novel insights into the molecular mechanisms governing T cell brain residency after brain ischemia. Boosting the intrinsic pro-regenerative role of post-stroke brain T_{RM} could represent a novel cell-based therapeutic approach for functional recovery.

Introduction

Stroke is a leading cause of death and disability worldwide, with the global incidence projected to increase in the next years (Pu et al., 2023; Feigin et al., 2021). While advancements in acute stroke treatment like thrombolysis and thrombectomy have positively impacted stroke management for the acute phase, specific interventions targeting long-term disability in the chronic phase of the disease are still limited to rehabilitation. Post-stroke neuroinflammation is a complex multifactorial phenomenon that drastically influences stroke outcome (Iadecola et al., 2020). Different immune cell subtypes have been shown to differentially impact injury progression and became target for therapeutic interventions. In particular, T cells were shown to significantly affect brain injury and functional outcome, and the contribution of different subtypes has been systematically investigated in the acute phase (Cramer et al., 2019a). Recently, we and others have surprisingly discovered that post-stroke neuroinflammation propagates over several months and particularly T cells can be detected still in the chronic phase after stroke, both in mice and humans (Doyle et al., 2015; Heindl et al., 2021; Shi et al., 2021). However, a mechanistic understanding of the recruitment, retention and function of this unexpected cell population in the chronically recovering brain after stroke is currently lacking.

Here, we performed an exhaustive characterization of chronic post-stroke T cells, focusing on the signaling pathways governing their accumulation. We identified that T cells acquire a phenotype of tissue-resident memory T cells (T_{RM}) in chronic post-stroke brains of mice and patients. T_{RM} constitute a non-recirculating population that act as a first line of defense in border tissues like skin and mucosae and are defined by a specific transcriptomic signature and expression of epitope markers (Schenkel and Masopust, 2014). In the brain, T_{RM} have been studied only in the context of viral infections (Steinbach et al., 2016; Vincenti et al., 2022; Ren et al., 2020), however, their role in sterile brain lesions such as stroke has so far not been recognized. Using single-cell transcriptomics, genetic models and adoptive cell transfers we were able to uncover the key chemoattractant factors and MHC-dependence of T_{RM} retention. Additionally, we describe that T_{RM} are critical for functional recovery in the chronic post-stroke phase.

Results and discussion

Stroke induces the development of a cerebral, tissue-resident memory T cell population

Consistent with previous reports (Heindl et al., 2021; Doyle et al., 2015), we observed accumulation of both CD4+ T_{helper} and CD8+ $T_{cytotoxic}$ cells 28d after stroke (**Fig. 1A**). Also, we confirmed CD3+ T cell accumulation in human brain samples obtained from chronic stroke patients (**Fig. 1B**). To further characterize post-stroke T cells, we performed single-cell mRNA sequencing (scSeq) of isolated CD3+ T cells from brain and blood at an acute (3d) and chronic (28d) time point after experimental stroke (**Fig. 1C**), which retrieved a heterogenous clustering of T cell subpopulations across the organs and time points (**Fig. 1D**). We identified the accumulation of a distinct brain-specific cell cluster in the chronic post-stroke time point within the CD8+ $T_{cytotoxic}$ cells (i.e. cluster 7), while this pattern was less prominent for CD4+ T_{helper} cells (**Fig. 1E** and **Fig. S1A**). To pinpoint the cellular identity of the chronic brain-specific cluster 7, we analyzed differentially expressed genes (DEGs) and observed upregulation of tissue homing (*Cxcr3* and *Cxcr6*) and retention molecules (*Itga4*, *Itgb1*, *Itgal* and *Cd44*), as well as downregulation of mediators of tissue egress (e.g. *Cd62l*, *S1pr1* and *Klf2*) (**Fig. 1F**), suggesting a non-circulating tissue-resident phenotype. Moreover, T cells of cluster 7 showed an upregulation of both inhibitory (*Pdcd1*, *Ctla4*, *Tigit* and *Lag3*) and

effector molecules (*Ifng*, *Gzmk* and *Fasl*), which is a typical hallmark of tissue-resident memory T cells (T_{RM}) (Szabo et al., 2019). Similarly, CD4+ T cells exhibited a prominent brain cluster (cluster 3) showing a comparable set of DEGs which points to a T_{RM} phenotype (**Fig. S1B**). To confirm the T_{RM} phenotype of post-stroke T cells, we performed flow cytometry for established T_{RM} epitope markers at different time points after stroke. The percentage of T_{RM} (here defined as CD44+CD69+KLRG1−) increased from the acute to the chronic phase, when it reached a plateau (**Fig. 1G**). Strikingly, CD69+ cells were also detected in brain sections from a stroke patient's brain, two months post-ischemia (**Fig. 1H**). Taken together, our data clearly demonstrate the previously unrecognized phenomenon of the accumulation of a chronic T_{RM} cell population in brains after an ischemic brain lesion, both in mice and humans.

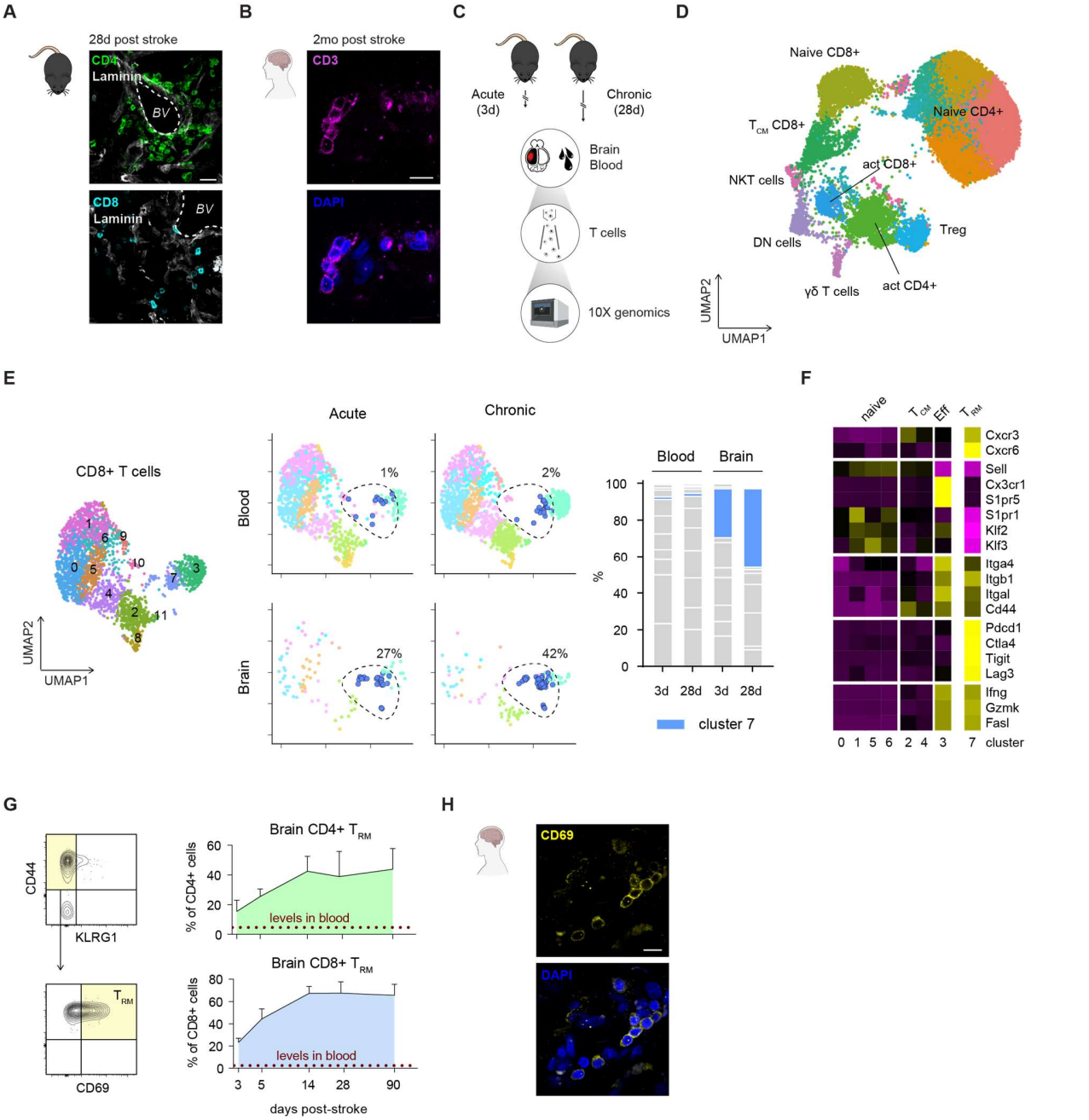

legend on the next page

Figure 1. Characterization of brain T cells in the chronic phase after ischemic stroke. (A) Representative images of CD4+ T_{helper} and CD8+ $T_{cytotoxic}$ cells in the mouse brain tissue, 28d after stroke induction. Dashed lines show the inner lumen of a blood vessel (BV). Scale bar = 20 µm. **(B)** Representative image of CD3+ T cells from human brain tissue, 2 months after stroke. Scale bar = 20 µm. **(C)** Schematic of the single-cell mRNA sequencing (scSeq) experimental design: CD3+ T cells were isolated from blood and brain at an acute (3d) and chronic (28d) time point after stroke, FACS sorted and processed following the 10x Genomics pipeline. **(D)** Uniform Manifold Approximation and Projection (UMAP) plot of 16´484 combined brain and blood T cells, colored by identified clusters and labelled based on the top differentially expressed genes (DEGs). T_{CM}: central memory T cells; NKT cells: natural killer T cells; act: activated; DN: double negative. Treg: regulatory T cells. **(E)** UMAP plots of 2´724 CD8+ T cells, combined (left) and subset by organ and time point (center). Dashed lines encircle cells from cluster 7, of which percentage is reported. Bar plot show the percentages of different clusters per sample, with a focus on cluster 7 (right). **(F)** Heatmap showing normalized expressions of tissue-resident memory T cell (T_{RM}) signature genes across different clusters. Eff: effector. **(G)** Gating strategy used to identify T_{RM} (left). Longitudinal analysis of the percentage of CD4+ and CD8+ T cells showing T_{RM} markers in the post-stroke brain (right). 3d, 5d, 14d, 28d and 90d: n = 5, 8, 9, 12 and 9. **(H)** Representative image of CD69+ bona-fide T_{RM} from human brain tissue, 2 months after stroke. Scale bar = 20 µm.

Post-stroke T_{RM} differentiate locally and form a homeostatically maintained cell population

Next, we aimed to explore the origin and fate of the T_{RM} population in brains chronically after stroke. Employing pseudotime analysis on the scSeq of $T_{cytotoxic}$ cells (**Fig. 2A**), we uncovered a differentiation trajectory of brain T_{RM} originating from naive and central memory T cells in the blood. To pinpoint the timeframe of T cell invasion, we labelled circulating T cells over 3d via i.v. injection of a fluorescently-labelled anti-CD45 antibody. We observed that T cells predominantly invade the brain acutely after stroke (0d-3d) and just in a limited amount during the subacute phase (14d-17d) (**Fig. 2B**). Since these results indicate that blood-to-brain migration does not contribute substantially to the maintenance of the T_{RM} population chronically in the brain, we further explored potential local clonal expansion. Using single-cell T cell receptor profiling for full-length V(D)J sequences in combination with the mRNA scSeq, we detected that CD8+ brain T cells showed a prominent clonal expansion specifically in the chronic phase, while CD4+ T cells exhibited only a negligible clonal expansion (**Fig. 2C** and **Fig. S1C**). Based on these results, we aimed to assess whether MHC-dependent antigen presentation is necessary for post-stroke T_{RM} development. We observed that chronically after stroke, still a high number of MHC class I+ and II+ cells can be found in the brain (**Fig. 2D** and **Fig. S2A**). Therefore, we used inducible gene knock-out models for either MHC class I or II, which show a very high, long-lasting recombination efficacy and minimally affect peripheral T cell numbers (**Fig. S2B** and **S2C**). Consistently with our results on clonal T_{helper} versus $T_{cytotoxic}$ cell expansion, MHC-I knock-out prevented the accumulation of CD8+ T_{RM}, while CD4+ T_{RM} numbers were unchanged. On the other hand, MHC-II knock-out did surprisingly not affect the cell count of either post-stroke T_{RM} population (**Fig. 2E**), suggesting an MHC-II-independent recruitment and retention of T_{RM} after stroke. Microglia are an important player in post-stroke neuroinflammation (Iadecola et al., 2020) and can function as antigen-presenting cells (APCs) (Goddery et al., 2021). Therefore we investigated whether microglia contribute to the establishment of the post-stroke T_{RM} population—potentially via MHC-I-dependent antigen presentation. To test this hypothesis, we depleted microglia using the CSF1R antagonist PLX5622 from 7d before stroke induction until 28d after stroke, resulting in a near-complete depletion of microglia in the peri-lesional brain cortex (**Fig. 2F**). Surprisingly, microglia depletion did not affect the post-stroke T_{RM} accumulation (**Fig. 2G**), suggesting that other cell types, such as astrocytes, monocyte-derived macrophages (moMΦ) or other invading immune cells, likely act as the main APCs. MoMΦ have been shown to accumulate in chronic stroke brain (Werner et al., 2020). Interestingly, Iba1+ cells in the lesion core were not affected by the PLX5622 treatment (**Fig. 2H**). Combining immunofluorescence and single-molecule fluorescent *in situ* hybridization (smFISH), we showed that the lesion core is populated

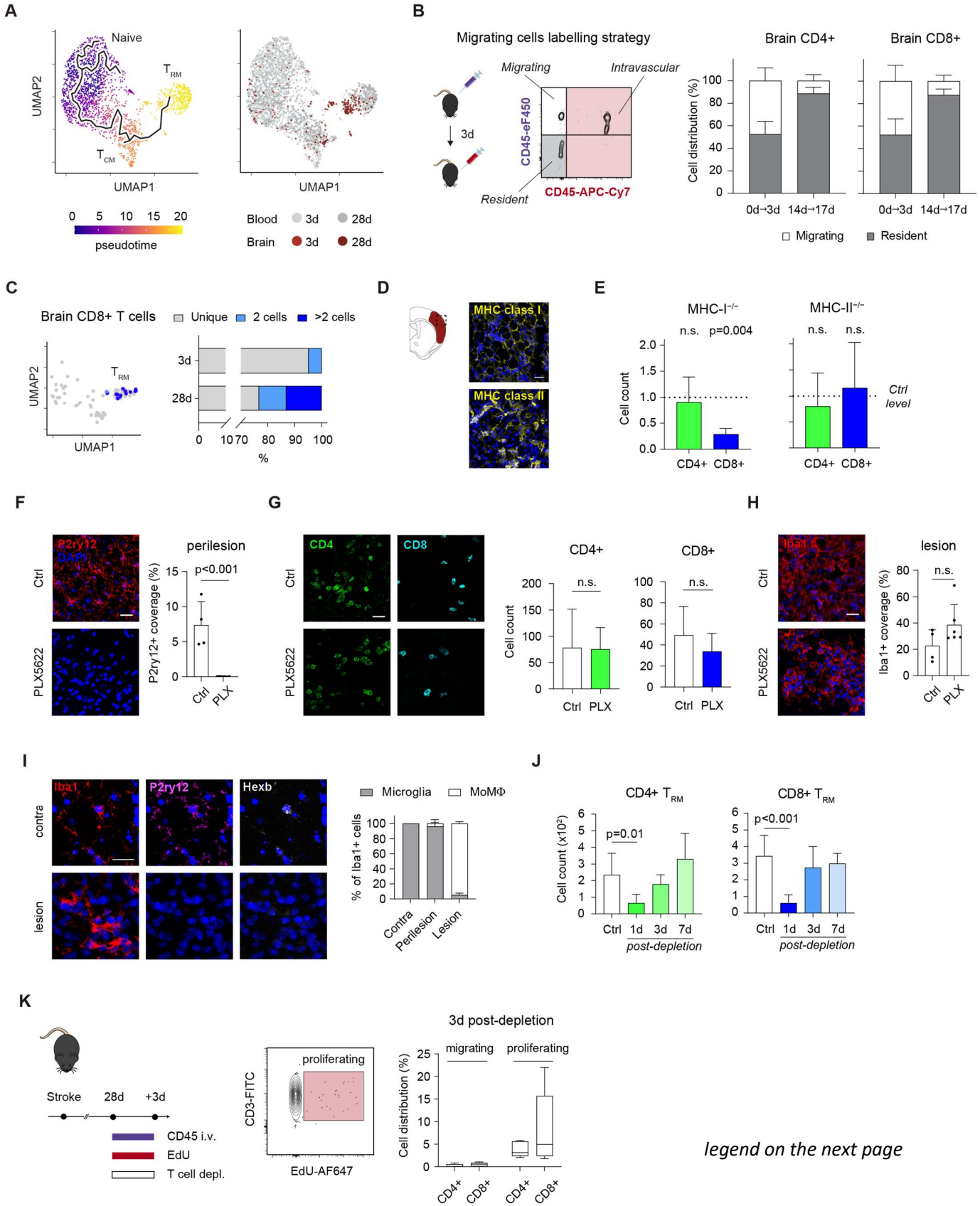

legend on the next page

Figure 2. Dynamics and mechanisms of post-stroke T_{RM} invasion and accumulation. (A) UMAP plots of CD8+ T cells showing pseudotime-based differentiation trajectory (left) and organ/timepoint distribution (right). **(B)** Schematic of experimental design for labelling and tracking of circulating T cells and corresponding gating strategy (left). Percentages of migrating and resident T cells in different time windows after stroke induction (right). 0d-3d and 14d-17d: n = 5. **(C)** UMAP of brain CD8+ T cells showing overrepresentation of clonally expanded cells in the T_{RM} cluster (left). Percentage of clonally expanded cells in the brain at 3d and 28d after stroke. **(D)** Representative images of brain slices 28d post-stroke, showing high density of MHC class I+ and class II+ cells in the lesion area. Scale bar = 20 µm. **(E)** Flow cytometric quantification of post-stroke brain CD4+ and CD8+ T_{RM} after induction of MHC class I or MHC class II deficiency. Cell numbers were normalized to control levels. For MHC-$I^{-/-}$, Ctrl: n = 19, KO: n = 13. For MHC-$II^{-/-}$, Ctrl: n = 10, KO: n = 12. Unpaired t test. **(F)** Representative images of P2ry12+ microglia cells in the perilesional area in control vs. PLX5622 diet-fed mice (scale bar = 20 µm) and quantification of coverage, showing near-complete depletion of microglia. Ctrl: n = 4, PLX: n = 6. Unpaired t test. **(G)** Representative images of CD4+ and CD8+ T cells in control vs. PLX5622 diet-fed mice (left). Intralesional cells were quantified and no significant difference was observed between groups. Ctrl: n = 10, PLX: n = 6. Unpaired t test. **(H)** Representative images of Iba1+ macrophages from the lesion core in control vs. PLX5622 diet-fed mice (scale bar = 20 µm) and quantification of coverage, showing no significant difference. Ctrl: n = 4, PLX: n = 6. Unpaired t test. **(I)** Representative images of combined immunofluorescence for P2ry12 and Iba1 and Hexb smFISH, showing accumulation of *bona fide* monocyte-derived macrophages (moMΦ) in the lesion core, compared to perilesional and contralateral cortex populated mainly by microglia. n = 6. Scale bar = 20 µm. **(J)** Number of post-stroke T_{RM} at 28d after stroke in control conditions and at different time points after intra-cisterna magna (i.c.m.) injection of depleting antibodies. Ctrl, 1d, 3d and 7d: n = 12, 7, 5 and 6. One-way ANOVA. **(K)** Schematic of experimental design for combined tracking of circulating T cells (as described in *B*), EdU incorporation and i.c.m. T cell depletion (left). Gating strategy to identify EdU+ proliferating cells (middle). Percentage of CD4+ and CD8+ T cells, 3d after T cell depletion, that show a migrating or proliferating phenotype. n = 5.

mainly by phagocytes that do not express microglia-specific markers (P2ry12 and Hexb, Masuda et al., 2020), therefore identifiable as moMΦ (**Fig. 2I**). These results suggest that moMΦ are likely sufficient to induce and maintain the population of post-stroke T_{RM}. Next, we attempted to locally deplete post-stroke T_{RM} by injections of CD4- and CD8-specific antibodies to the cerebrospinal fluid via the cisterna magna. Interestingly, while the injection induced a significant depletion of post-stroke T_{RM}, the T_{RM} population reemerged at comparable population size within one week (**Fig. 2J**), suggesting that the cell niche of post-stroke T_{RM} is homeostatically maintained chronically after stroke. Consistently, we detected 3d after T_{RM} depletion a consistent amount of proliferating T cells, suggesting local homeostatic proliferation for population size maintenance, while invasion of circulating T cells—marked by antibody labeling in the circulation—did not contribute to the reemerging T_{RM} population (**Fig. 2K**).

Post-stroke T_{RM} accumulation depends on chemokine signaling

Next, we searched for the potential molecular mechanisms driving accumulation and maintenance of post-stroke T_{RM} within the brain. Spatial distribution analysis revealed that the vast majority of T cells accumulate within the lesion core, suggesting the presence of a specific chemotactic signal that is directing this compartmentalized accumulation (**Fig. 3A**). Our scSeq dataset revealed a significant upregulation in the chemokine receptors CXCR3 and CXCR6 in post-stroke T_{RM}. We confirmed the abundant expression of these receptors also at the protein level by flow cytometry (**Fig. 3B**). Moreover, the chemokine ligands of these receptors, namely CXCL9 and -10 for CXCR3, and CXCL16 for CXCR6, are also upregulated after stroke with a particular peak in the early chronic phase – corresponding to the dynamics of chronic post-stroke T cell accumulation (**Fig. 3C**) and unlike the expression of other cytokines and chemokines which peak in the acute phase within the first hours and days after stroke (Lambertsen et al., 2012). Using a combination of histological analysis of T cell localization in relation to the lesion border—defined based on astrocytic GFAP signal—and smFISH analysis for mRNA abundance of specific chemokines, we detected a closely matching spatial expression of CXCL9, -10 and -16 with the local accumulation of T cells at the transition zone between lesion core and peri-lesional tissue (**Fig. 3D**). Additionally, smFISH and

histological co-localization analysis revealed that the main cellular source of the analyzed chemokines was Iba1+ microglia/macrophages, with a minor contribution of GFAP+ astrocytes specifically for CXCL10 (**Fig. 3E**). To assess whether this potential chemokine signaling is necessary for post-stroke T_{RM}

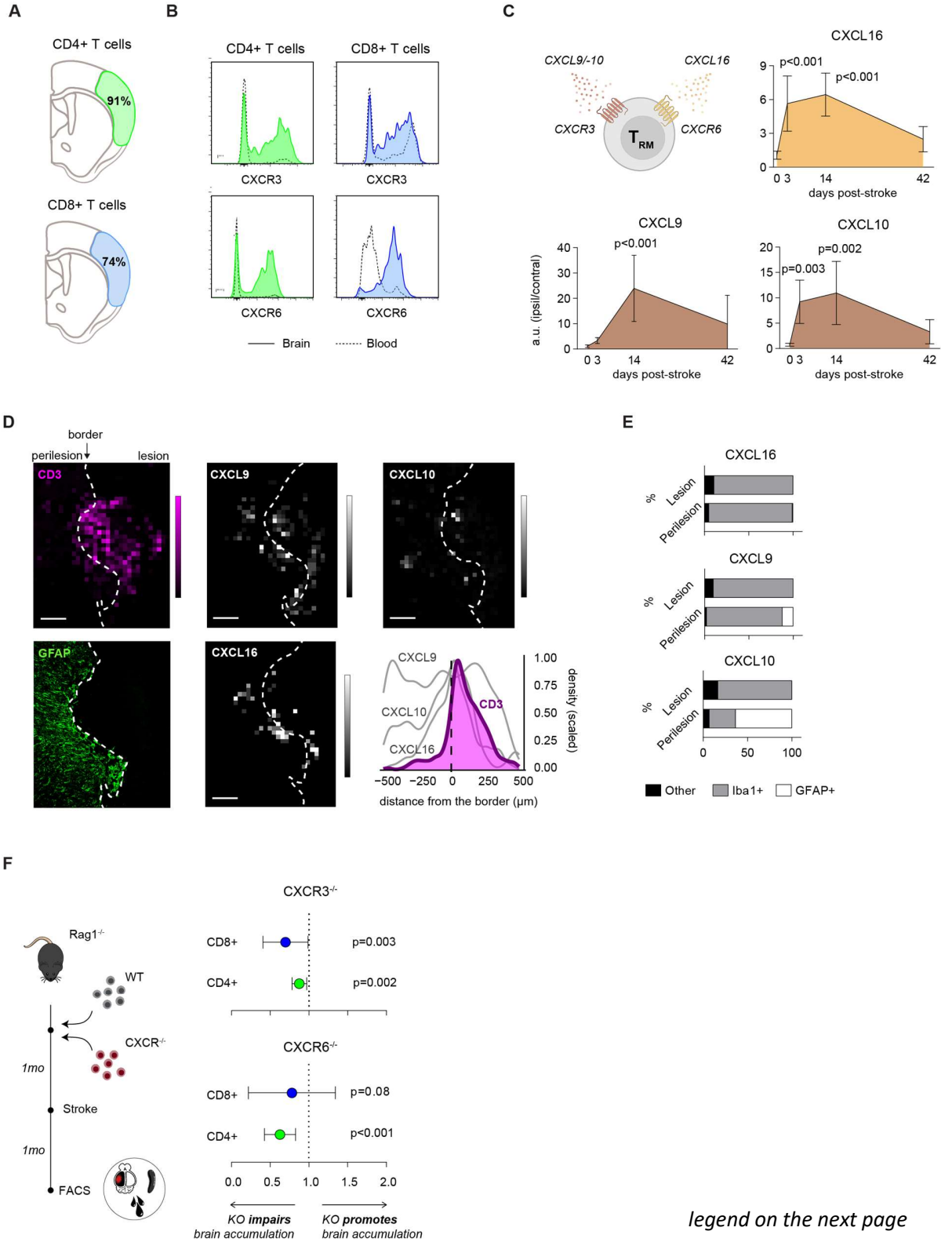

legend on the next page

Figure 3. Chemokine signaling contributes to post-stroke T_{RM} accumulation. (A) Schematics representing the predominant accumulation of CD4+ and CD8+ T cells within the lesion core, 28d after stroke. n = 6. **(B)** Histograms showing expression levels of the chemokine receptors CXCR3 and CXCR6 in CD4+ and CD8+ T cells, measured by flow cytometry. Brain and blood cells are represented with a solid or dashed line, respectively. n = 4. **(C)** Schematic of T_{RM}-specific chemokine receptors and their cognate ligands (upper left). RNA expression levels of the chemokines CXCL9, -10 and -16 at different time points after stroke, measured by quantitative RT-PCR. 0d, 3d, 14d and 42d: n = 4, 10, 5 and 10. One-way ANOVA. **(D)** Representative heatmap of fluorescent intensity of CD3, showing T cell accumulation mainly in the lesion area, and of smFISH probes for CXCL9, -10 and -16 in consecutive sections, 14 days post-stroke. Representative image of GFAP staining, utilized to define the lesion border (bottom left). Spatial distribution (quantified as distance from lesion border) of CD3+ T cells, as well as individual smFISH puncta for chemokines, showing a high overlap (bottom right). CD3, CXCL9, -10 and -16: n = 3, 5, 5 and 5. **(E)** Percentage of GFAP+ astrocytes, Iba1+ microglia/macrophages and other cell types expressing the chemokines CXCL9, -10 and -16 in the lesion core and perilesional cortex. n = 5. **(F)** Schematic of experimental design for the adoptive transfer of WT and chemokine receptor KO (CXCR3 or -6) in $Rag1^{-/-}$ mice (left). Accumulation index shows the relative accumulation of KO T cells over WT in the brain, compared to a reference peripheral organ (spleen). $CXCR3^{-/-}$ and $CXCR6^{-/-}$: n = 10. Paired t test.

accumulation, we adoptively transferred wildtype (WT) and CXCR3 or -6 knock-out (KO) T cells into $Rag1^{-/-}$ mice and compared the WT-to-KO chimerism in spleen and brain at 28d after stroke (**Fig. 3F**). We detected an impaired accumulation of CXCR3/-6 KO T cells in the brain compared to the spleen chimerism, suggesting a critical role for CXCR3/-6 signaling for development of the post-stroke T_{RM} population. CXCR3 signaling is generally implicated in T cell infiltration of inflamed tissues, including the central nervous system (Zhang et al., 2008; Sporici and Issekutz, 2010). CXCR6 is important for the maintenance, but not initial invasion, of T cells in several organs including the brain (Rosen et al., 2022; Tse et al., 2014). Based on this, we speculate that CXCR3 and CXCR6 might have complementary roles in brain invasion and maintenance of post-stroke T_{RM}; however, further experiments exploring the complex chemokine networks and their specific role for recruitment, retention and life cycle of brain T_{RM} are required. Analysis of these chemokines or their receptors as potential therapeutic targets for post-stroke chronic neuroinflammation warrants further studies.

Post-stroke T_{RM} affect functional outcome after stroke

Finally, we aimed to assess if T cells have a functional role during recovery in the chronic phase after experimental stroke. For this, we assessed the reorganization of cortical neuronal network function after a photothrombotic lesion in the motor cortex using repetitive *in vivo* widefield imaging in lymphocyte-deficient ($Rag1^{-/-}$) and immunocompetent (WT) Thy1-GCamp6s reporter mice (Cramer et al., 2019b). Focusing on interhemispheric connectivity of corresponding brain areas as the most dominant type of cortical connectivity in the mouse brain, we identified that lymphocyte-deficient mice showed a substantial deficit in recovering connectivity strength of various functional connections in comparison to immunocompetent animals (**Fig. 4A**) At the microanatomical level, this effect was paralleled by a reduced dendritic spine density in $Rag1^{-/-}$ mice compared to WT animals (**Fig. 4B**), suggesting a pro-regenerative effect of lymphocytes that promote neuronal plasticity. While lymphocyte-deficient $Rag1^{-/-}$ mice show a dominant phenotype, they also have the limitation of a constitutive absence of both B and T cells. Therefore, we used antibody-mediated depletion of CD4+ and CD8+ T cells, in order to address the role of T cells specifically in the recovery phase. Multiple CD4- and CD8-specific antibody injections starting from 14d after stroke efficiently resulted in nearly complete depletion of brain T cells (**Fig. 4C**). We have previously demonstrated that the effect of brain-invading T cells after stroke is largely exerted by modulating microglial activity (Benakis et al., 2022). Therefore, we performed automated microglia morphology analysis comparing T cell-depleted and control mice at 28d after stroke (Heindl et al., 2018). Indeed, microglia of

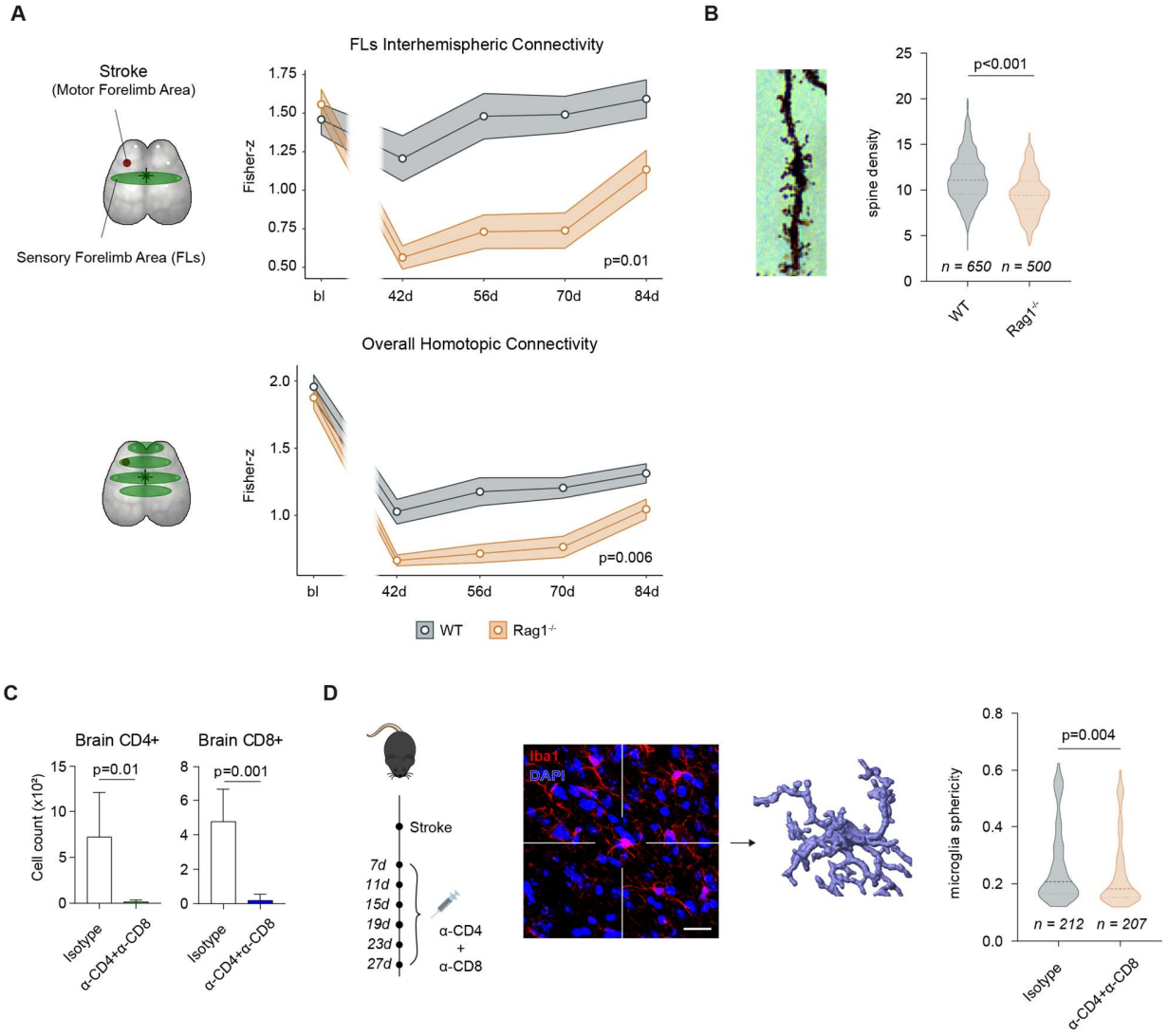

Figure 4. T cells contribute to functional recovery in the chronic phase after stroke. (A) Schematic representation of functional connectivity parameters (left). Functional connectivity strength (indicated as Fisher-z transformed correlation coefficient) between the two homotopic sensory forelimb areas (upper) and all homotopic areas (lower) at different time points after stroke in WT and Rag1$^{-/-}$ mice. WT: n = 13, Rag1$^{-/-}$: n = 11. Mixed-effects model. **(B)** Spine density, quantified by Golgi-Cox staining, in WT and Rag1$^{-/-}$ mice. U test. **(C)** Quantification of brain T cell depletion after two weeks of treatment (from 14d to 28d). Isotype: n = 4, α-CD4+α-CD8: n = 5. Unpaired t test. **(D)** Schematic of CD4+ and CD8+ T cell depletion with antibodies (left). Representative image of Iba1+ microglial cells and example of an automatically reconstructed cell (center). Microglia sphericity, used as a proxy for activation status, is shown for isotype control and T cell-depleted group (right). U test.

animals with brain T_{RM} depletion showed a less ameboid morphology, which corresponds to a less reactive state, suggesting that indeed post-stroke brain T_{RM} can functionally affect microglia reactivity (**Fig. 4D**).

While we cannot unambiguously define the exact contribution of different T cell subpopulations to stroke recovery, here we showed that lymphocytes deficiency significantly affects stroke outcome. Further studies will be required to define the exact mechanisms by which T_{RM} can modulate functional recovery, neuronal plasticity and network reorganization—which is likely a multifactorial process dependent on cell-cell-contact dependent mechanisms and secreted factors by the post-stroke T_{RM}. Recent studies have highlighted

how different T cell subtypes can polarize microglia into distinct "activation states" in different neurological disorders (Rosen et al., 2022; Yshii et al., 2022; Su et al., 2023). Therefore, T cell-microglia crosstalk is likely to play a pivotal role in T cell-mediated promotion of functional recovery. In addition, T cell-derived cytokines can directly affect neuronal function and modulate behavior as it has been previously demonstrated for T cell-derived cytokines including IL-4, IL-10 and IFN-γ in other brain disorders – but not yet explored in recovery from ischemic brain lesions (Filiano et al., 2016; Alves de Lima et al., 2020).

Post-stroke T_{RM} mainly localize in the lesion core, where they secrete soluble mediators that can permeate through the glial scar directly into the brain parenchyma (Zbesko et al., 2018), positioning them in an ideal niche to affect neuronal function in the reorganizing peri-lesional tissue. In our study we identified both, the local T_{RM}-recruiting/retaining chemokines and the local expression of MHC-I by lesional macrophages as a likely cause of the compartmentalized clustering of T_{RM} in the post-ischemic brain. Another surprising observation of our experiments was the identification of brain T_{RM} as a *de novo* established cell population which is not only retained in the recovering brain but in fact forms a self-maintained population, as demonstrated in our T_{RM}-depletion and repopulation experiments. These findings suggest the development of an immunological niche for T_{RM} cells in the post-ischemic brain, however, the molecular cues involved in the regulation of this non-physiological population in the brain are currently unknown. A better understanding on these T_{RM}-specific mechanisms and their contribution to post-stroke recovery might open up novel directions for immunomodulatory stroke therapies to promote post-stroke recovery.

Materials and methods

Animals

All experiments in this study were conducted in accordance with the national guidelines for animal experiments and approved by the German governmental committees (Regierungpraesidium Oberbayern, Munich, Germany). Wild-type C57BL6/J male mice were purchased from Charles River. $Rag1^{-/-}$, eGFP reporter (C57BL/6-Tg (CAG-EGFP)131Osb/LeySopJ), Ai9 tdTomato reporter (B6.Cg-Gt(ROSA)26Sortm9(CAG-tdTomato)Hze/J), and Thy1-GCaMP6 (C57BL/6J-Tg(Thy1-GCaMP6s)GP4.3Dkim/J) were bred and housed at the animal core facility of the Center for Stroke and Dementia Research (Munich, Germany). $Cxcr3^{-/-}$ (B6.129P2-Cxcr3tm1Dgen/J) and $Cxcr6^{-/-}$ mice (B6.129P2-Cxcr6tm1Litt/J) were purchased from the Jackson Laboratory. β2 microglobulin $B2m^{fl/fl}$ mice (B6(Cg)-B2mtm1c(EUCOMM)Hmgu/J, Bern et al., 2019) were crossed with R26-CreERT2 (B6.129-Gt(ROSA)26Sortm1(cre/ERT2)Tyj/J) to obtain a global inducible MHC class I knock-out (here termed MHC-$I^{-/-}$). Histocompatibility 2, class II antigen, beta 2 I-$AB^{fl/fl}$ mice (B6.129X1-H2-Ab1tm1Koni/J) were crossed with R26-CreERT2 mice (Gt(ROSA)26Sortm2(cre/ERT2)Brn) to obtain a global inducible MHC class II knock-out (here termed MHC-$II^{-/-}$). To induce the knock-out, mice were treated with i.p. injection of tamoxifen at a concentration of 100 mg/kg for the MHC-$I^{-/-}$ mice and 20 mg/kg for MHC-$II^{-/-}$ mice, for five consecutive days, two weeks before stroke induction. Thy1-GcaMP6 and $Rag1^{-/-}$ mice were crossed to obtain Thy1-GcaMP6 : $Rag1^{-/-}$. All the animals were housed under controlled temperature (22 ± 2°C) with a 12-h light/dark cycle and access to food and water ad libitum. All animal experiments are reported in accordance with the ARRIVE guidelines (Kilkenny et al., 2010).

Animal treatments

For microglia depletion, mice were fed with PLX5622 chow (Plexxikon Inc.), from 2 weeks before until 4 weeks after stroke, when mice were sacrificed for histological analysis. For T cell-depletion, mice were i.p. injected with a bolus of 100 µg of α-CD4 (clone: YTS 191, catalog no.: BE0119; Bio X Cell) and 100 µg of α-CD8a (clone: 2.43, catalog no.: BE0061; Bio X Cell), 1 week after stroke. Follow-up injections of 50 µg of α-CD4 and 50 µg of α-CD8a were repeated every 4 days after the first injection, to maintain a high level of T cell depletion, until mice were sacrificed for histological analysis. Control injections were performed using a correspondent amount of isotype control antibody (LTF-2, catalog no.: BE0090; Bio X Cell).

Experimental stroke model

dMCAo

Experimental stroke was induced by permanent occlusion of the distal middle cerebral artery as previously described (Llovera et al., 2014). Briefly, mice were anaesthetized with isoflurane, delivered in 30% O_2/70% N_2O, and positioned to their side. Body temperature was maintained at 37°C with a mouse warming pad. Dexpanthenol eye ointment was applied to both eyes. An incision between the ear and the eye was used to expose the temporal muscle. The muscle was detached from the bone and a hole was drilled on top of the middle cerebral artery. The vessel was coagulated with electrocoagulation forceps and the muscle was

placed back. Finally, the wound sutured and mice were allowed to wake up from anesthesia in a heating chamber.

Photothrombosis

Photothrombotic lesions were induced as previously described (Llovera et al., 2021). Briefly, mice were anaesthetized as described above and placed in a stereotactic frame. The skull was exposed and the lesion location was marked in the left hemisphere (1.5 mm lateral and 1.0 mm rostral to bregma). Animals received 10 µl/g body weight of 1% Rose Bengal (198250-5g; Sigma-Aldrich) in saline and right after injection the lesion area was illuminated for 20 min with a laser (Cobolt Jive 50, 561 nm power at 25mV). The illuminated area was set to 2mm diameter with an adjustable iris.

Intra-cisterna magna injection of α-CD4 and α-CD8 antibodies

Mice were anesthetized and fixed in a stereotaxic frame, with the head slightly tilted to form an angle of 120° in relation to the body. A small incision was made in the neck region between the ears to expose the neck muscles, which separated along the midline to expose the cisterna magna (CM). Cannulas composed of a glass capillary (ID, inner diameter 0.67 mm; OD, outside diameter, 1.20 mm) attached to a polyethylene tubing (ID 0.86 mm and OD 1.52 mm; Fisher Scientific UK Ltd.) were used to perform the CM injections. Glass capillaries were sharpened using a flaming micropipette puller (P-1000, Sutter Instrument GmbH) and filled with a mixture of 3 µg of α-CD4 (clone: YTS 191, catalog no.: BE0119; Bio X Cell) and 3 µg of α-CD8a (clone: 2.43, catalog no.: BE0061; Bio X Cell) in a total volume of 10 µL. Control injections were performed with 6 µg of isotype control antibody (LTF-2, catalog no.: BE0090; Bio X Cell). Capillaries were fixed to the micromanipulator arm of the stereotaxic and injections were performed at a rate of 1 µL/min. At the end of the injection, mice were sutured and allowed to recover.

***In vivo* widefield neuronal calcium imaging**

In vivo widefield calcium imaging was performed as previously described (Cramer et al., 2019b). Briefly, Thy1-GCaMP6s heterozygous mice with either a WT or Rag1$^{-/-}$ background underwent scalp removal and the exposed skull was covered with transparent dental cement. Mice were mildly anesthetized (0.5 mg/kg body weight of medetomidine with 0.75%isoflurane inhalation) and immobilized in a stereotactic frame. Resting-state in vivo imaging was performed using a custom-made macroscopic imaging setup. Mouse cortex was illuminated with 450-nm blue light from an LED source. Resting state calcium activity was recorded for 4 min (6 × 1,000 frames) with a high-precision 2/3" Interline charge-coupled device camera (Adimec-1000m/D, pixel size 7.4 × 7.4 µm, acquisition at 20–22°C; Adimec) at a 25-Hz frame rate using longDaq software (Optical Imaging).

***In vivo* calcium imaging analysis**

Functional imaging data were analyzed as described previously (Cramer et al., 2019b). Specifically, functional connectivity was calculated as pairwise Fisher's z-transformed Pearson's correlation between the time course of each of eight previously defined seeds, corresponding to rostral forelimb area (RFL), caudal

forelimb area (CFL), forelimb sensory (FLs) and hindlimb sensory (HLs) for left and right hemispheres. Overall homotopic connectivity corresponds to the mean of all coefficients of each homotopic connection between the seeds in both hemispheres. Left intrahemispheric connectivity corresponds to the mean of the coefficient of each connection between the seeds located in the left hemisphere. Fisher's z-transformed Pearson's correlation was calculated using MATLAB (MathWorks R2016b with Optimization Toolbox, Statistics and Machine Learning Toolbox, Signal Processing Toolbox and Image Processing Toolbox; MathWorks).

Immunofluorescence of mouse coronal brain sections

Mice were transcardially perfused with saline and 4% paraformaldehyde solution. To prevent tissue damage associated with the dissection of the brain, the whole skull was isolated, post-fixed with 4% paraformaldehyde overnight at 4°C and then decalcified in 0.3 M EDTA for 7 days. Subsequently, the brains were dehydrated for 2d in 30% sucrose in PBS and then snap-frozen in isopentane. Immunofluorescence was performed on 20-µm-thick coronal sections. Sections were fixed with cold acetone for 10 min at RT and washed with PBS before blocking with goat or donkey serum blocking buffer for 1 h at room temperature. Subsequently, sections were stained overnight at 4°C with primary antibody (CD3e, 1:200, hamster anti-mouse, clone 500A2; BD Pharmingen; CD4, 1:100, rat anti-mouse, clone GK1.5; abcam; CD8a, 1:100, rat anti-mouse, clone 53-6.7; eBioscience; CD69, 1:100, goat anti-mouse, polyclonal; R&D system; laminin, rabbit anti-mouse; clone L9393; Sigma Aldrich; MHC class I, 1:100, goat anti-rat, clone ER-HR52; Santa Cruz, MHC class II, 1:100, goat anti-rat, clone IBL-5/22; Santa Cruz; P2ry12, 1:200, goat anti-rabbit, polyclonal; Invitrogen; Iba1, 1:200, rabbit anti-mouse, polyclonal; Wako; Iba1, 1:200, goat anti-mouse, polyclonal; Wako). After washing with PBS, secondary antibody staining was applied for 2 h at RT (goat anti-hamster, Alexa Fluor 594; Thermo Fisher Scientific; donkey anti-rat, Alexa Fluor 647; abcam; donkey anti-goat, Alexa Fluor 594; Invitrogen; donkey anti-rabbit, Alexa Fluor 488; Invitrogen; goat anti-rat, Alexa Fluor 647; Invitrogen; goat anti-rabbit, Alexa Fluor 594; Invitrogen; donkey anti-goat, Alexa Fluor 594; Invitrogen; donkey anti-rabbit, Alexa Fluor 488; Invitrogen; goat anti-chicken, Alexa Fluor 488; Invitrogen). Nuclei were stained with DAPI (1:4´000; Invitrogen) for 5 min at RT and the sections were mounted with Fluoromount^{TM} Aqueous Mounting medium. Images were acquired in a confocal microscope (LSM 880, Carl Zeiss, Germany). For the quantification of T cell distribution and cell count, combined tile and z-scan were acquired in the lesion area and quantified with the Cell Counter plugin in FIJI. The count of extralesional cells were performed online at an immunofluorescence microscope. Coverage analysis was performed in FIJI, following manual selection of a threshold that was kept consistent across images.

Human brain sample and immunofluorescence

Ethical approval for the use of human postmortem material was granted according to institutional ethics board protocol and national regulations by the Hungarian Medical Research Council Scientific and Research Ethics Board (19312/2016/EKU). Clinical information of the donor patient is summarized below:

	Age	Sex	Cause of death	*Post-mortem* delay	Timepoint after stroke
	78	male	acute heart and respiratory failure	3 hours 49 min	2 months

Brain samples were fixed in 4% paraformaldehyde and sectioned at a vibratome. Free-floating brain sections were washed with 0.1 phosphate buffer and 1X TBS before blocking with human serum albumin blocking buffer for 1 h at room temperature. Subsequently, sections were stained for 48h at 4°C with primary antibody (CD3, 1:100, mouse anti-human, clone F7.2.38; Invitrogen; CD69, 1:100, rabbit anti-human, clone EPR21814; abcam). After washing with TBS, secondary antibody staining was applied overnight at 4°C (goat anti-mouse, Alexa Fluor 647; Invitrogen; goat anti-rabbit, Alexa Fluor 647; Invitrogen). Nuclei were stained with DAPI (1:4´000; Invitrogen) for 2 min at RT and the sections were mounted with Fluoromount^{TM} Aqueous Mounting medium. Images were acquired in a confocal microscope (LSM 880, Carl Zeiss, Germany).

Microglia morphology analysis

Automated microglia morphology analysis was performed as previously published (Heindl et al., 2018). Briefly, mice were transcardially perfused with saline and 4% paraformaldehyde solution. The brains were post-fixed with 4% paraformaldehyde overnight at 4°C and dehydrated for 2 d in 30% sucrose in PBS. Then the brains were embedded in 4% agarose and cut in 100-µm-thick sections at a Leica Vibratome. Immunofluorescence was performed as described above, using Iba1 (1:200, rabbit anti-mouse, polyclonal; Wako) as primary and antibodies goat anti-rabbit Alexa Fluor 594 (Invitrogen) as secondary antibody. Z-stack images were acquired with a 40× objective in a resolution of 1´024 × 1´024 pixels (x–y-pixel size = 0.15598 µm) and a slice distance (z) of 0.4 µm. The raw confocal z-stacks were then analyzed using the Microglia Morphology Quantification Tool (MMQT) for automated analysis of microglial morphology (https://github.com/isdneuroimaging/mmqt).

Single-molecule fluorescence *in situ* hybridization (smFISH)

Single-molecule fluorescence *in situ* hybridization (smFISH) was performed using the RNAscope^{TM} Multiplex Fluorescent Reagent Kit v2 (Advanced Cell Diagnostics) following manufacturer's protocols. Briefly, cryo-sections were washed and incubated in RNAscope^{TM} hydrogen peroxide. Antigen retrieval and protease III treatment were performed as per protocol. Sections were then incubated with the probe (*Mm-Cxcl9*, *Mm-Cxcl10*, *Mm-Cxcl16* and *Mm-Hexb*) for 2 hr at 40°C and then immediately washed with wash buffer. Next, sections were incubated with RNAscope^{TM} Multiplex FL v2 AMP1, AMP2, and AMP3 and then probes were counterstained with TSA Plus Cy5. Subsequently, the immunofluorescence staining protocol described above was used. Chemokine smFISH was combined with Iba1 and GFAP staining and Iba1+, GFAP+ or Iba1-GFAP- cells coexpressing the probe were quantified in the lesion and perilesional area. For the quantification of chemokine density, single spots were automatically detected using Imaris x64

(8.4.0; Bitplane), while position of CD3+ T cells was evaluated manually. Data were combined and visualized using a custum R script. Hexb smFISH was combined with Iba1 and P2ry12 and the number of microglia (Iba1+P2ry12+Hexb+) and macrophages (Iba1+P2ry12–Hexb–) was quantified in the lesion, perilesional and contralateral cortex.

Organ collection and cell isolation

Mice were overdosed with anesthesia and transcardially perfused with saline containing 2U/mL heparin. Both brain and spleen were dissected, and blood was collected through cardiac puncture in EDTA tubes. In a subset of experiments, mice were injected i.v. with 3 µg CD45-eFluor450 (clone 30-F11; Invitrogen), 3 min before transcardiac perfusion, to exclude blood contamination in the brain parenchyma. For brain, both hemispheres were carefully removed, separated, and tissue was mechanically dissociated with Dounce homogenizer. Mononuclear cells were enriched using discontinuous 70%/30% Percoll gradients. Then, cells were isolated, filtered and washed in FACS buffer. Spleen was mashed on a 40-µm filter. Cells were incubated in red blood cell (RBC) lysis buffer for 2 minutes. Mononuclear cells from blood were isolated using Histopaque gradient.

Flow cytometry

For differentiation of live and dead cells, we stained cells with the Zombie NIR Fixable Viability Kit according to the manufacturer's instructions (Biolegend). Nonspecific binding was blocked by incubation for 10 min at 4°C with anti-CD16/CD32 antibody (1:100, clone 93; eBioscience) and cells were stained with the appropriate antibodies for 15 min at 4°C. Whenever 2 or more antibodies were conjugated with Brilliant Violet fluorophores, antibodies were mixed in Brilliant Stain Buffer (BD biosciences) instead of standard FACS buffer. The following antibodies were used for extracellular staining: CD45-eFluor450 (1:200, clone 30-F11; eBioscience), CD45-APC/Cy7 (1:200, clone 30-F11; Biolegend), CD44-BV510 (1:200, clone IM7; Biolegend), CD44-AlexaFluor532 (1:200, clone IM7; eBioscience), CD69-FITC (1:100, clone H1.2F3; eBioscience), CD69-BV480 (1:50, clone H1.2F3; BD biosciences), Klrg1-PE (1:200, clone 2F1/KLRG1; Biolegend), CD4-PerCP/Cy5.5 (1:200, clone RM4-5; eBioscience), CD4-APC/Fire810 (1:500, clone GK1.5; Biolegend), CD103-PE/Cy7 (1:200, clone 2E7; eBioscience), CD3-BV421 (1:50, clone 17A2; Biolegend), CD3-FITC (1:200, clone 17A2; eBioscience), CD3-APC (1:200, clone 17A2; eBioscience), CD8a-BV510 (1:100, clone 53-6.7; BD biosciences), CD8a-PE (1:200, clone 53-6.7; eBioscience), CD8a-APC/Cy7 (1:200, clone 53-6.7; Biolegend), CD62L-BV650 (1:100, clone MEL-14; BD biosciences), B220-BV785 (1:200, RA3-6B2; Biolegend), CD11b-FITC (1:200, clone M1/70; BD biosciences), CD11b-PerCP/Cy5.5 (1:200, clone M1/70; eBioscience), CD11b-PE (1:200, clone M1/70; eBioscience), CD11b-PE/Cy7 (1:200, clone M1/70; eBioscience), CD19-PE/Cy7 (1:200, clone eBio1D3 (1D3); eBioscience), CD19-BV570 (1:200,6D5; Biolegend), PD-1-BV605 (1:100, clone J43; BD biosciences), Lag-3-PE (1:200, clone eBioC9B7W (C9B7W); eBioscience), H2Kb-APC (1:100, clone AF6-88.5; Biolegend), H2Db-PE/Cy7 (1:100, clone KH95; Biolegend), MHC-II-PE (1:500, clone NMR-4, eBioscience). When chemokine receptors were stained, antibodies were incubated for 15 minutes at RT before all the other extracellular markers. The antibodies used were CXCR3-BV421 (1:100, clone CXCR3-173; Biolegend) and CXCR6-PE/Cy7 (1:200, clone SA051D1; Biolegend). For intracellular staining, Foxp3 / Transcription Factor Staining Buffer Set (eBioscience) was used following the provider guidelines and the

antibody FoxP3-AF647 (1:100, clone MF-14; BioLegend) was used. Samples were acquired using a Northern lights™ flow cytometer (Cytek Biosciences, US) and analyzed with FlowJo v10.9.

Single-cell mRNA sequencing and TCR profiling

Mononuclear cell suspensions from brain and blood were incubated with anti-CD16/CD32 antibody to block nonspecific binding and stained with CD45-eFluor450 (1:400, clone 30-F11; eBioscience), CD3-APC (1:200, clone 17A2; eBioscience), CD11b-PE/Cy7 (1:200, clone M1/70; eBioscience), TotalSeq-C0001 CD4 (1:50, Biolegend) and TotalSeq-C0002 CD8a (1:50, Biolegend). Cell suspensions from different mice were also stained with four unique hashtag antibodies (1:50, TotalSeq-C0301, -C0302, -C0303 and -C0304, Biolegend). All surface antibodies and hashtag antibodies were incubated for 30 min at 4ºC. Then, cell suspensions were pooled together by organ, labelled with propidium iodide to exclude dead cells and sorted for PI-CD45+CD11b-CD3+ (SH800S Cell Sorter, Sony Biotechnology). Sorted cells were centrifuged and resuspended to a final concentration of 1000 cells/µl. ScSseq and cell hashing libraries were prepared using the 10x Chromium Single Cell 5′ Solution combined feature barcoding technology for cell surface proteins. VDJ libraries were prepared using 10x Chromium Next GEM Single Cell V(D)J Reagent Kits.

Quality control of all cDNA samples was performed with a Bioanalyzer 2100 (Agilent Technologies) and libraries were quantified with the Qubit dsDNA HS kit. Gene expression libraries were sequenced on an Illumina NextSeq 1000 using 20,000 reads per cell. Cell-surface protein expression and VDJ sequence libraries were sequenced on an Illumina NextSeq 1000 aiming for 5,000 reads per cell.

Single-cell sequencing data processing and analysis

Cell Ranger software was used for initial sample demultiplexing, raw data processing, alignment to the mouse mm10 reference genome and summary of unique molecular identifier (UMI) counts. Barcodes with UMI counts that did not pass the threshold for cell detection were excluded. Cell Ranger-generated matrices were further analyzed using the R package Seurat. As additional quality control steps, the following cells were excluded: (1) cells with no or more than one hashtag oligos (doublets) detected; (2) cells with a number of detected genes <200 or >2500; (4) cells with >5% of counts that belonged to mitochondrial genes. Raw gene counts for cells that passed this additional quality control were log-normalized, scaled and regressed against the number of UMIs and mitochondrial RNA content per cell to remove unwanted sources of variation. Data was subjected to principal component analysis, using the variable features obtained with the MeanVarPlot method. Unsupervised clusters were obtained by the Louvain clustering method and visualized using Uniform Manifold Approximation and Projection (UMAP) representations. Clusters of non-T cells clusters were excluded (5% of total cells). Subsequent analysis was conducted separately for CD8+ and CD4+ T cells, based on the cell surface protein expression of these markers. After subsetting, normalization, scaling, dimensionality reduction and clustering were performed again. Differentially expressed genes between clusters were calculated using the FindMarkers function. Pseudotime analysis was computed on the corresponding UMAP projections using Monocle 3 (Cao et al., 2019). Clonality analysis was conducted using the scRepertoire package (Borcherding and Bormann, 2020). Clones were defined using the most stringer criterion, namely the correspondence of gene usage and nucleotide sequence.

Migration vs. proliferation assay of brain T cells

To track migration of T cells from the blood circulation into the brain parenchyma, mice were injected i.v. with 3 µg CD45-eFluor450 (clone 30-F11; Invitrogen). After 3 days, mice were injected i.v. with 3 µg of CD45 conjugated with a different fluorophore (APC-/Cy7, clone 30-F11; Biolegend), 3 min before transcardiac perfusion, to exclude blood contamination in the brain parenchyma. Brain and blood where then processed for flow cytometry. In a subset of experiments, migration assessment was combined with an in vivo cell proliferation assay, where mice were treated with EdU (0.5 mg/ml; Invitrogen) in sucrose-enriched drinking water (5 g sucrose in 100 ml) for 3 d, concomitantly with the first CD45 antibody i.v. injection. EdU was detected using a Click-iT EdU Alexa Fluor 647 Flow Cytometry Assay Kit (C10419; Invitrogen) following the manufacturer's instructions. Gating strategy was based on an untreated negative control sample.

Adoptive transfer of T cells into RAG$^{-/-}$ mice

T cells were isolated as described above. A cohort of 10 Rag1$^{-/-}$ mice was adoptively transferred with a mixture of eGFP and CXCR3$^{-/-}$ T cells, injected i.p. at 4-6 week of age. A different cohort of 10 Rag1$^{-/-}$ mice was adoptively transferred with a mixture of tdTomato and CXCR6$^{-/-}$ T cells. Approximately $6 \cdot 10^6$ WT and $6 \cdot 10^6$ knock-out cells were injected. Mice were left for one month, to allow the reconstitution of the T cell population, before inducing stroke.

RNA extraction and qPCR

Ipsi- and contralateral brain cortex was microdissected and stored in RNAlater®. Tissue was dissociated using innuSPEED Lysis A tubes. RNA was extracted from the lysate using MaXtract High Density tubes (Qiagen), following manufacturer´s instruction, and further purified using the RNeasy Mini Kit (Qiagen). RNA quantity was measured with Nanodrop and samples were diluted to the lowest concentration. cDNA was synthetized using the High-Capacity cDNA Reverse Transcription Kit (ThermoFisher). The following primers were used:

	forward	Reverse
PPIA	ACACGCCATAATGGCACTGG	ATTTGCCATGGACAAGATGCC
CXCL9	CGCTGTTCTTTTCCTCTTGGG	CATTCCTTATCACTAGGGTTCCTCG
CXCL10	CCACGTGTTGAGATCATTGCC	GAGGCTCTCTGCTGTCCATC
CXCL16	TCGTACCATTTCTTCTGGCACC	CATGACCAGTTCCACACTCTTTGC

The QuantiNova SYBR Green PCR Kit (Qiagen) was used with a LightCycler 480 II (Roche). All gene expression was expressed relative to the PPIA house keeping gene and calculated using the relative standard curve method.

Golgi-Cox staining

Mice were perfused 84d after photothrombosis with saline and then aldehyde fixative solution (003780; Bioenno). Brains were carefully dissected and post-fixed at 4°C overnight. 100 µm-thick brain slices were obtained with a vibratome and stained with impregnation slice Golgi Kit (003760; Bioenno) solution for 5d in darkness, as per manufacturer´s guidelines (Bioenno). Images of dendrites were collected in the perilesional area, in cortical layer II/III. Collectively, images of 25 dendrites per animal (5 dendrites from 5 neurons) in both ipsi- and contralateral hemispheres were acquired using an Axio Imager.M2 at a 100× magnification (EC Plan-Neofluar objective, numerical aperture [NA] = 1.3, oil immersion, acquisition at 18–20°C) using the AxioCam MRc and AxioVision 4.8.2 software. Dendrites were then 3D reconstructed and the spine density evaluated using Imaris x64 (8.4.0; Bitplane).

Statistics

Data were analyzed using GraphPad Prism (v8.4). Summary data were plotted as mean ± standard deviation. 2-group experiments were analysed with a Student's t test or, in case of a non-normal distrubution, Mann-Whitney U test. Experiments with more than 2 groups were analysed using one-way ANOVA. *In vivo* calcium imaging data were analysed using a mixed-effects model. A p-value lower than 0.05 was considered statistically significant.

Author contributions. A. Ricci conceptualized experiments, performed most of the experiments, analyzed the data and wrote the manuscript; S. Heindl performed and analyzed experiments. O. Carofiglio and A. Simats performed experiments; E. Beltran contributed to the analysis of sequencing data. R. Fekete and A. Denes selected and provided the human tissue samples. S. Bittner provided experimental resources. A. Liesz initiated the study, conceptualized and supervised the research and wrote the manuscript. All authors reviewed the manuscript.

Acknowledgement. We would like to thank Kerstin Thuß-Silczak and Christina Bauer for technical support. We would also like to thank Prof. Wayne Yokoyama for providing the $B2m^{fl/fl}$ mice. This work was funded by the European Research Council (ERC-StGs 802305), the Hungarian Brain Research Program (2017-1.2.1-NKP-2017-00002) and the German Research Foundation (DFG) under Germany's Excellence Strategy (EXC 2145 SyNergy – ID 390857198), through the CRC TRR274 (ID 408885537), the CRC TRR355 (ID 490846870) and under the grants LI-2534/6-1 and LI-2534/7-1.

Competing interests. All authors state that they have no competing financial interest related to the presented work besides the listed funding sources.

References

Alves de Lima, K., J. Rustenhoven, S. Da Mesquita, M. Wall, A.F. Salvador, I. Smirnov, G. Martelossi Cebinelli, T. Mamuladze, W. Baker, Z. Papadopoulos, M.B. Lopes, W.S. Cao, X.S. Xie, J. Herz, and J. Kipnis. 2020. Meningeal γδ T cells regulate anxiety-like behavior via IL-17a signaling in neurons. *Nat Immunol*. 21:1421–1429. doi:10.1038/s41590-020-0776-4.

Benakis, C., A. Simats, S. Tritschler, S. Heindl, S. Besson-Girard, G. Llovera, K. Pinkham, A. Kolz, A. Ricci, F.J. Theis, S. Bittner, Ö. Gökce, A. Peters, and A. Liesz. 2022. T cells modulate the microglial response to brain ischemia. *Elife*. 11. doi:10.7554/ELIFE.82031.

Bern, M.D., B.A. Parikh, L. Yang, D.L. Beckman, J. Poursine-Laurent, and W.M. Yokoyama. 2019. Inducible down-regulation of MHC class I results in natural killer cell tolerance. *J Exp Med*. 216:99–116. doi:10.1084/jem.20181076.

Borcherding, N., and N.L. Bormann. 2020. scRepertoire: An R-based toolkit for single-cell immune receptor analysis. *F1000Res*. 9:47. doi:10.12688/f1000research.22139.1.

Cao, J., M. Spielmann, X. Qiu, X. Huang, D.M. Ibrahim, A.J. Hill, F. Zhang, S. Mundlos, L. Christiansen, F.J. Steemers, C. Trapnell, and J. Shendure. 2019. The single-cell transcriptional landscape of mammalian organogenesis. *Nature*. 566:496–502. doi:10.1038/s41586-019-0969-x.

Cramer, J. V., C. Benakis, and A. Liesz. 2019a. T cells in the post-ischemic brain: Troopers or paramedics? *J Neuroimmunol*. 326:33–37. doi:10.1016/j.jneuroim.2018.11.006.

Cramer, J. V., B. Gesierich, S. Roth, M. Dichgans, M. Düring, and A. Liesz. 2019b. In vivo widefield calcium imaging of the mouse cortex for analysis of network connectivity in health and brain disease. *Neuroimage*. 199:570–584. doi:10.1016/J.NEUROIMAGE.2019.06.014.

Doyle, K.P., L.N. Quach, M. Solé, R.C. Axtell, T.-V. V Nguyen, G.J. Soler-Llavina, S. Jurado, J. Han, L. Steinman, F.M. Longo, J.A. Schneider, R.C. Malenka, and M.S. Buckwalter. 2015. B-lymphocyte-mediated delayed cognitive impairment following stroke. *J Neurosci*. 35:2133–45. doi:10.1523/JNEUROSCI.4098-14.2015.

Feigin, V.L., B.A. Stark, C.O. Johnson, G.A. Roth, C. Bisignano, G.G. Abady, M. Abbasifard, M. Abbasi-Kangevari, F. Abd-Allah, V. Abedi, A. Abualhasan, N.M. Abu-Rmeileh, A.I. Abushouk, O.M. Adebayo, G. Agarwal, P. Agasthi, B.O. Ahinkorah, S. Ahmad, S. Ahmadi, Y. Ahmed Salih, B. Aji, S. Akbarpour, R.O. Akinyemi, H. Al Hamad, F. Alahdab, S.M. Alif, V. Alipour, S.M. Aljunid, S. Almustanyir, R.M. Al-Raddadi, R. Al-Shahi Salman, N. Alvis-Guzman, R. Ancuceanu, D. Anderlini, J.A. Anderson, A. Ansar, I.C. Antonazzo, J. Arabloo, J. Ärnlöv, K.D. Artanti, Z. Aryan, S. Asgari, T. Ashraf, M. Athar, A. Atreya, M. Ausloos, A.A. Baig, O.C. Baltatu, M. Banach, M.A. Barboza, S.L. Barker-Collo, T.W. Bärnighausen, M.T.U. Barone, S. Basu, G. Bazmandegan, E. Beghi, M. Beheshti, Y. Béjot, A.W. Bell, D.A. Bennett, I.M. Bensenor, W.M. Bezabhe, Y.M. Bezabih, A.S. Bhagavathula, P. Bhardwaj, K. Bhattacharyya, A. Bijani, B. Bikbov, M.M. Birhanu, A. Boloor, A. Bonny, M. Brauer, H. Brenner, D. Bryazka, Z.A. Butt, F.L. Caetano dos Santos, I.R. Campos-Nonato, C. Cantu-Brito, J.J. Carrero, C.A. Castañeda-Orjuela, A.L. Catapano, P.A. Chakraborty, J. Charan, S.G. Choudhari, E.K. Chowdhury, D.-T. Chu, S.-C. Chung, D. Colozza, V.M. Costa, S. Costanzo, M.H. Criqui, O. Dadras, B. Dagnew, X. Dai, K. Dalal, A.A.M.

Damasceno, E. D'Amico, L. Dandona, et al. 2021. Global, regional, and national burden of stroke and its risk factors, 1990–2019: a systematic analysis for the Global Burden of Disease Study 2019. *Lancet Neurol*. 20:795–820. doi:10.1016/S1474-4422(21)00252-0.

Filiano, A.J., Y. Xu, N.J. Tustison, R.L. Marsh, W. Baker, I. Smirnov, C.C. Overall, S.P. Gadani, S.D. Turner, Z. Weng, S.N. Peerzade, H. Chen, K.S. Lee, M.M. Scott, M.P. Beenhakker, V. Litvak, and J. Kipnis. 2016. Unexpected role of interferon-γ in regulating neuronal connectivity and social behaviour. *Nature*. 535:425–9. doi:10.1038/nature18626.

Goddery, E.N., C.E. Fain, C.G. Lipovsky, K. Ayasoufi, L.T. Yokanovich, C.S. Malo, R.H. Khadka, Z.P. Tritz, F. Jin, M.J. Hansen, and A.J. Johnson. 2021. Microglia and Perivascular Macrophages Act as Antigen Presenting Cells to Promote CD8 T Cell Infiltration of the Brain. *Front Immunol*. 12. doi:10.3389/fimmu.2021.726421.

Heindl, S., B. Gesierich, C. Benakis, G. Llovera, M. Duering, and A. Liesz. 2018. Automated Morphological Analysis of Microglia After Stroke. *Front Cell Neurosci*. 12. doi:10.3389/FNCEL.2018.00106.

Heindl, S., A. Ricci, O. Carofiglio, Q. Zhou, T. Arzberger, N. Lenart, N. Franzmeier, T. Hortobagyi, P.T. Nelson, A.M. Stowe, A. Denes, D. Edbauer, and A. Liesz. 2021. Chronic T cell proliferation in brains after stroke could interfere with the efficacy of immunotherapies. *J Exp Med*. 218. doi:10.1084/jem.20202411.

Iadecola, C., M.S. Buckwalter, and J. Anrather. 2020. Immune responses to stroke: mechanisms, modulation, and therapeutic potential. *Journal of Clinical Investigation*. 130:2777–2788. doi:10.1172/JCI135530.

Kilkenny, C., W.J. Browne, I.C. Cuthill, M. Emerson, and D.G. Altman. 2010. Improving Bioscience Research Reporting: The ARRIVE Guidelines for Reporting Animal Research. *PLoS Biol*. 8:e1000412. doi:10.1371/JOURNAL.PBIO.1000412.

Lambertsen, K.L., K. Biber, and B. Finsen. 2012. Inflammatory Cytokines in Experimental and Human Stroke. *Journal of Cerebral Blood Flow & Metabolism*. 32:1677–1698. doi:10.1038/jcbfm.2012.88.

Llovera, G., K. Pinkham, and A. Liesz. 2021. Modeling Stroke in Mice: Focal Cortical Lesions by Photothrombosis. *J Vis Exp*. 2021. doi:10.3791/62536.

Llovera, G., S. Roth, N. Plesnila, R. Veltkamp, and A. Liesz. 2014. Modeling stroke in mice: permanent coagulation of the distal middle cerebral artery. *J Vis Exp*. doi:10.3791/51729.

Masuda, T., L. Amann, R. Sankowski, O. Staszewski, M. Lenz, P. d´Errico, N. Snaidero, M.J. Costa Jordão, C. Böttcher, K. Kierdorf, S. Jung, J. Priller, T. Misgeld, A. Vlachos, M. Meyer-Luehmann, K.-P. Knobeloch, and M. Prinz. 2020. Novel Hexb-based tools for studying microglia in the CNS. *Nat Immunol*. 21:802–815. doi:10.1038/s41590-020-0707-4.

Pu, L., L. Wang, R. Zhang, T. Zhao, Y. Jiang, and L. Han. 2023. Projected Global Trends in Ischemic Stroke Incidence, Deaths and Disability-Adjusted Life Years From 2020 to 2030. *Stroke*. 54:1330–1339. doi:10.1161/STROKEAHA.122.040073.

Ren, H.M., E.M. Kolawole, M. Ren, G. Jin, C.S. Netherby-Winslow, Q. Wade, Shwetank, Z.S.M. Rahman, B.D. Evavold, and A.E. Lukacher. 2020. IL-21 from high-affinity CD4 T cells drives differentiation of brain-resident CD8 T cells during persistent viral infection. *Sci Immunol*. 5. doi:10.1126/sciimmunol.abb5590.

Rosen, S.F., A.L. Soung, W. Yang, S. Ai, M. Kanmogne, V.A. Davé, M. Artyomov, J.A. Magee, and R.S. Klein. 2022. Single-cell RNA transcriptome analysis of CNS immune cells reveals CXCL16/CXCR6 as maintenance factors for tissue-resident T cells that drive synapse elimination. *Genome Med*. 14:108. doi:10.1186/s13073-022-01111-0.

Schenkel, J.M., and D. Masopust. 2014. Tissue-Resident Memory T Cells. *Immunity*. 41:886–897. doi:10.1016/j.immuni.2014.12.007.

Shi, L., Z. Sun, W. Su, F. Xu, D. Xie, Q. Zhang, X. Dai, K. Iyer, T.K. Hitchens, L.M. Foley, S. Li, D.B. Stolz, K. Chen, Y. Ding, A.W. Thomson, R.K. Leak, J. Chen, and X. Hu. 2021. Treg cell-derived osteopontin promotes microglia-mediated white matter repair after ischemic stroke. *Immunity*. 54:1527-1542.e8. doi:10.1016/J.IMMUNI.2021.04.022.

Sporici, R., and T.B. Issekutz. 2010. CXCR3 blockade inhibits T-cell migration into the CNS during EAE and prevents development of adoptively transferred, but not actively induced, disease. *Eur J Immunol*. 40:2751–61. doi:10.1002/eji.200939975.

Steinbach, K., I. Vincenti, M. Kreutzfeldt, N. Page, A. Muschaweckh, I. Wagner, I. Drexler, D. Pinschewer, T. Korn, and D. Merkler. 2016. Brain-resident memory T cells represent an autonomous cytotoxic barrier to viral infection. *Journal of Experimental Medicine*. 213:1571–1587. doi:10.1084/jem.20151916.

Su, W., J. Saravia, I. Risch, S. Rankin, C. Guy, N.M. Chapman, H. Shi, Y. Sun, A. Kc, W. Li, H. Huang, S.A. Lim, H. Hu, Y. Wang, D. Liu, Y. Jiao, P.-C. Chen, H. Soliman, K.-K. Yan, J. Zhang, P. Vogel, X. Liu, G.E. Serrano, T.G. Beach, J. Yu, J. Peng, and H. Chi. 2023. CXCR6 orchestrates brain CD8+ T cell residency and limits mouse Alzheimer's disease pathology. *Nat Immunol*. 24:1735–1747. doi:10.1038/s41590-023-01604-z.

Szabo, P.A., M. Miron, and D.L. Farber. 2019. Location, location, location: Tissue resident memory T cells in mice and humans. *Sci Immunol*. 4. doi:10.1126/sciimmunol.aas9673.

Tse, S.-W., A.J. Radtke, D.A. Espinosa, I.A. Cockburn, and F. Zavala. 2014. The chemokine receptor CXCR6 is required for the maintenance of liver memory $CD8^+$ T cells specific for infectious pathogens. *J Infect Dis*. 210:1508–16. doi:10.1093/infdis/jiu281.

Vincenti, I., N. Page, K. Steinbach, A. Yermanos, S. Lemeille, N. Nunez, M. Kreutzfeldt, B. Klimek, G. Di Liberto, K. Egervari, M. Piccinno, G. Shammas, A. Mariotte, N. Fonta, N. Liaudet, D. Shlesinger, A.R. Liuzzi, I. Wagner, C. Saadi, C. Stadelmann, S. Reddy, B. Becher, and D. Merkler. 2022. Tissue-resident memory CD8+ T cells cooperate with CD4+ T cells to drive compartmentalized immunopathology in the CNS. *Sci Transl Med*. 14:eabl6058. doi:10.1126/scitranslmed.abl6058.

Werner, Y., E. Mass, P. Ashok Kumar, T. Ulas, K. Händler, A. Horne, K. Klee, A. Lupp, D. Schütz, F. Saaber, C. Redecker, J.L. Schultze, F. Geissmann, and R. Stumm. 2020. Cxcr4 distinguishes HSC-

derived monocytes from microglia and reveals monocyte immune responses to experimental stroke. *Nat Neurosci*. 23:351–362. doi:10.1038/s41593-020-0585-y.

Yshii, L., E. Pasciuto, P. Bielefeld, L. Mascali, P. Lemaitre, M. Marino, J. Dooley, L. Kouser, S. Verschoren, V. Lagou, H. Kemps, P. Gervois, A. de Boer, O.T. Burton, J. Wahis, J. Verhaert, S.H.K. Tareen, C.P. Roca, K. Singh, C.E. Whyte, A. Kerstens, Z. Callaerts-Vegh, S. Poovathingal, T. Prezzemolo, K. Wierda, A. Dashwood, J. Xie, E. Van Wonterghem, E. Creemers, M. Aloulou, W. Gsell, O. Abiega, S. Munck, R.E. Vandenbroucke, A. Bronckaers, R. Lemmens, B. De Strooper, L. Van Den Bosch, U. Himmelreich, C.P. Fitzsimons, M.G. Holt, and A. Liston. 2022. Astrocyte-targeted gene delivery of interleukin 2 specifically increases brain-resident regulatory T cell numbers and protects against pathological neuroinflammation. *Nat Immunol*. 23:878–891. doi:10.1038/s41590-022-01208-z.

Zbesko, J.C., T.-V. V Nguyen, T. Yang, J.B. Frye, O. Hussain, M. Hayes, A. Chung, W.A. Day, K. Stepanovic, M. Krumberger, J. Mona, F.M. Longo, and K.P. Doyle. 2018. Glial scars are permeable to the neurotoxic environment of chronic stroke infarcts. *Neurobiol Dis*. 112:63–78. doi:10.1016/j.nbd.2018.01.007.

Zhang, B., Y.K. Chan, B. Lu, M.S. Diamond, and R.S. Klein. 2008. CXCR3 mediates region-specific antiviral T cell trafficking within the central nervous system during West Nile virus encephalitis. *J Immunol*. 180:2641–9. doi:10.4049/jimmunol.180.4.2641.

Supplemental material

Figure S1

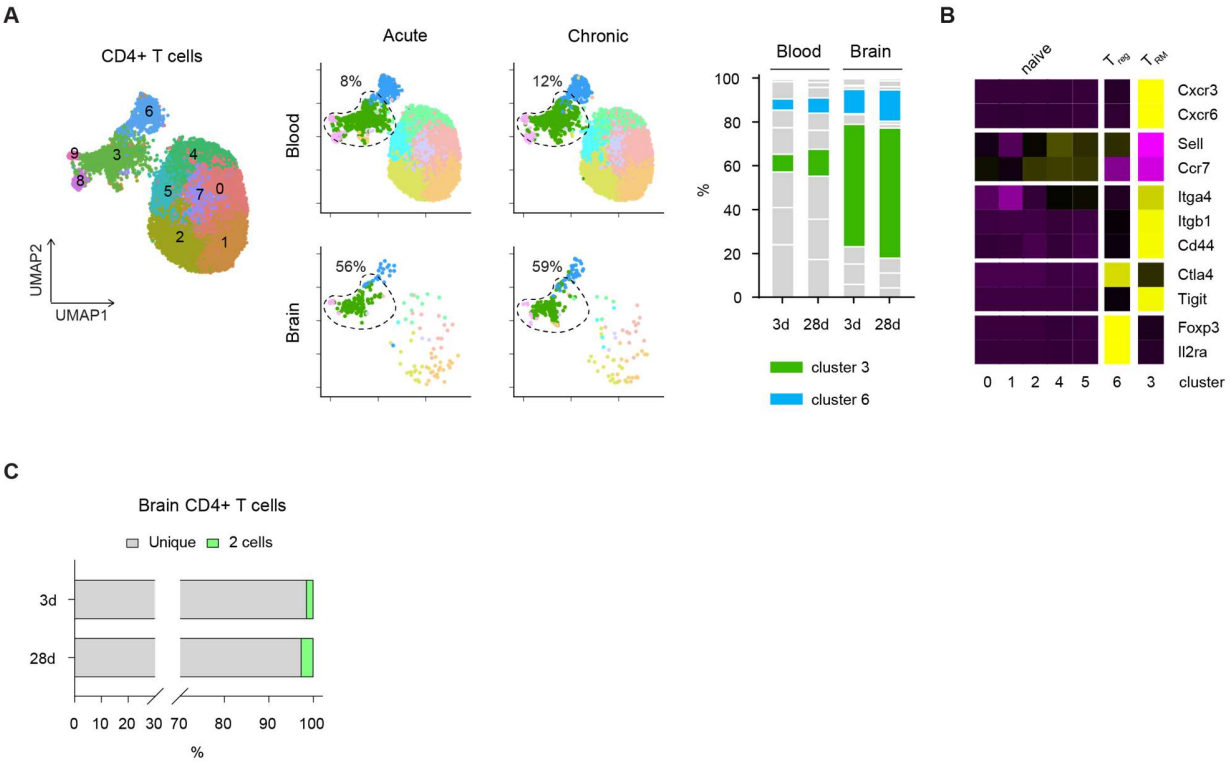

Figure S1. Characterization of brain CD4+ T cells after stroke. (A) UMAP of 11´978 CD4+ T cells, combined (left) and subset by organ and time point (center). Dashed lines encircle cells from cluster 3, whose percentage is reported. Bar plot show the percentages of different clusters per sample, with a focus on cluster 3 and cluster 6, corresponding to Treg (right). **(B)** Heatmap showing normalized expressions of T_{RM} signature genes across different clusters. **(C)** Percentage of clonally expanded CD4+ T cells in the brain at 3d and 28d after stroke.

Figure S2

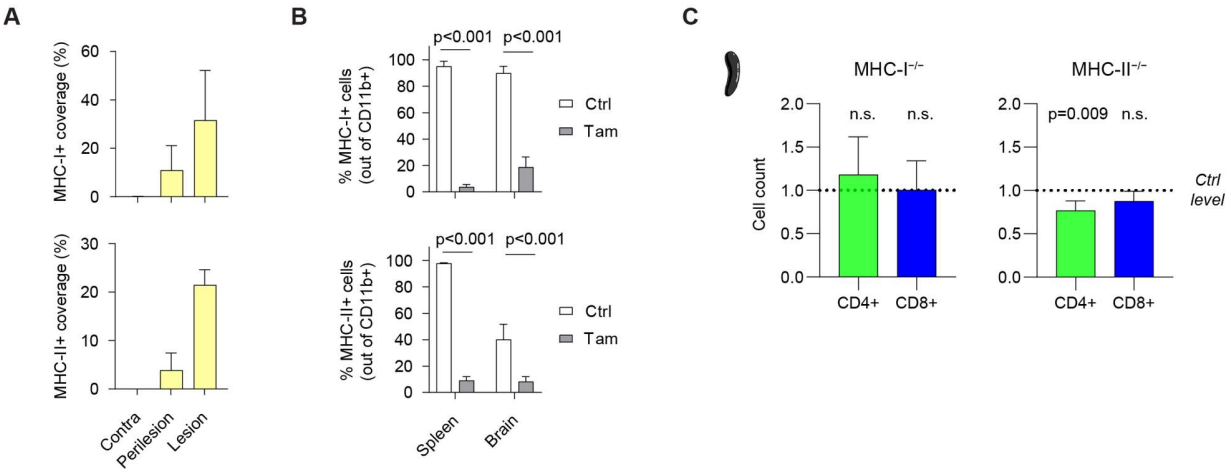

Figure S2. Role of MHC-I and -II in post-stroke T_{RM} accumulation (A) Quantification of MHC class I and II coverage in the lesion core and contralateral and perilesional cortex. n= 4. **(B)** Quantification of KO efficiency in MHC-I$^{-/-}$ and MHC-II$^{-/-}$ in spleen and brain (CD45hi cells), showing a high degree of induced recombination. For MHC-I$^{-/-}$, Ctrl and KO: n = 13. For MHC-II$^{-/-}$, Ctrl: n = 9, KO: n = 12. Unpaired t test. **(C)** Flow cytometric quantification of CD4+ and CD8+ T cells in spleen, after induction of MHC class I or MHC class II knock-out. Cell numbers were normalized to control levels. Overall, knock-out does not affect the number of peripheral T cells, with the exception of a minor reduction of CD4+ T cells upon MHC-II knock-out induction. For MHC-I$^{-/-}$, Ctrl: n = 12, KO: n = 11. For MHC-II$^{-/-}$, Ctrl: n = 7, KO: n = 10. Unpaired t test.

4 DISCUSSION

4.1 THE CHALLENGE OF BENCH-TO-BEDSIDE TRANSLATION IN THE STROKE FIELD

Considerable attention has been directed toward unraveling the role of T cells during the acute phase following ischemic stroke, with preliminary investigations highlighting their deleterious impact on stroke outcomes (Hum et al., 2007; Kleinschnitz et al., 2010). This has prompted preclinical endeavors aimed at acutely impeding T cell trafficking into the post-ischemic brain. Notable approaches, such as anti-CD49d blockade and Fingolimod, have demonstrated promising and reproducible results in preclinical studies (Dang et al., 2021; Llovera et al., 2015), thereby instigating their translation from bench to bedside, as evidenced by the initiation of several clinical trials.

Despite the initial promise, the efficacy of an anti-CD49d antibody, Natalizumab, was assessed in two phase II clinical trials, ACTION and ACTION II, both showing no improvement in clinical outcome in the treatment arm (Elkind et al., 2020; Elkins et al., 2017). In contrast, Fingolimod positively affected stroke outcomes in multiple exploratory clinical trials (Bai et al., 2022). A detailed comparison of these results requires an examination of the mechanistic differences between the two approaches. Natalizumab specifically targets the CD49d-mediated mechanism of tissue invasion, whereas Fingolimod sequesters T cells within secondary lymphoid organs, preventing tissue invasion by any conceivable mechanism. The CD49d-mediated extravasation holds pivotal significance for blood-brain barrier (BBB) crossing and subsequent brain invasion (Engelhardt & Sorokin, 2009). Notably, in the context of stroke, alternative invasion routes through the choroid plexus and meninges may contribute, and their molecular mediators, distinct from CD49d, remain incompletely characterized (Benakis et al., 2018). Future strategies for acute tissue invasion blockade must account for this heterogeneity to optimize efficacy.

An additional facet to consider in elucidating the translational failure of Natalizumab lies in the discordance between experimental designs in preclinical studies and clinical trials. Mouse model experiments predominantly focused on acute stroke outcomes (Liesz et al., 2011). Furthermore, the first preclinical randomized controlled multicenter trial (pRCT) addressing anti-CD49d therapy revealed efficacy solely in small-sized strokes (Llovera et al., 2015). In contrast, clinical trials predominantly emphasized chronic-phase endpoints,

specifically 90 days post-stroke. Our investigation adopted a reverse translational approach, uncovering that CD49d blockade lacked long-term efficacy in a mouse model of experimental stroke, attributable to T cell accumulation during the chronic phase via local proliferation (Heindl et al., 2021). This underscores the critical importance of aligning experimental designs closely between preclinical and clinical studies to mitigate variables that could compromise the outcomes of resource-intensive clinical trials.

In response to the overarching challenge of failed translation in clinical practice, particularly in the realm of neuroprotective agents, international collaborative efforts have culminated in the formulation of guidelines known as the STAIR guidelines (Stroke Therapy Academic Industry Roundtable, 1999). These guidelines have evolved with additional recommendations (Lapchak et al., 2013), emphasizing crucial aspects such as randomization, reproducibility across diverse laboratories, and the inclusion of factors like sex, age, and comorbidities. Adhering to these guidelines in preclinical research is paramount for identifying robust therapeutic targets with an enhanced likelihood of success when translated to human patients.

An added complexity inherent to the investigation of long-term recovery in stroke research lies in the transient nature of behavioral deficits observed in animal models (Balkaya et al., 2013). The occurrence of spontaneous recovery poses a challenge to the comprehensive evaluation of treatment efficacy during the chronic phase post-stroke. Overcoming this challenge necessitates the implementation of alternative methodologies that can provide a nuanced understanding of the recovery process. In both of our investigations, we employed wide-field calcium imaging to explore functional recovery dynamics (Cramer et al., 2019). This approach enabled the discernment of functional differences among experimental groups for up to three months following stroke induction (Ricci et al., 2024). Beyond its heightened sensitivity, wide-field calcium imaging offers an additional advantage over behavioral assessments by obviating the need for manual scoring, thereby mitigating potential biases introduced by the experimenter. Utilizing calcium imaging for the examination of long-term outcomes following stroke represents a robust methodology that enhances the sensitivity and objectivity of preclinical studies.

4.2 Post-Stroke T Cells as a Tissue-Resident Memory Population

While numerous studies have extensively characterized lymphocyte subsets in the acute phase following a stroke, the immunological landscape in the chronic post-stroke phase

remains elusive. Stubbe et al. initially demonstrated the presence of Treg in the chronic post-stroke brain (Stubbe et al., 2013), followed by confirmation of the presence of B cells and various T cell subtypes (Doyle et al., 2015; Xie et al., 2019). However, a comprehensive characterization of the specific phenotype of these cells was yet to be described.

Our first study unveiled a diverse population of T cell subsets, including activated CD4+ and CD8+ T cells, Treg, and γδ T cells in the chronic post-stroke brain (Heindl et al., 2021). Building upon this, our second study delved into an in-depth characterization of post-stroke T cells, elucidating their acquisition of a tissue-resident memory (T_{RM}) phenotype (Ricci et al., 2024). Traditionally, brain T_{RM} have been studied in models of brain infections, playing a pivotal role as the first line of defense against re-infections. However, recent insights indicate their contribution to a pro-inflammatory milieu within brain tissue across various neurological conditions, including autoimmunity, neurodegeneration, and even after traumatic brain injury (Altendorfer et al., 2022; Beltrán et al., 2019; Chen et al., 2023; Daglas et al., 2019; Machado-Santos et al., 2018; Su et al., 2023). This broad occurrence of T_{RM} across diverse diseases suggests a general phenomenon associated with brain tissue damage.

It is noteworthy that post-stroke T_{RM}, while sharing a primary genetic signature described in the literature (Szabo et al., 2019), exhibit distinct characteristics. The integrin CD103 is a distinctive marker of T_{RM} in various organs, including the brain. Whether post-stroke T_{RM} also express this marker requires further investigation. Furthermore, unlike virus infection-generated T_{RM} persisting beyond the blood-brain barrier, post-stroke T cells primarily localize in the lesion core, where vessels lack astrocyte association and display intrinsic leakiness. Consequently, peripheral injection of depleting antibodies effectively eliminates post-stroke T_{RM}.

By definition, T_{RM} do not rely on continuous replenishment from circulating cells. We demonstrated that brain invasion is very limited in the sub-acute phase. Furthermore, depletion experiments revealed that post-stroke T_{RM} can replenish the brain niche within one week via local proliferation, suggesting homeostatic maintenance (Ricci et al., 2024). In this experiment, we tracked blood-to-brain transmigration via an intravenously injected fluorescently labeled antibody over three days. This approach, while experimentally simple, has limitations such as the decrease in fluorescent signal over time and the restricted observation period. A definitive proof that post-stroke T cells are functionally T_{RM} could come from parabiosis experiments, in which the circulatory systems of two individuals are experimentally connected. In this setting, we would expect that, after the establishment of the post-stroke T cell population, no significant contribution would come from the parabiont. Alternatively, one would need to prove that post-stroke T cells are long-lived and stable by labeling them in a spatially specific manner. Such a condition could be achieved by

photoconversion, a technique that allows shifting the emission spectrum of a fluorescent protein such as Kikume Green-Red in a site-specific manner (Nowotschin & Hadjantonakis, 2009). Unfortunately, this system also suffers from a relatively short time window during which the photoconversion persists (around three days), which is related to protein turnover. Recently, a mouse model expressing a photoactivatable Cre recombinase (PA-Cre) has been developed (Morikawa et al., 2020). This system combines the spatial specificity of a light-induced trigger with the long-term modification of Cre-induced genetic modifications. Combined with a reporter protein, the PA-Cre system would allow labeling post-stroke T_{RM} and following them long-term to study their turnover.

Several cytokines have been implicated in T_{RM} formation and maintenance, including IL-7, IL-15, and TGF-β (Szabo et al., 2019). Interestingly, TGF-β levels are increased in the brain chronically after a stroke (Zbesko et al., 2018). In the acute phase, TGF-β is secreted mainly by microglia and macrophages (Doyle et al., 2010), however the cellular source of this cytokine in the chronic phase has not been described. Studies blocking TGF-β signaling specifically in T cells, for example, by adoptive transfer of TGF-β receptor knock-out cells, could assess whether this cytokine is necessary for post-stroke T_{RM} formation in the context of stroke. Altering TGF-β signaling specifically in T cell is crucial to avoid possible confounding effects, given the highly pleiotropic nature of this cytokine.

Notably, CD8+ T_{RM} formed after viral infections depend on CD4+ T cell-derived IL-21 for their establishment (Ren et al., 2020). In our study, we did not address the potential cross-talk between CD4+ and CD8+ T cells. Depletion experiments for either of the two populations could shed light on these mechanisms and simultaneously discern the subpopulation-specific contribution to stroke recovery.

In our local depletion approach, we observed that post-stroke T_{RM} returns to pre-depletion levels within one week, suggesting the presence of a molecular mechanism that regulates the amount of T cells that can persist within the brain. T cells, particularly Treg, are uniquely dependent on the cytokine IL-2 for their survival, of which they are the main cellular source. In the brain, as opposed to other organs, IL-2 levels are ~tenfold lower than the serum, however the levels of this cytokine are increased in the chronic post-stroke brain (Ito et al., 2019). Therefore, it is plausible that the local production of IL-2 regulates the T cell population size within the post-stroke brain and it favors the proliferation of T cells upon depletion. Based on this hypothesis, we would expect that either increasing IL-2 availability within the brain or injecting an IL-2 neutralizing antibody should affect post-stroke T_{RM} population size. This phenomenon has clear implications when devising approaches aimed at depleting post-stroke T_{RM} to investigate in detail their function. In fact, the short time window during which depletion persists makes challenging to highlight the function of post-

stroke T_{RM}. Alternatively, chronic implants to the lateral ventricles connected with osmotic minipumps allow the infusion of compounds, for example depleting antibodies, long-term and with the advantage of a mostly local action. Such approaches will be crucial to investigate the role of specific cell subpopulations and signaling molecules in the chronic phase after stroke.

In our local depletion strategy, we observed that post-stroke T_{RM} return to pre-depletion levels within one week, indicating the presence of a molecular mechanism governing the number of T cells in the brain. T cells, especially Treg, rely significantly on the cytokine IL-2 for survival, and they are the primary cellular source of this cytokine. In the brain, IL-2 levels are approximately tenfold lower than in the serum (Yshii et al., 2022). Nevertheless, post-stroke brains exhibit increased levels of IL-2, particularly in the chronic phase (Ito et al., 2019). Hence, it is conceivable that locally produced IL-2 regulates T cell population size within the post-stroke brain and promotes T cell proliferation following depletion. Based on this hypothesis, we anticipate that either enhancing IL-2 availability within the brain or administering an IL-2 neutralizing antibody would impact post-stroke T_{RM} population size. This insight holds significant implications for developing strategies to deplete post-stroke T_{RM} and investigate their functions in detail. The brief duration of the depletion window poses challenges in elucidating the role of post-stroke T_{RM}. Alternatively, chronic implantation of cannulas into the lateral ventricles, connected to osmotic minipumps, enables the long-term infusion of compounds such as depleting antibodies, offering the advantage of mostly local action. Such approaches are pivotal for exploring the roles of specific cell subpopulations and signaling molecules during the chronic phase following a stroke.

4.3 The Role of T Cells in Chronic Stroke Outcome

The contribution of lymphocyte subsets to stroke outcome has been extensively studied in the acute phase, with a limited focus on the chronic phase, potentially due to the inherent challenges in investigating long-term functional outcomes after stroke induction.

The majority of research has centered around the role of Treg, which has been demonstrated to restrict astrogliosis and promote white matter integrity, thereby exerting an overall beneficial effect on chronic outcome (Ito et al., 2019; Shi et al., 2021). Building upon these findings, therapeutic approaches have been developed to enhance Treg numbers and improve outcomes. One such approach involves injecting IL-2:IL-2 antibody complexes, effectively increasing the number of Treg (Shi et al., 2021). However, this method lacks brain specificity, potentially leading to global immunosuppression. An alternative strategy

capitalizes on IL-2-induced Treg expansion through the delivery of IL-2 using an adeno-associated viral (AAV) vector. This system ensures spatial and temporal specificity through a triple-lock mechanism: (1) the AAV capsid's brain tropism, (2) transcriptional control under the astrocyte-specific GFAP promoter, and (3) the use of the Tet-On system, inducing transcription upon doxycycline injection (Yshii et al., 2022). Tested in various experimental neurological disease models, including stroke, this system has demonstrated a neuroprotective effect. However, when the triple-lock IL-2 delivery was applied in a "therapeutic fashion", namely after stroke induction, it did not exhibit any beneficial effects. It is crucial to note that the functional outcome in this study was solely assessed by infarct volume; more comprehensive approaches may be necessary to unveil a positive effect.

Initial investigations have revealed the detrimental role of CD8+ T cells in the chronic phase (Selvaraj et al., 2021), while B cells have exhibited both positive and negative effects (Doyle et al., 2015; Ortega et al., 2020). Although these studies highlight the influence of lymphocytes on chronic outcomes, the underlying mechanisms remain poorly understood. Our study demonstrated that lymphocyte-deficient $Rag1^{-/-}$ mice exhibit a clear deficit in the recovery of functional connectivity after stroke, indicating that under normal conditions, they surprisingly promote the natural recovery process (Ricci et al., 2024). While this effect was robust, it is important to note that $Rag1^{-/-}$ mice have the limitations of constitutive lymphocyte absence and a compensatory high level of NK cells. Additionally, CD4+ T cell deficiency has been shown to affect microglia maturation and their synapse pruning activity (Pasciuto et al., 2020). Further experiments are required to elucidate whether lymphocyte deficiency has a direct effect on functional connectivity or if it is partially mediated by microglia.

Microglia are among the first cells to respond to ischemic injury, particularly to danger signals released by damaged neurons. It has been demonstrated that T cells play a crucial role in finely tuning the microglial response in the acute phase, suggesting that this intercellular crosstalk is central to stroke outcome (Benakis et al., 2022). Others have shown that the beneficial effects of Treg on chronic stroke outcome are critically mediated by microglia (Ito et al., 2019; Shi et al., 2021), supporting the notion that the relatively small population of post-stroke T cells has a significantly amplified impact through microglial interactions (Ricci & Liesz, 2023). Our study revealed that even in the chronic phase, T cells can influence microglial reactivity, assessed through their morphology as a proxy (Ricci et al., 2024). Future experiments will be essential to explore the functional implications of this altered reactivity, particularly in assessing whether subacute T cell depletion affects microglial phagocytosis, synaptic pruning activity, and secretory function. As mentioned previously, experiments investigating the specific deletion of CD4+ or CD8+ T cells, and potentially B

cell depletion, will be crucial to unravel the distinct and potentially diverging contributions of lymphocyte subsets to the recovery of neuronal connectivity.

It is noteworthy that the majority of post-stroke T cells localize within the lesion core (Ricci et al., 2024), indicating that secreted factors likely mediate the crosstalk between T cells and nearby neuronal tissue. Upon stroke induction, the infarct region becomes enclosed over time by reactive astrocytes, forming a glial scar (Zhang et al., 2018). While the glial scar restricts axon regeneration, it serves as a crucial barrier to confine tissue damage (Pekny & Pekna, 2014). However, in the chronic phase after stroke, the glial scar does not form a perfect barrier; instead, solutes up to 70 kDa (approximately albumin molecular weight) can permeate from the lesion core to the perilesional brain tissue (Zbesko et al., 2018). Consequently, T cell-secreted factors can easily access the perilesional tissue, influencing the cells in that region.

In addition to the aforementioned effects on microglia, T cell cytokines can also directly impact neuronal function. For instance, IFN-γ has been shown to affect cortical connectivity and social behavior, while IL-17a signals directly to neurons, regulating anxiety-like behavior (Alves de Lima et al., 2020; Filiano et al., 2016). Whether T cells can promote functional connectivity after a stroke by directly influencing neurons is an intriguing possibility that requires further investigation. In the era of single-cell RNA sequencing, it is now possible to sample all cell types in a specific tissue or organ and infer potential cell-cell interactions (Jin et al., 2021). This holistic approach will prove pivotal in understanding the neuroimmune interactions governing functional recovery chronically after a stroke.

4.4 Antigen-Dependent Mechanisms After Stroke

Ischemic stroke leads to consistent brain tissue damage and subsequent release of danger signals and brain antigens. These brain antigens can be transported via lymphatic vessels in the dura mater to the deep cervical lymph nodes, where they have the potential to trigger an immune response (Louveau et al., 2015). Indeed, brain antigens have been identified in draining lymph nodes after stroke (Planas et al., 2012). The question of whether ischemic stroke can instigate an autoimmune response against brain antigens has been the subject of extensive debate (Javidi & Magnus, 2019). Several research groups have reported signs of clonal expansion in brain-invading T cells after stroke (Ito et al., 2019; Liesz et al., 2013), and there is evidence indicating that T cells can respond to brain antigens after stroke induction (Ortega et al., 2015).

In our study, we demonstrated that T cells undergo local proliferation in the post-stroke brain (Heindl et al., 2021) and that this local proliferation can replenish the brain niche following antibody-mediated depletion (Ricci et al., 2024). Furthermore, we detected clonal expansion in CD8+ T cells and not in CD4+ T cells. Notably, inducible knock-out of MHC class I prevented the accumulation of CD8+ T cells in the brain, while MHC class II knock-out did not affect CD4+ T cells. A prior report demonstrated that CD8+ T cells depend on antigen recognition, as ovalbumin-specific CD8+ T cells exhibited a deficit in brain accumulation in the acute phase (Mracsko et al., 2014). Since we induced the knock-out before stroke induction, we cannot distinguish whether this mechanism plays a role in CD8+ T cell accumulation or retention. Further experiments varying the timing of knock-out induction will help elucidate this point. In addition, it would be interesting to combine the depletion approach via antibodies with the induction of MHCs knock-out, to determine whether homeostatic repopulation also relies on antigen presentation.

In the study conducted by Ito and colleagues, they demonstrated deficits in brain accumulation of ovalbumin-specific CD4+ T cells after stroke, suggesting that this specific subpopulation also requires antigen recognition for development. Additionally, they reported signs of clonal expansion in brain Treg (Ito et al., 2019). In contrast, our observations did not reveal CD4+ T cell clonal expansion, and we found no MHC class II dependence for brain accumulation. These disparities could be attributed to differences in stroke models employed in the respective studies. Ito et al. utilized the proximal middle cerebral artery occlusion (pMCAo) model, resulting in a large infarct affecting both the striatum and cortex. Conversely, our study primarily used the distal middle cerebral artery occlusion model (dMCAo), inducing a much smaller, cortex-confined lesion. Importantly, the pMCAo model induces the formation of a brain-resident CD4+ T cell population that is one order of magnitude more numerous than the dMCAo model. Therefore, it is conceivable that we could not observe CD4+ T cell clonal expansion simply because we were unable to analyze a sufficient number of cells to detect this subtle phenomenon. Alternatively, the immune response triggered by these two different stroke models might differ to the extent that only pMCAo induces CD4+ T cell clonal expansion.

It is crucial to highlight that our MHCs knock-out approach impacted all cells, given that the Cre driver utilized was situated under the ubiquitous *ROSA26* locus. This broad impact prompts considerations about the potential initiation of an antigen-dependent response in the periphery (e.g., at the level of the draining lymph nodes), locally within the CNS, or a combination of both mechanisms being significant for post-stroke CD8+ T cell accumulation. Specifically, the dura mater, the outermost meningeal layer, harbors local APCs and patrolling T cells, potentially serving as a site for the recognition of cerebrospinal fluid (CSF)-

derived antigens (Rustenhoven et al., 2021). The contribution of meningeal layers to post-stroke neuroinflammation remains largely unexplored. Given the complex immune milieu characterizing this compartment, investigating whether the meninges can act as a site for antigen presentation to T cells after stroke would be intriguing. Despite the challenges associated with discerning the site and cell type specificity of antigen presentation after stroke, the use of cell type-specific Cre driver lines holds promise for elucidating this phenomenon.

When discussing antigen-dependent T cell responses, it is crucial to emphasize that antigen dependency does not necessarily correspond to antigen specificity. In the context of inflammation, T cell proliferation could be primarily driven by a robust cytokine response, to the extent that even weak MHC-TCR interactions might be sufficient for clonal expansion. In such cases, the T cell response would be stochastic rather than antigen-specific. To conclusively demonstrate that stroke induces an antigen-specific response, it is essential to show that T cells can selectively respond to brain antigens. Even in the field of multiple sclerosis, a well-studied autoimmune disease of the central nervous system, identifying specific antigens responsible for the disease has proven extremely challenging (Hohlfeld et al., 2016). In the stroke field, the use of preclinical models could be fundamental to demonstrate whether, in principle, a sterile ischemic injury can trigger an immune response against brain antigens. For instance, the presence of public clones among experimental replicates would pave the way to describing such a phenomenon. With currently available techniques, candidate TCRs could be resurrected and extensively studied both *in vitro* and *in vivo*.

4.5 The Role of Chemokine Receptors in Tissue-Residency

One of the most salient features of T_{RM} is the expression of specific chemokine receptors, namely CXCR3 and CXCR6. We demonstrated that post-stroke T cells also express these receptors, distinguishing them starkly from circulating T cells (Ricci et al., 2024). Consistently, their respective ligands, CXCL9 and CXCL10 for CXCR3, and CXCL16 for CXCR6, are upregulated in the post-stroke brain, particularly during the sub-acute phase, in contrast to other chemokines such as MIP-1α and MCP-1, which exhibit a more transient acute peak of expression (C. Yang et al., 2019).

In our adoptive transfer experiments, we showed that both CXCR3 and CXCR6 are necessary for the formation of the post-stroke T_{RM} population. However, this approach cannot

distinguish whether T cells need these receptors to acutely invade the ischemic brain or if they are necessary for their maintenance. To distinguish between these two possibilities, pharmacological blockage of the receptors or inducible knockout models would allow interference with chemokine signaling selectively in the acute or subacute phase. While several compounds exist for CXCR3 that work as antagonists, the same is not true for CXCR6, as there are no available molecules for use in murine models. The development of such compounds will likely open a new avenue of possibilities that goes beyond their use in neurological conditions.

CXCR3 has been widely recognized as a critical mediator for T cell invasion in inflamed tissues. Its ligands, CXCL9 and CXCL10, are upregulated in various pathological conditions related to cell-mediated immunity, such as infections, graft rejection, and autoimmunity. However, the role of CXCR3 in neuroinflammation is complex and context-dependent. In CNS infections, CXCR3 appears necessary for brain invasion, crucial for pathogen control but also linked to deleterious post-infection sequelae. On the other hand, in the context of CNS autoimmunity, CXCR3 is not essential for T cell tissue entry, except for Treg (Müller et al., 2010). In the case of stroke, our data suggest an important role for CXCR3 in tissue invasion.

An additional aspect is that CXCL9 and CXCL10 are classically upregulated in response to interferon γ (IFN-γ), a cytokine produced mostly by NK and T cells, and to a lesser extent by macrophages. In the acute phase after stroke, IFN-γ signaling has been linked to the upregulation of CXCL10 (Seifert et al., 2014), but the cellular source of this cytokine has not been described. In the single-cell dataset generated by Garcia-Bonilla and coworkers, *Ifng* appears to be expressed by T and NK cells 14 days after stroke induction (Garcia-Bonilla et al., 2023). Interestingly, IFN-γ levels remain elevated up to 7 weeks after experimental stroke (Zbesko et al., 2018). It is tempting to speculate that locally secreted IFN-γ by T cells induces the expression of CXCL9 and CXCL10, thereby maintaining the T cell population and creating a self-perpetuating feedback loop. Moreover, IFN-γ has been linked to scar formation in experimental autoimmune encephalomyelitis, and CNS fibroblasts express CXCL9 and CXCL10 (Dorrier et al., 2021), introducing a potential new player to this intercellular crosstalk. Although we observed that the majority of CXCL9- and CXCL10-producing cells within the lesion core are Iba1+ myeloid cells, we did not specifically stain for fibroblast markers, and therefore, we cannot exclude that this cell population also contributes to chemokine secretion and T cell brain residency.

CXCR6 is a chemokine receptor whose role is beginning to be elucidated. Several reports suggest that, unlike other chemokine receptors, CXCR6 is not involved in acute tissue invasion but instead in tissue maintenance, albeit through different mechanisms depending

on the organ. For example, in the lung, CXCR6 is associated with continuous recruitment from the periphery after the establishment of the T_{RM} population (Wein et al., 2019). In the liver, CXCR6-deficient T cells fail to express typical T_{RM} markers (Tse et al., 2014), while in the dermis, CXCR6 deficiency is mainly related to lower survival (Heim et al., 2023). In a model of brain viral infection, CXCR6 is also not necessary for acute viral control but for long-term maintenance, specifically of the CD8+ population (Rosen et al., 2022). Interestingly, CXCR6 knockout significantly affects CD4+ post-stroke T cells. Although we did not reach statistical significance to affirm the same about CD8+ T cells, this is likely due to the high variability that a complex experiment such as WT-and-KO T cell adoptive transfer entails.

Notably, CXCR6 expression has been linked to TCR signaling. Antigen stimulation of skin T cells, in particular, promotes a "chemotactic switch," with the downregulation of S1PR1 and the upregulation of CXCR6. This process is critically dependent on the transcription factor Blimp1 (Abdelbary et al., 2023), whose critical role in T_{RM} formation was identified previously (Mackay et al., 2016). In line with this data, brain-resident CXCR6+ T cells show a high level of clonal expansion in a mouse model of AD, and CXCR6 is critically involved in the establishment of tissue residency (Su et al., 2023). Based on these findings, it is tempting to speculate that the reduction of CD8+ post-stroke T_{RM} in the context of MHC-$I^{-/-}$ can be attributable to the incapability of expressing a tissue residency differentiation program. On the other hand, the mechanisms that can maintain CD4+ post-stroke T_{RM} even in the absence of MHC-II stimulation are a fascinating topic that requires further investigation.

5 REFERENCES

Abdelbary, M., Hobbs, S. J., Gibbs, J. S., Yewdell, J. W., & Nolz, J. C. (2023). T cell receptor signaling strength establishes the chemotactic properties of effector CD8+ T cells that control tissue-residency. *Nature Communications*, *14*(1), 3928. https://doi.org/10.1038/s41467-023-39592-1

Allen, C., Thornton, P., Denes, A., McColl, B. W., Pierozynski, A., Monestier, M., Pinteaux, E., Rothwell, N. J., & Allan, S. M. (2012). Neutrophil Cerebrovascular Transmigration Triggers Rapid Neurotoxicity through Release of Proteases Associated with Decondensed DNA. *The Journal of Immunology*, *189*(1), 381–392. https://doi.org/10.4049/jimmunol.1200409

Altendorfer, B., Unger, M. S., Poupardin, R., Hoog, A., Asslaber, D., Gratz, I. K., Mrowetz, H., Benedetti, A., de Sousa, D. M. B., Greil, R., Egle, A., Gate, D., Wyss-Coray, T., & Aigner, L. (2022). Transcriptomic Profiling Identifies CD8+ T Cells in the Brain of Aged and Alzheimer's Disease Transgenic Mice as Tissue-Resident Memory T Cells. *The Journal of Immunology*, *209*(7), 1272–1285. https://doi.org/10.4049/jimmunol.2100737

Alves de Lima, K., Rustenhoven, J., Da Mesquita, S., Wall, M., Salvador, A. F., Smirnov, I., Martelossi Cebinelli, G., Mamuladze, T., Baker, W., Papadopoulos, Z., Lopes, M. B., Cao, W. S., Xie, X. S., Herz, J., & Kipnis, J. (2020). Meningeal γδ T cells regulate anxiety-like behavior via IL-17a signaling in neurons. *Nature Immunology*, *21*(11), 1421–1429. https://doi.org/10.1038/s41590-020-0776-4

Bai, P., Zhu, R., Wang, P., Jiang, F., Zhen, J., Yao, Y., Zhao, C., Liang, Z., Wang, M., Liu, B., Li, M., Li, N., & Yuan, J. (2022). The efficacy and safety of fingolimod plus standardized treatment versus standardized treatment alone for acute ischemic stroke: A systematic review and meta-analysis. *Pharmacology Research & Perspectives*, *10*(3). https://doi.org/10.1002/prp2.972

Balkaya, M., Kröber, J. M., Rex, A., & Endres, M. (2013). Assessing Post-Stroke Behavior in Mouse Models of Focal Ischemia. *Journal of Cerebral Blood Flow & Metabolism*, *33*(3), 330–338. https://doi.org/10.1038/jcbfm.2012.185

Becker, K., Kindrick, D., Relton, J., Harlan, J., & Winn, R. (2001). Antibody to the α4 Integrin Decreases Infarct Size in Transient Focal Cerebral Ischemia in Rats. *Stroke*, *32*(1), 206–211. https://doi.org/10.1161/01.STR.32.1.206

Becktel, D. A., Zbesko, J. C., Frye, J. B., Chung, A. G., Hayes, M., Calderon, K., Grover, J. W., Li, A., Garcia, F. G., Tavera-Garcia, M. A., Schnellmann, R. G., Wu, H.-J. J., Nguyen, T.-V. V., & Doyle, K. P. (2022). Repeated Administration of 2-Hydroxypropyl-β-Cyclodextrin (HPβCD) Attenuates the Chronic Inflammatory Response to Experimental Stroke. *The Journal of Neuroscience*, *42*(2), 325–348. https://doi.org/10.1523/JNEUROSCI.0933-21.2021

Beltrán, E., Gerdes, L. A., Hansen, J., Flierl-Hecht, A., Krebs, S., Blum, H., Ertl-Wagner, B., Barkhof, F., Kümpfel, T., Hohlfeld, R., & Dornmair, K. (2019). Early adaptive immune activation detected in monozygotic twins with prodromal multiple sclerosis. *The Journal of Clinical Investigation*, *129*(11), 4758–4768. https://doi.org/10.1172/JCI128475

Benakis, C., Llovera, G., & Liesz, A. (2018). The meningeal and choroidal infiltration routes for leukocytes in stroke. *Therapeutic Advances in Neurological Disorders*, *11*, 175628641878370. https://doi.org/10.1177/1756286418783708

Benakis, C., Simats, A., Tritschler, S., Heindl, S., Besson-Girard, S., Llovera, G., Pinkham, K., Kolz, A., Ricci, A., Theis, F. J., Bittner, S., Gökce, Ö., Peters, A., & Liesz, A. (2022). T cells modulate the microglial response to brain ischemia. *ELife*, *11*. https://doi.org/10.7554/ELIFE.82031

Chen, X., Firulyova, M., Manis, M., Herz, J., Smirnov, I., Aladyeva, E., Wang, C., Bao, X., Finn, M. B., Hu, H., Shchukina, I., Kim, M. W., Yuede, C. M., Kipnis, J., Artyomov, M. N., Ulrich, J. D., & Holtzman, D. M. (2023). Microglia-mediated T cell infiltration drives neurodegeneration in tauopathy. *Nature*, *615*(7953), 668–677. https://doi.org/10.1038/s41586-023-05788-0

Cramer, J. V., Gesierich, B., Roth, S., Dichgans, M., Düring, M., & Liesz, A. (2019). In vivo widefield calcium imaging of the mouse cortex for analysis of network connectivity in health and brain disease. *NeuroImage*, *199*, 570–584. https://doi.org/10.1016/J.NEUROIMAGE.2019.06.014

Daglas, M., Draxler, D. F., Ho, H., McCutcheon, F., Galle, A., Au, A. E., Larsson, P., Gregory, J., Alderuccio, F., Sashindranath, M., & Medcalf, R. L. (2019). Activated CD8+ T Cells Cause Long-Term Neurological Impairment after Traumatic Brain Injury in Mice. *Cell Reports*, *29*(5), 1178-1191.e6. https://doi.org/10.1016/j.celrep.2019.09.046

Dang, C., Lu, Y., Li, Q., Wang, C., & Ma, X. (2021). Efficacy of the sphingosine-1-phosphate receptor agonist fingolimod in animal models of stroke: an updated meta-analysis. *International Journal of Neuroscience*, *131*(1), 85–94. https://doi.org/10.1080/00207454.2020.1733556

Donkor, E. S. (2018). Stroke in the 21st Century: A Snapshot of the Burden, Epidemiology, and Quality of Life. *Stroke Research and Treatment*, *2018*, 3238165. https://doi.org/10.1155/2018/3238165

Dorrier, C. E., Aran, D., Haenelt, E. A., Sheehy, R. N., Hoi, K. K., Pintarić, L., Chen, Y., Lizama, C. O., Cautivo, K. M., Weiner, G. A., Popko, B., Fancy, S. P. J., Arnold, T. D., & Daneman, R. (2021). CNS fibroblasts form a fibrotic scar in response to immune cell infiltration. *Nature Neuroscience*, *24*(2), 234–244. https://doi.org/10.1038/s41593-020-00770-9

Doyle, K. P., Cekanaviciute, E., Mamer, L. E., & Buckwalter, M. S. (2010). TGFβ signaling in the brain increases with aging and signals to astrocytes and innate immune cells in the weeks after stroke. *Journal of Neuroinflammation*, *7*, 62. https://doi.org/10.1186/1742-2094-7-62

Doyle, K. P., Quach, L. N., Solé, M., Axtell, R. C., Nguyen, T.-V. V, Soler-Llavina, G. J., Jurado, S., Han, J., Steinman, L., Longo, F. M., Schneider, J. A., Malenka, R. C., & Buckwalter, M. S. (2015). B-lymphocyte-mediated delayed cognitive impairment following stroke. *The Journal of Neuroscience : The Official Journal of the Society for Neuroscience*, *35*(5), 2133–2145. https://doi.org/10.1523/JNEUROSCI.4098-14.2015

Elkind, M. S. V., Veltkamp, R., Montaner, J., Johnston, S. C., Singhal, A. B., Becker, K., Lansberg, M. G., Tang, W., Kasliwal, R., & Elkins, J. (2020). Natalizumab in acute ischemic stroke (ACTION II). *Neurology*, *95*(8), e1091–e1104. https://doi.org/10.1212/WNL.0000000000010038

Elkins, J., Veltkamp, R., Montaner, J., Johnston, S. C., Singhal, A. B., Becker, K., Lansberg, M. G., Tang, W., Chang, I., Muralidharan, K., Gheuens, S., Mehta, L., & Elkind, M. S. V. (2017). Safety and efficacy of natalizumab in patients with acute ischaemic stroke (ACTION): a randomised, placebo-controlled, double-blind phase 2 trial. *The Lancet Neurology*, *16*(3), 217–226. https://doi.org/10.1016/S1474-4422(16)30357-X

Engelhardt, B., & Sorokin, L. (2009). The blood–brain and the blood–cerebrospinal fluid barriers: function and dysfunction. *Seminars in Immunopathology*, *31*(4), 497–511. https://doi.org/10.1007/s00281-009-0177-0

Fan, L., Zhang, C.-J., Zhu, L., Chen, J., Zhang, Z., Liu, P., Cao, X., Meng, H., & Xu, Y. (2020). FasL-PDPK1 Pathway Promotes the Cytotoxicity of CD8+ T Cells During Ischemic Stroke. *Translational Stroke Research*, *11*(4), 747–761. https://doi.org/10.1007/s12975-019-00749-0

Feigin, V. L., Stark, B. A., Johnson, C. O., Roth, G. A., Bisignano, C., Abady, G. G., Abbasifard, M., Abbasi-Kangevari, M., Abd-Allah, F., Abedi, V., Abualhasan, A., Abu-Rmeileh, N. M., Abushouk, A. I., Adebayo, O. M., Agarwal, G., Agasthi, P., Ahinkorah, B. O., Ahmad, S., Ahmadi, S., … Murray, C. J. L. (2021). Global, regional, and national burden of stroke and its risk factors, 1990–2019: a systematic analysis for the Global Burden of Disease Study 2019. *The Lancet Neurology*, *20*(10), 795–820. https://doi.org/10.1016/S1474-4422(21)00252-0

Filiano, A. J., Xu, Y., Tustison, N. J., Marsh, R. L., Baker, W., Smirnov, I., Overall, C. C., Gadani, S. P., Turner, S. D., Weng, Z., Peerzade, S. N., Chen, H., Lee, K. S., Scott, M. M., Beenhakker, M. P., Litvak, V., & Kipnis, J. (2016). Unexpected role of interferon-γ in regulating neuronal connectivity and social behaviour. *Nature*, *535*(7612), 425–429. https://doi.org/10.1038/nature18626

Frieser, D., Pignata, A., Khajavi, L., Shlesinger, D., Gonzalez-Fierro, C., Nguyen, X.-H., Yermanos, A., Merkler, D., Höftberger, R., Desestret, V., Mair, K. M., Bauer, J., Masson, F., & Liblau, R. S. (2022). Tissue-resident CD8 $^{+}$ T cells drive compartmentalized and chronic autoimmune damage against CNS neurons. *Science Translational Medicine*, *14*(640). https://doi.org/10.1126/scitranslmed.abl6157

Fu, Y., Zhang, N., Ren, L., Yan, Y., Sun, N., Li, Y.-J., Han, W., Xue, R., Liu, Q., Hao, J., Yu, C., & Shi, F.-D. (2014). Impact of an immune modulator fingolimod on acute ischemic stroke. *Proceedings of the National Academy of Sciences*, *111*(51), 18315–18320. https://doi.org/10.1073/pnas.1416166111

Garcia-Bonilla, L., Faraco, G., Moore, J., Murphy, M., Racchumi, G., Srinivasan, J., Brea, D., Iadecola, C., & Anrather, J. (2016). Spatio-temporal profile, phenotypic diversity, and fate of recruited monocytes into the post-ischemic brain. *Journal of Neuroinflammation*, *13*(1), 285. https://doi.org/10.1186/s12974-016-0750-0

Garcia-Bonilla, L., Moore, J. M., Racchumi, G., Zhou, P., Butler, J. M., Iadecola, C., & Anrather, J. (2014). Inducible Nitric Oxide Synthase in Neutrophils and Endothelium Contributes to Ischemic Brain Injury in Mice. *The Journal of Immunology*, *193*(5), 2531–2537. https://doi.org/10.4049/jimmunol.1400918

Garcia-Bonilla, L., Shahanoor, Z., Sciortino, R., Nazarzoda, O., Racchumi, G., Iadecola, C., & Anrather, J. (2023). Brain and blood single-cell transcriptomics in acute and subacute phases after experimental stroke. *BioRxiv : The Preprint Server for Biology*. https://doi.org/10.1101/2023.03.31.535150

Gelderblom, M., Leypoldt, F., Steinbach, K., Behrens, D., Choe, C.-U., Siler, D. A., Arumugam, T. V, Orthey, E., Gerloff, C., Tolosa, E., & Magnus, T. (2009). Temporal and spatial dynamics of cerebral immune cell accumulation in stroke. *Stroke*, *40*(5), 1849–1857. https://doi.org/10.1161/STROKEAHA.108.534503

Gelderblom, M., Weymar, A., Bernreuther, C., Velden, J., Arunachalam, P., Steinbach, K., Orthey, E., Arumugam, T. V., Leypoldt, F., Simova, O., Thom, V., Friese, M. A., Prinz, I., Hölscher, C., Glatzel, M., Korn, T., Gerloff, C., Tolosa, E., & Magnus, T. (2012). Neutralization of the IL-17 axis diminishes neutrophil invasion and protects from ischemic stroke. *Blood*, *120*(18), 3793–3802. https://doi.org/10.1182/blood-2012-02-412726

Heim, T. A., Lin, Z., Steele, M. M., Mudianto, T., & Lund, A. W. (2023). CXCR6 promotes dermal CD8⁺ T cell survival and transition to long-term tissue residence. *BioRxiv*, 2023.02.14.528487. https://doi.org/10.1101/2023.02.14.528487

Heindl, S., Ricci, A., Carofiglio, O., Zhou, Q., Arzberger, T., Lenart, N., Franzmeier, N., Hortobagyi, T., Nelson, P. T., Stowe, A. M., Denes, A., Edbauer, D., & Liesz, A. (2021). Chronic T cell proliferation in brains after stroke could interfere with the efficacy of immunotherapies. *The Journal of Experimental Medicine*, *218*(8). https://doi.org/10.1084/jem.20202411

Hohlfeld, R., Dornmair, K., Meinl, E., & Wekerle, H. (2016). The search for the target antigens of multiple sclerosis, part 1: autoreactive CD4+ T lymphocytes as pathogenic effectors and therapeutic targets. *The Lancet Neurology*, *15*(2), 198–209. https://doi.org/10.1016/S1474-4422(15)00334-8

Hum, P. D., Subramanian, S., Parker, S. M., Afentoulis, M. E., Kaler, L. J., Vandenbark, A. A., & Offner, H. (2007). T- and B-Cell-Deficient Mice with Experimental Stroke have Reduced Lesion Size and Inflammation. *Journal of Cerebral Blood Flow & Metabolism*, *27*(11), 1798–1805. https://doi.org/10.1038/sj.jcbfm.9600482

Iadecola, C., & Anrather, J. (2011). The immunology of stroke: from mechanisms to translation. *Nature Medicine*, *17*(7), 796–808. https://doi.org/10.1038/nm.2399

Ito, M., Komai, K., Mise-Omata, S., Iizuka-Koga, M., Noguchi, Y., Kondo, T., Sakai, R., Matsuo, K., Nakayama, T., Yoshie, O., Nakatsukasa, H., Chikuma, S., Shichita, T., & Yoshimura, A. (2019). Brain regulatory T cells suppress astrogliosis and potentiate neurological recovery. *Nature*, *565*(7738), 246–250. https://doi.org/10.1038/s41586-018-0824-5

Javidi, E., & Magnus, T. (2019). Autoimmunity After Ischemic Stroke and Brain Injury. *Frontiers in Immunology*, *10*. https://doi.org/10.3389/fimmu.2019.00686

Jin, S., Guerrero-Juarez, C. F., Zhang, L., Chang, I., Ramos, R., Kuan, C.-H., Myung, P., Plikus, M. V., & Nie, Q. (2021). Inference and analysis of cell-cell communication using CellChat. *Nature Communications*, *12*(1), 1088. https://doi.org/10.1038/s41467-021-21246-9

Kelly-Hayes, M., Beiser, A., Kase, C. S., Scaramucci, A., D'Agostino, R. B., & Wolf, P. A. (2003). The influence of gender and age on disability following ischemic stroke: the Framingham study. *Journal of Stroke and Cerebrovascular Diseases : The Official Journal of National Stroke Association*, *12*(3), 119–126. https://doi.org/10.1016/S1052-3057(03)00042-9

Klein, R. S., Lin, E., Zhang, B., Luster, A. D., Tollett, J., Samuel, M. A., Engle, M., & Diamond, M. S. (2005). Neuronal CXCL10 directs CD8+ T-cell recruitment and control of West Nile virus encephalitis. *Journal of Virology*, *79*(17), 11457–11466. https://doi.org/10.1128/JVI.79.17.11457-11466.2005

Kleinschnitz, C., Schwab, N., Kraft, P., Hagedorn, I., Dreykluft, A., Schwarz, T., Austinat, M., Nieswandt, B., Wiendl, H., & Stoll, G. (2010). Early detrimental T-cell effects in experimental cerebral ischemia are neither related to adaptive immunity nor thrombus formation. *Blood*, *115*(18), 3835–3842. https://doi.org/10.1182/blood-2009-10-249078

Langhauser, F., Kraft, P., Göb, E., Leinweber, J., Schuhmann, M. K., Lorenz, K., Gelderblom, M., Bittner, S., Meuth, S. G., Wiendl, H., Magnus, T., & Kleinschnitz, C. (2014). Blocking of α4 Integrin Does Not Protect From Acute Ischemic Stroke in Mice. *Stroke*, *45*(6), 1799–1806. https://doi.org/10.1161/STROKEAHA.114.005000

Lapchak, P. A., Zhang, J. H., & Noble-Haeusslein, L. J. (2013). RIGOR Guidelines: Escalating STAIR and STEPS for Effective Translational Research. *Translational Stroke Research*, *4*(3), 279–285. https://doi.org/10.1007/s12975-012-0209-2

Li, C., Zhu, B., Son, Y. M., Wang, Z., Jiang, L., Xiang, M., Ye, Z., Beckermann, K. E., Wu, Y., Jenkins, J. W., Siska, P. J., Vincent, B. G., Prakash, Y. S., Peikert, T., Edelson, B. T., Taneja, R., Kaplan, M. H., Rathmell, J. C., Dong, H., … Sun, J. (2019). The Transcription Factor Bhlhe40 Programs Mitochondrial Regulation of Resident CD8+ T Cell Fitness and Functionality. *Immunity*, *51*(3), 491-507.e7. https://doi.org/10.1016/j.immuni.2019.08.013

Liesz, A., Karcher, S., & Veltkamp, R. (2013). Spectratype analysis of clonal T cell expansion in murine experimental stroke. *Journal of Neuroimmunology*, *257*(1–2), 46–52. https://doi.org/10.1016/j.jneuroim.2013.01.013

Liesz, A., & Kleinschnitz, C. (2016). Regulatory T Cells in Post-stroke Immune Homeostasis. *Translational Stroke Research*, *7*(4), 313–321. https://doi.org/10.1007/s12975-016-0465-7

Liesz, A., Suri-Payer, E., Veltkamp, C., Doerr, H., Sommer, C., Rivest, S., Giese, T., & Veltkamp, R. (2009). Regulatory T cells are key cerebroprotective immunomodulators in acute experimental stroke. *Nature Medicine*, *15*(2), 192–199. https://doi.org/10.1038/nm.1927

Liesz, A., Zhou, W., Mracskó, É., Karcher, S., Bauer, H., Schwarting, S., Sun, L., Bruder, D., Stegemann, S., Cerwenka, A., Sommer, C., Dalpke, A. H., & Veltkamp, R. (2011). Inhibition of lymphocyte trafficking shields the brain against deleterious neuroinflammation after stroke. *Brain*, *134*(3), 704–720. https://doi.org/10.1093/brain/awr008

Llovera, G., Hofmann, K., Roth, S., Salas-Pérdomo, A., Ferrer-Ferrer, M., Perego, C., Zanier, E. R., Mamrak, U., Rex, A., Party, H., Agin, V., Fauchon, C., Orset, C., Haelewyn, B., De Simoni, M.-G., Dirnagl, U., Grittner, U., Planas, A. M., Plesnila, N., … Liesz, A. (2015). Results of a preclinical randomized controlled multicenter trial (pRCT): Anti-CD49d treatment for acute brain ischemia. *Science Translational Medicine*, *7*(299). https://doi.org/10.1126/scitranslmed.aaa9853

Louveau, A., Smirnov, I., Keyes, T. J., Eccles, J. D., Rouhani, S. J., Peske, J. D., Derecki, N. C., Castle, D., Mandell, J. W., Lee, K. S., Harris, T. H., & Kipnis, J. (2015). Structural and functional features of central nervous system lymphatic vessels. *Nature*, *523*(7560), 337–341. https://doi.org/10.1038/nature14432

Machado-Santos, J., Saji, E., Tröscher, A. R., Paunovic, M., Liblau, R., Gabriely, G., Bien, C. G., Bauer, J., & Lassmann, H. (2018). The compartmentalized inflammatory response in the multiple sclerosis brain is composed of tissue-resident CD8+ T lymphocytes and B cells. *Brain : A Journal of Neurology*, *141*(7), 2066–2082. https://doi.org/10.1093/brain/awy151

Mackay, L. K., Minnich, M., Kragten, N. A. M., Liao, Y., Nota, B., Seillet, C., Zaid, A., Man, K., Preston, S., Freestone, D., Braun, A., Wynne-Jones, E., Behr, F. M., Stark, R., Pellicci, D. G., Godfrey, D. I., Belz, G. T., Pellegrini, M., Gebhardt, T., … van Gisbergen, K. P. J. M. (2016). Hobit and Blimp1 instruct a universal transcriptional program of tissue

residency in lymphocytes. *Science*, *352*(6284), 459–463. https://doi.org/10.1126/science.aad2035

Merkler, D., Vincenti, I., Masson, F., & Liblau, R. S. (2022). Tissue-resident CD8 T cells in central nervous system inflammatory diseases: present at the crime scene and …guilty. *Current Opinion in Immunology*, *77*, 102211. https://doi.org/10.1016/j.coi.2022.102211

Milner, J. J., Toma, C., Yu, B., Zhang, K., Omilusik, K., Phan, A. T., Wang, D., Getzler, A. J., Nguyen, T., Crotty, S., Wang, W., Pipkin, M. E., & Goldrath, A. W. (2017). Runx3 programs CD8+ T cell residency in non-lymphoid tissues and tumours. *Nature*, *552*(7684), 253–257. https://doi.org/10.1038/nature24993

Morikawa, K., Furuhashi, K., de Sena-Tomas, C., Garcia-Garcia, A. L., Bekdash, R., Klein, A. D., Gallerani, N., Yamamoto, H. E., Park, S.-H. E., Collins, G. S., Kawano, F., Sato, M., Lin, C.-S., Targoff, K. L., Au, E., Salling, M. C., & Yazawa, M. (2020). Photoactivatable Cre recombinase 3.0 for in vivo mouse applications. *Nature Communications*, *11*(1), 2141. https://doi.org/10.1038/s41467-020-16030-0

Morrison, H. W., & Filosa, J. A. (2013). A quantitative spatiotemporal analysis of microglia morphology during ischemic stroke and reperfusion. *Journal of Neuroinflammation*, *10*(1), 782. https://doi.org/10.1186/1742-2094-10-4

Mracsko, E., Liesz, A., Stojanovic, A., Lou, W. P.-K., Osswald, M., Zhou, W., Karcher, S., Winkler, F., Martin-Villalba, A., Cerwenka, A., & Veltkamp, R. (2014). Antigen Dependently Activated Cluster of Differentiation 8-Positive T Cells Cause Perforin-Mediated Neurotoxicity in Experimental Stroke. *The Journal of Neuroscience*, *34*(50), 16784–16795. https://doi.org/10.1523/JNEUROSCI.1867-14.2014

Mueller, S. N., Gebhardt, T., Carbone, F. R., & Heath, W. R. (2013). Memory T Cell Subsets, Migration Patterns, and Tissue Residence. *Annual Review of Immunology*, *31*(1), 137–161. https://doi.org/10.1146/annurev-immunol-032712-095954

Müller, M., Carter, S., Hofer, M. J., & Campbell, I. L. (2010). Review: The chemokine receptor CXCR3 and its ligands CXCL9, CXCL10 and CXCL11 in neuroimmunity - a tale of conflict and conundrum. *Neuropathology and Applied Neurobiology*, *36*(5), 368–387. https://doi.org/10.1111/j.1365-2990.2010.01089.x

Neumann, J., Riek-Burchardt, M., Herz, J., Doeppner, T. R., König, R., Hütten, H., Etemire, E., Männ, L., Klingberg, A., Fischer, T., Görtler, M. W., Heinze, H.-J., Reichardt, P., Schraven, B., Hermann, D. M., Reymann, K. G., & Gunzer, M. (2015). Very-late-antigen-4 (VLA-4)-mediated brain invasion by neutrophils leads to interactions with

microglia, increased ischemic injury and impaired behavior in experimental stroke. *Acta Neuropathologica*, *129*(2), 259–277. https://doi.org/10.1007/s00401-014-1355-2

Nowotschin, S., & Hadjantonakis, A.-K. (2009). Use of KikGR a photoconvertible green-to-red fluorescent protein for cell labeling and lineage analysis in ES cells and mouse embryos. *BMC Developmental Biology*, *9*(1), 49. https://doi.org/10.1186/1471-213X-9-49

Ortega, S. B., Noorbhai, I., Poinsatte, K., Kong, X., Anderson, A., Monson, N. L., & Stowe, A. M. (2015). Stroke induces a rapid adaptive autoimmune response to novel neuronal antigens. *Discovery Medicine*, *19*(106), 381–392.

Ortega, S. B., Torres, V. O., Latchney, S. E., Whoolery, C. W., Noorbhai, I. Z., Poinsatte, K., Selvaraj, U. M., Benson, M. A., Meeuwissen, A. J. M., Plautz, E. J., Kong, X., Ramirez, D. M., Ajay, A. D., Meeks, J. P., Goldberg, M. P., Monson, N. L., Eisch, A. J., & Stowe, A. M. (2020). B cells migrate into remote brain areas and support neurogenesis and functional recovery after focal stroke in mice. *Proceedings of the National Academy of Sciences*, *117*(9), 4983–4993. https://doi.org/10.1073/pnas.1913292117

Otxoa-de-Amezaga, A., Miró-Mur, F., Pedragosa, J., Gallizioli, M., Justicia, C., Gaja-Capdevila, N., Ruíz-Jaen, F., Salas-Perdomo, A., Bosch, A., Calvo, M., Márquez-Kisinousky, L., Denes, A., Gunzer, M., & Planas, A. M. (2019). Microglial cell loss after ischemic stroke favors brain neutrophil accumulation. *Acta Neuropathologica*, *137*(2), 321–341. https://doi.org/10.1007/s00401-018-1954-4

Pan, Y., Tian, T., Park, C. O., Lofftus, S. Y., Mei, S., Liu, X., Luo, C., O'Malley, J. T., Gehad, A., Teague, J. E., Divito, S. J., Fuhlbrigge, R., Puigserver, P., Krueger, J. G., Hotamisligil, G. S., Clark, R. A., & Kupper, T. S. (2017). Survival of tissue-resident memory T cells requires exogenous lipid uptake and metabolism. *Nature*, *543*(7644), 252–256. https://doi.org/10.1038/nature21379

Pasciuto, E., Burton, O. T., Roca, C. P., Lagou, V., Rajan, W. D., Theys, T., Mancuso, R., Tito, R. Y., Kouser, L., Callaerts-Vegh, Z., de la Fuente, A. G., Prezzemolo, T., Mascali, L. G., Brajic, A., Whyte, C. E., Yshii, L., Martinez-Muriana, A., Naughton, M., Young, A., … Liston, A. (2020). Microglia Require CD4 T Cells to Complete the Fetal-to-Adult Transition. *Cell*, *182*(3), 625-640.e24. https://doi.org/10.1016/j.cell.2020.06.026

Pedragosa, J., Miró-Mur, F., Otxoa-de-Amezaga, A., Justicia, C., Ruíz-Jaén, F., Ponsaerts, P., Pasparakis, M., & Planas, A. M. (2020). CCR2 deficiency in monocytes impairs angiogenesis and functional recovery after ischemic stroke in mice. *Journal of Cerebral*

Blood Flow & Metabolism, *40*(1_suppl), S98–S116. https://doi.org/10.1177/0271678X20909055

Pekny, M., & Pekna, M. (2014). Astrocyte Reactivity and Reactive Astrogliosis: Costs and Benefits. *Physiological Reviews*, *94*(4), 1077–1098. https://doi.org/10.1152/physrev.00041.2013

Planas, A. M., Gómez-Choco, M., Urra, X., Gorina, R., Caballero, M., & Chamorro, Á. (2012). Brain-Derived Antigens in Lymphoid Tissue of Patients with Acute Stroke. *The Journal of Immunology*, *188*(5), 2156–2163. https://doi.org/10.4049/jimmunol.1102289

Pu, L., Wang, L., Zhang, R., Zhao, T., Jiang, Y., & Han, L. (2023). Projected Global Trends in Ischemic Stroke Incidence, Deaths and Disability-Adjusted Life Years From 2020 to 2030. *Stroke*, *54*(5), 1330–1339. https://doi.org/10.1161/STROKEAHA.122.040073

Recommendations for Standards Regarding Preclinical Neuroprotective and Restorative Drug Development. (1999). *Stroke*, *30*(12), 2752–2758. https://doi.org/10.1161/01.STR.30.12.2752

Relton, J. K., Sloan, K. E., Frew, E. M., Whalley, E. T., Adams, S. P., & Lobb, R. R. (2001). Inhibition of α4 Integrin Protects Against Transient Focal Cerebral Ischemia in Normotensive and Hypertensive Rats. *Stroke*, *32*(1), 199–205. https://doi.org/10.1161/01.STR.32.1.199

Ren, H. M., Kolawole, E. M., Ren, M., Jin, G., Netherby-Winslow, C. S., Wade, Q., Shwetank, Rahman, Z. S. M., Evavold, B. D., & Lukacher, A. E. (2020). IL-21 from high-affinity CD4 T cells drives differentiation of brain-resident CD8 T cells during persistent viral infection. *Science Immunology*, *5*(51). https://doi.org/10.1126/sciimmunol.abb5590

Ricci, A., & Liesz, A. (2023). A tale of two cells: Regulatory T cell–microglia cross-talk in the ischemic brain. *Science Translational Medicine*, *15*(721). https://doi.org/10.1126/scitranslmed.adj0052

Rosen, S. F., Soung, A. L., Yang, W., Ai, S., Kanmogne, M., Davé, V. A., Artyomov, M., Magee, J. A., & Klein, R. S. (2022). Single-cell RNA transcriptome analysis of CNS immune cells reveals CXCL16/CXCR6 as maintenance factors for tissue-resident T cells that drive synapse elimination. *Genome Medicine*, *14*(1), 108. https://doi.org/10.1186/s13073-022-01111-0

Rustenhoven, J., Drieu, A., Mamuladze, T., de Lima, K. A., Dykstra, T., Wall, M., Papadopoulos, Z., Kanamori, M., Salvador, A. F., Baker, W., Lemieux, M., Da Mesquita, S., Cugurra, A., Fitzpatrick, J., Sviben, S., Kossina, R., Bayguinov, P., Townsend, R. R.,

Zhang, Q., … Kipnis, J. (2021). Functional characterization of the dural sinuses as a neuroimmune interface. *Cell*, *184*(4), 1000-1016.e27. https://doi.org/10.1016/j.cell.2020.12.040

Schenkel, J. M., & Masopust, D. (2014). Tissue-Resident Memory T Cells. *Immunity*, *41*(6), 886–897. https://doi.org/10.1016/j.immuni.2014.12.007

Seifert, H. A., Collier, L. A., Chapman, C. B., Benkovic, S. A., Willing, A. E., & Pennypacker, K. R. (2014). Pro-Inflammatory Interferon Gamma Signaling is Directly Associated with Stroke Induced Neurodegeneration. *Journal of Neuroimmune Pharmacology*, *9*(5), 679–689. https://doi.org/10.1007/s11481-014-9560-2

Selvaraj, U. M., Ujas, T. A., Kong, X., Kumar, A., Plautz, E. J., Zhang, S., Xing, C., Sudduth, T. L., Wilcock, D. M., Turchan-Cholewo, J., Goldberg, M. P., & Stowe, A. M. (2021). Delayed diapedesis of CD8 T cells contributes to long-term pathology after ischemic stroke in male mice. *Brain, Behavior, and Immunity*, *95*, 502–513. https://doi.org/10.1016/j.bbi.2021.05.001

Shi, L., Sun, Z., Su, W., Xu, F., Xie, D., Zhang, Q., Dai, X., Iyer, K., Hitchens, T. K., Foley, L. M., Li, S., Stolz, D. B., Chen, K., Ding, Y., Thomson, A. W., Leak, R. K., Chen, J., & Hu, X. (2021). Treg cell-derived osteopontin promotes microglia-mediated white matter repair after ischemic stroke. *Immunity*, *54*(7), 1527-1542.e8. https://doi.org/10.1016/J.IMMUNI.2021.04.022

Shichita, T., Sugiyama, Y., Ooboshi, H., Sugimori, H., Nakagawa, R., Takada, I., Iwaki, T., Okada, Y., Iida, M., Cua, D. J., Iwakura, Y., & Yoshimura, A. (2009). Pivotal role of cerebral interleukin-17–producing γδT cells in the delayed phase of ischemic brain injury. *Nature Medicine*, *15*(8), 946–950. https://doi.org/10.1038/nm.1999

Smolders, J., Heutinck, K. M., Fransen, N. L., Remmerswaal, E. B. M., Hombrink, P., ten Berge, I. J. M., van Lier, R. A. W., Huitinga, I., & Hamann, J. (2018). Tissue-resident memory T cells populate the human brain. *Nature Communications*, *9*(1), 4593. https://doi.org/10.1038/s41467-018-07053-9

Sporici, R., & Issekutz, T. B. (2010). CXCR3 blockade inhibits T-cell migration into the CNS during EAE and prevents development of adoptively transferred, but not actively induced, disease. *European Journal of Immunology*, *40*(10), 2751–2761. https://doi.org/10.1002/eji.200939975

Steinbach, K., Vincenti, I., Kreutzfeldt, M., Page, N., Muschaweckh, A., Wagner, I., Drexler, I., Pinschewer, D., Korn, T., & Merkler, D. (2016). Brain-resident memory T cells

represent an autonomous cytotoxic barrier to viral infection. *Journal of Experimental Medicine*, *213*(8), 1571–1587. https://doi.org/10.1084/jem.20151916

Stubbe, T., Ebner, F., Richter, D., Engel, O., Klehmet, J., Royl, G., Meisel, A., Nitsch, R., Meisel, C., & Brandt, C. (2013). Regulatory T cells accumulate and proliferate in the ischemic hemisphere for up to 30 days after MCAO. *Journal of Cerebral Blood Flow and Metabolism : Official Journal of the International Society of Cerebral Blood Flow and Metabolism*, *33*(1), 37–47. https://doi.org/10.1038/jcbfm.2012.128

Su, W., Saravia, J., Risch, I., Rankin, S., Guy, C., Chapman, N. M., Shi, H., Sun, Y., KC, A., Li, W., Huang, H., Lim, S. A., Hu, H., Wang, Y., Liu, D., Jiao, Y., Chen, P.-C., Soliman, H., Yan, K.-K., … Chi, H. (2023). CXCR6 orchestrates brain CD8+ T cell residency and limits mouse Alzheimer's disease pathology. *Nature Immunology*, *24*(10), 1735–1747. https://doi.org/10.1038/s41590-023-01604-z

Szabo, P. A., Miron, M., & Farber, D. L. (2019). Location, location, location: Tissue resident memory T cells in mice and humans. *Science Immunology*, *4*(34). https://doi.org/10.1126/sciimmunol.aas9673

Szalay, G., Martinecz, B., Lénárt, N., Környei, Z., Orsolits, B., Judák, L., Császár, E., Fekete, R., West, B. L., Katona, G., Rózsa, B., & Dénes, Á. (2016). Microglia protect against brain injury and their selective elimination dysregulates neuronal network activity after stroke. *Nature Communications*, *7*(1), 11499. https://doi.org/10.1038/ncomms11499

Tse, S.-W., Radtke, A. J., Espinosa, D. A., Cockburn, I. A., & Zavala, F. (2014). The chemokine receptor CXCR6 is required for the maintenance of liver memory $CD8^+$ T cells specific for infectious pathogens. *The Journal of Infectious Diseases*, *210*(9), 1508–1516. https://doi.org/10.1093/infdis/jiu281

Vincenti, I., Page, N., Steinbach, K., Yermanos, A., Lemeille, S., Nunez, N., Kreutzfeldt, M., Klimek, B., Di Liberto, G., Egervari, K., Piccinno, M., Shammas, G., Mariotte, A., Fonta, N., Liaudet, N., Shlesinger, D., Liuzzi, A. R., Wagner, I., Saadi, C., … Merkler, D. (2022). Tissue-resident memory $CD8^+$ T cells cooperate with $CD4^+$ T cells to drive compartmentalized immunopathology in the CNS. *Science Translational Medicine*, *14*(640). https://doi.org/10.1126/scitranslmed.abl6058

Wakim, L. M., Woodward-Davis, A., & Bevan, M. J. (2010). Memory T cells persisting within the brain after local infection show functional adaptations to their tissue of residence. *Proceedings of the National Academy of Sciences*, *107*(42), 17872–17879. https://doi.org/10.1073/pnas.1010201107

Wattananit, S., Tornero, D., Graubardt, N., Memanishvili, T., Monni, E., Tatarishvili, J., Miskinyte, G., Ge, R., Ahlenius, H., Lindvall, O., Schwartz, M., & Kokaia, Z. (2016). Monocyte-Derived Macrophages Contribute to Spontaneous Long-Term Functional Recovery after Stroke in Mice. *The Journal of Neuroscience*, *36*(15), 4182–4195. https://doi.org/10.1523/JNEUROSCI.4317-15.2016

Wein, A. N., McMaster, S. R., Takamura, S., Dunbar, P. R., Cartwright, E. K., Hayward, S. L., McManus, D. T., Shimaoka, T., Ueha, S., Tsukui, T., Masumoto, T., Kurachi, M., Matsushima, K., & Kohlmeier, J. E. (2019). CXCR6 regulates localization of tissue-resident memory CD8 T cells to the airways. *The Journal of Experimental Medicine*, *216*(12), 2748–2762. https://doi.org/10.1084/jem.20181308

Weitbrecht, L., Berchtold, D., Zhang, T., Jagdmann, S., Dames, C., Winek, K., Meisel, C., & Meisel, A. (2021). CD4+ T cells promote delayed B cell responses in the ischemic brain after experimental stroke. *Brain, Behavior, and Immunity*, *91*, 601–614. https://doi.org/10.1016/j.bbi.2020.09.029

Werner, Y., Mass, E., Ashok Kumar, P., Ulas, T., Händler, K., Horne, A., Klee, K., Lupp, A., Schütz, D., Saaber, F., Redecker, C., Schultze, J. L., Geissmann, F., & Stumm, R. (2020). Cxcr4 distinguishes HSC-derived monocytes from microglia and reveals monocyte immune responses to experimental stroke. *Nature Neuroscience*, *23*(3), 351–362. https://doi.org/10.1038/s41593-020-0585-y

Xie, L., Li, W., Hersh, J., Liu, R., & Yang, S.-H. (2019). Experimental ischemic stroke induces long-term T cell activation in the brain. *Journal of Cerebral Blood Flow & Metabolism*, *39*(11), 2268–2276. https://doi.org/10.1177/0271678X18792372

Xie, L., Sun, F., Wang, J., Mao, X., Xie, L., Yang, S.-H., Su, D.-M., Simpkins, J. W., Greenberg, D. A., & Jin, K. (2014). mTOR Signaling Inhibition Modulates Macrophage/Microglia-Mediated Neuroinflammation and Secondary Injury via Regulatory T Cells after Focal Ischemia. *The Journal of Immunology*, *192*(12), 6009–6019. https://doi.org/10.4049/jimmunol.1303492

Yang, C., Hawkins, K. E., Doré, S., & Candelario-Jalil, E. (2019). Neuroinflammatory mechanisms of blood-brain barrier damage in ischemic stroke. *American Journal of Physiology-Cell Physiology*, *316*(2), C135–C153. https://doi.org/10.1152/ajpcell.00136.2018

Yang, K., & Kallies, A. (2021). Tissue-specific differentiation of CD8+ resident memory T cells. *Trends in Immunology*, *42*(10), 876–890. https://doi.org/10.1016/j.it.2021.08.002

Yshii, L., Pasciuto, E., Bielefeld, P., Mascali, L., Lemaitre, P., Marino, M., Dooley, J., Kouser, L., Verschoren, S., Lagou, V., Kemps, H., Gervois, P., de Boer, A., Burton, O. T., Wahis, J., Verhaert, J., Tareen, S. H. K., Roca, C. P., Singh, K., … Liston, A. (2022). Astrocyte-targeted gene delivery of interleukin 2 specifically increases brain-resident regulatory T cell numbers and protects against pathological neuroinflammation. *Nature Immunology*, *23*(6), 878–891. https://doi.org/10.1038/S41590-022-01208-Z

Zbesko, J. C., Frye, J. B., Becktel, D. A., Gerardo, D. K., Stokes, J., Calderon, K., Nguyen, T.-V. V., Bhattacharya, D., & Doyle, K. P. (2021). IgA natural antibodies are produced following T-cell independent B-cell activation following stroke. *Brain, Behavior, and Immunity*, *91*, 578–586. https://doi.org/10.1016/j.bbi.2020.09.014

Zbesko, J. C., Nguyen, T.-V. V, Yang, T., Frye, J. B., Hussain, O., Hayes, M., Chung, A., Day, W. A., Stepanovic, K., Krumberger, M., Mona, J., Longo, F. M., & Doyle, K. P. (2018). Glial scars are permeable to the neurotoxic environment of chronic stroke infarcts. *Neurobiology of Disease*, *112*, 63–78. https://doi.org/10.1016/j.nbd.2018.01.007

Zhang, R., Wu, Y., Xie, F., Zhong, Y., Wang, Y., Xu, M., Feng, J., Charish, J., Monnier, P. P., & Qin, X. (2018). RGMa mediates reactive astrogliosis and glial scar formation through TGFβ1/Smad2/3 signaling after stroke. *Cell Death & Differentiation*, *25*(8), 1503–1516. https://doi.org/10.1038/s41418-018-0058-y

6 COPYRIGHT AND AI USE INFORMATION

Figure number	1
License number	5706351079191
License date	Jan 12, 2024
Licensed content publisher	Wolters Kluwer Health, Inc.
Licensed content publication	Stroke
Licensed content title	Temporal and Spatial Dynamics of Cerebral Immune Cell Accumulation in Stroke
Licensed content author	Mathias Gelderblom, Frank Leypoldt, Karin Steinbach, et al

Figure number	2
License number	5701911068423
License date	Jan 04, 2024
Licensed content publisher	Elsevier
Licensed content publication	Journal of Neuroimmunology
Licensed content title	T cells in the post-ischemic brain: Troopers or paramedics?
Licensed content author	Julia V. Cramer,Corinne Benakis,Arthur Liesz

Figure number	3
License number	5701911387600
License date	Jan 04, 2024
Licensed content publisher	Springer Nature
Licensed content publication	Seminars in Immunopathology

Licensed content title	Regulatory T lymphocytes as a therapy for ischemic stroke
Licensed content author	Miao Wang et al

Figure number	4
License number	5701920054806
License date	Jan 04, 2024
Licensed content publisher	Elsevier
Licensed content publication	Immunity
Licensed content title	Tissue-Resident Memory T Cells
Licensed content author	Jason M. Schenkel,David Masopust

Section 3.1.1 and 3.2.1 were created with the aid of ChatGPT

Abstract and section 1, 2 and 4 were corrected with the aid of ChatGPT

7 CURRICULUM VITAE

EDUCATION

Oct 2019-Present	PhD student Graduate School of Systemic Neurosciences, Munich (Germany)
Oct 2018-Oct 2019	Fast-track student (Computational Track) Graduate School of Systemic Neurosciences, Munich (Germany)
Sep 2016-Sep 2018	Master's degree in Neuroscience (110/110 with honours) University of Pisa (Italy) Thesis: "Discovery of prognostic markers and development of a stem cell-based therapy in mouse models of focal stroke"
Oct 2013-Oct 2018	Biology Student Scuola Normale Superiore (Italy) http://en.sns.it
Jan 2018-Jul 2018	Preparatory exams for Teaching Activity Psychology, Pedagogy, Anthropology and Education Methods
Sep 2013-Jul 2016	Bachelor's degree in Biological Science (110/110 with honours) University of Pisa (Italy) Thesis: "The role of a-synuclein in cellular physiology and neurodegeneration"

TRAINING

Mar 2019-Present	PhD Project Prof. Arthur Liesz, Institute for Stroke and Dementia Research, Munich Project: "The role of T cells in the Chronic Phase after Stroke"
Oct 2017-Sep 2018	Research internship Prof. Matteo Caleo, National Research Council (CNR), Pisa (Italy) Project: "Discovery of prognostic markers and development of a stem cell-based therapy in mouse models of focal stroke"
Jul 2017-Aug 2017	Summer Research Program Prof. Carmen Sandi, Laboratory of Behavioral Genetics (EPFL), Lausanne Project: "Characterization of Adult Hippocampal Neurogenesis in High and Low Anxious Rats"
Dec 2015-May 2016	Research internship Dr. Emanuela Colla, Bio@SNS laboratory, Pisa (Italy) Project: "Study of a-synuclein protein aggregates endocytosis and its cytotoxic effect in primary and secondary cell lines"

8 LIST OF PUBLICATIONS

1. **Ricci, A.**, & Liesz, A. (2023). A tale of two cells: Regulatory T cell–microglia cross-talk in the ischemic brain. Science Translational Medicine, 15(721). https://doi.org/10.1126/scitranslmed.adj0052

2. Benakis, C., Simats, A., Tritschler, S., Heindl, S., Besson-Girard, S., Llovera, G., Pinkham, K., Kolz, A., **Ricci, A.**, Theis, F. J., Bittner, S., Gökce, Ö., Peters, A., & Liesz, A. (2022). T cells modulate the microglial response to brain ischemia. ELife, 11. https://doi.org/10.7554/ELIFE.82031

3. Schafflick, D., Wolbert, J., Heming, M., Thomas, C., Hartlehnert, M., Börsch, A.-L., **Ricci, A.**, Martín-Salamanca, S., Li, X., Lu, I.-N., Pawlak, M., Minnerup, J., Strecker, J.-K., Seidenbecher, T., Meuth, S. G., Hidalgo, A., Liesz, A., Wiendl, H., & Meyer Zu Horste, G. (2021). Single-cell profiling of CNS border compartment leukocytes reveals that B cells and their progenitors reside in non-diseased meninges. Nature Neuroscience, 24(9), 1225–1234. https://doi.org/10.1038/s41593-021-00880-y

4. Heindl, S., **Ricci, A.**, Carofiglio, O., Zhou, Q., Arzberger, T., Lenart, N., Franzmeier, N., Hortobagyi, T., Nelson, P. T., Stowe, A. M., Denes, A., Edbauer, D., & Liesz, A. (2021). Chronic T cell proliferation in brains after stroke could interfere with the efficacy of immunotherapies. The Journal of Experimental Medicine, 218(8). https://doi.org/10.1084/jem.20202411

5. Roth, S., Cao, J., Singh, V., Tiedt, S., Hundeshagen, G., Li, T., Boehme, J. D., Chauhan, D., Zhu, J., **Ricci, A.**, Gorka, O., Asare, Y., Yang, J., Lopez, M. S., Rehberg, M., Bruder, D., Zhang, S., Groß, O., Dichgans, M., … Liesz, A. (2021). Post-injury immunosuppression and secondary infections are caused by an AIM2 inflammasome-driven signaling cascade. Immunity, 54(4), 648-659.e8. https://doi.org/10.1016/j.immuni.2021.02.004

6. Miraglia, F., **Ricci, A.**, Rota, L., & Colla, E. (2018). Subcellular localization of alpha-synuclein aggregates and their interaction with membranes. Neural Regeneration Research, 13(7), 1136–1144. https://doi.org/10.4103/1673-5374.235013

7. Colla, E., Panattoni, G., **Ricci, A.**, Rizzi, C., Rota, L., Carucci, N., Valvano, V., Gobbo, F., Capsoni, S., Lee, M. K., & Cattaneo, A. (2018). Toxic properties of microsome-associated alpha-synuclein species in mouse primary neurons. Neurobiology of Disease, 111, 36–47. https://doi.org/10.1016/j.nbd.2017.12.004

9 AFFIDAVIT

Eidesstattliche Versicherung/Affidavit

Alessio Ricci

(Studierende / Student)

Hiermit versichere ich an Eides statt, dass ich die vorliegende Dissertation

The Role of T Cells in the Chronic Phase after Stroke

selbstständig angefertigt habe, mich außer der angegebenen keiner weiteren Hilfsmittel bedient und alle Erkenntnisse, die aus dem Schrifttum ganz oder annähernd übernommen sind, als solche kenntlich gemacht und nach ihrer Herkunft unter Bezeichnung der Fundstelle einzeln nachgewiesen habe.

I hereby confirm that the dissertation The Role of T Cells in the Chronic Phase after Stroke is the result of my own work and that I have only used sources or materials listed and specified in the dissertation.

München / Munich

19.01.2024 (Datum / Date)

Alessio Ricci (Unterschrift / Signature)

10 DECLARATION OF AUTHOR CONTRIBUTION

Publication 1: (Heindl, Ricci, et al. 2021) 'Chronic T cell proliferation in brains after stroke could interfere with the efficacy of immunotherapies'

Heindl, S., **Ricci, A.**, Carofiglio, O., Zhou, Q., Arzberger, T., Lenart, N., Franzmeier, N., Hortobagyi, T., Nelson, P. T., Stowe, A. M., Denes, A., Edbauer, D., & Liesz, A.

Author contributions: S. Heindl conceptualized experiments, performed most of the experiments, analyzed the data, and wrote the manuscript. A. Ricci performed and analyzed experiments. O. Carofiglio, Q. Zhou, T. Arzberger, and N. Lenart performed experiments. N. Franzmeier analyzed FC data. T. Hortobagyi, P.T. Nelson, A.M. Stowe, and A. Denes selected and provided the human tissue samples. D. Edbauer provided experimental resources. A. Liesz initiated the study, conceptualized and supervised the research, and wrote the manuscript. All authors reviewed the manuscript.

My contribution to this publication in detail:

For this publication, I performed the multidimentional flow cytometry, from panel design and optimization, to actually perform the experiments and analyze the results (Fig. 2B to 2C). I set up the staining protocol for CD3. I performed the experiments with the cohort of mice that underwent distal middle cerebral artery occlusion (dMCAo), for which I quantified infarct volume (Fig. S1F), T cell density (Fig. S3B) and percentage of proliferating cells (Fig. S3D). I developed the script to quantify Clark-Evans agglomeration index to study T cell distribution in the tissue. I set up the method to label circulating cells to determine the contribution of tissue invasion and performed the experiment (Fig. S3C).

Publication 2: (Ricci et al. 2024) 'Stroke Induces Development of a Brain-Resident T cell Population which Promotes Functional Recovery'

Ricci, A., Heindl, S., Carofiglio, O., Simats, A., Bittner, S., Beltran, E., Fekete, R., Denes, A., & Liesz, A.

Author contributions: A. Ricci conceptualized experiments, performed most of the experiments, analyzed the data and wrote the manuscript; S. Heindl performed and analyzed experiments. O. Carofiglio and A. Simats performed experiments; E. Beltran contributed to the analysis of sequencing data. R. Fekete and A. Denes selected and provided the human tissue samples. S. Bittner provided experimental resources. A. Liesz initiated the study,

conceptualized and supervised the research and wrote the manuscript. All authors reviewed the manuscript.

My contribution to this publication in detail:

For this publication, I performed and analyzed all the experiments with the following exceptions:

- For the scSeq experiments, libraries were generated by A. Simats and preliminary data analysis was performed by E. Beltran.
- Experiment in Fig. 2I was performed and analyzed by O. Carofiglio.
- Experiment in Fig. 4A was performed and analyzed by S. Heindl.

Herewith, I confirm the contributions of Alessio Ricci to the articles.

Munich, 19.01.2024

Alessio Ricci	Dr. Steffanie Heindl (First author publication 1)
	Prof. Arthur Liesz (Supervisor)